# EVALUATION OF CRACKING POTENTIAL OF SUPERPAVE MIXTURES WITH HIGH RECLAIMED ASPHALT PAVEMENT CONTENT

by

ANANNA AHMED

B.Sc., Bangladesh University of Engineering and Technology, 2012

A THESIS

submitted in partial fulfillment of the requirements for the degree

MASTER OF SCIENCE

Department of Civil Engineering
College of Engineering

KANSAS STATE UNIVERSITY
Manhattan, Kansas

2015

Approved by:

Major Professor
Dr. Mustaque Hossain

# Abstract

Approximately 89% of 11,000 miles of Kansas roads are surfaced with asphalt. Hundreds of thousands of tons of reclaimed asphalt pavement (RAP) are produced annually in the United States, including in Kansas. This bulk volume of RAP must be economically managed in order to achieve environmental friendliness. Recycling of RAP conserves natural resources and reduces landfill usage. However, many agencies have reported that increased RAP content produces drier hot-mix asphalt (HMA) mixtures than virgin mixtures that are susceptible to premature cracking.

In this research, laboratory-produced Superpave HMA mixtures containing increased percentages (20, 30, and 40%) of RAP materials from three RAP sources (Shilling Construction Co., Konza Co., and the Kansas Department of Transportation's project, US 73) were studied for cracking performance. Mix designs were produced using Superpave design criteria for 12.5-mm nominal maximum aggregate size mixture. The static and repetitive Semicircular Bending (SCB) test, the Texas Overlay Tester test, the dynamic modulus test, and Viscoelastic Continuum Damage (VECD) tests were performed on laboratory-prepared samples. In general, cracking performance decreased with increased RAP content. The RAP from the US 73 project performed most consistently compared to other two sources of RAPs. Test results were analyzed using two-way Analysis of Variance (ANOVA), proving that mixtures containing 4.5% to 4.9% binder performed the best against cracking. The RAP source was found to have more effect on cracking propensity than RAP content. Mixtures with RAP content up to 40% performed satisfactorily. Tukey's pairwise comparison method was used to compare results from all tests; VECD was determined to be the most appropriate test to evaluate cracking propensity of HMA mixtures.

# Table of Contents

# List of Figures

# List of Tables

# Acknowledgements

I would like to acknowledge my sincerest gratefulness to my major professor, Dr. Mustaque Hossain, for his academic guidance and perennial support to me. I am very thankful to Dr. Robert Stokes and Dr. Kyle Riding for being part of my thesis committee and all their suggestions for making my thesis better. I appreciate the financial support from the Kansas Department of Transportation for completing this research work. I would like to thank Dr. Abigail Jager for consulting the statistical analysis for the study. I very thankfully acknowledge technical helps of Aswad Adib and statistical helps of Sharif Mahmood, two of my fellow graduate students. I am very thankful to my graduate colleagues and undergraduate assistants for fixing every problem I have ever faced during this research work.

Last but not least, I would like to take this opportunity to acknowledge the contribution of my parents and family in my journey.

# Dedication

This thesis is dedicated to my friends, here in Manhattan and back home in Bangladesh. It had been proverbially a long journey and they never let me stop from making it happen.

# Chapter 1 - Introduction

## 1.1 Background

Asphalt pavement recycling has become an integral part of pavement reconstruction and resurfacing in the United States and in many parts of the world. Scarcity of quality aggregates and increasing environmental concerns are intensifying the need for pavement recycling. Existing asphalt pavement materials are commonly removed during resurfacing, rehabilitation, and reconstruction operations. In the past, rehabilitation refuse of asphalt pavement was disposed of in landfills; however, recent principles of sustainable transportation systems have gained popularity and raised concerns regarding these landfills and their environmental impact.

Once removed and processed, pavement materials become reclaimed asphalt pavement (RAP) that contains valuable asphalt binder and aggregate, as shown in Figure 1.1. This RAP can replace expensive virgin aggregates and binders in HMA mixtures. According to the National Asphalt Pavement Association (NAPA), approximately 33 million metric tons of RAP materials are produced in the United States each year (NAPA 2013). The Federal Highway Administration (FHWA) recommends use of RAP for all new construction and rehabilitation work of asphalt pavements in order to achieve better or equal performance with maximum sustainability. According to FHWA, use of RAP is economical for the intermediate and surface layers of flexible pavements in which the aged binder from RAP can replace a portion of virgin binder.

**Figure 1.1 RAP from different sources and with various gradations**

Although RAP has been in use for the last three decades, recent interest has arisen regarding use of higher quantities of RAP. By definition, mixtures with high RAP content contain more than 25% RAP by weight of the mixture (FHWA 2011).

Initially, use of RAP in roadwork was confined to low-volume roads but RAP use has become increasingly more widespread nowadays. In 2007, typical hot-mix asphalt (HMA) mixture contained approximately 12% RAP. From 2007 to 2009, approximately 27 states increased the amount of RAP permitted in asphalt mixtures, and, as of 2009, 23 states gained experience about utilizing high-RAP mixtures. In 2011, over 40 state highway agencies allowed more than 30% RAP; however, only 11 states reported practically using 25% RAP or more (FHWA 2011). However, surface layer quality is of primary concern for states' Department of Transportations (DOTs). Although use of RAP in unbound layers has been practiced widely in the United States, the main factors influencing reluctance in accepting RAP usage include uncertainties in mix design, lack of information about production technology used for RAP sources, and uncertainties of resultant mixture qualities (Zaumanis and Mallick 2014). Research conducted by McDaniel et al. (2000) investigated the inclusion of RAP in the Surperpave mix design, resulting in development of Procedure M 323 by the American Association of State Highway and

Transportation Officials (AASHTO). Institutionalizing RAP use in addition to the rising price of virgin binder has resulted in increased quantities of RAP use in new HMA mixtures.

In 2009, the North Carolina DOT conducted a survey for AASHTO in order to evaluate RAP use by state DOTs, including Province of Ontario, Canada. According to the survey, four factors were identified that prevent DOTs from using high-RAP quantities in HMA mixtures: (1) specification limitations, (2) variability of RAP, (3) lack of availability of RAP, and (4) lack of experience with RAP. The survey also evaluated performance of pavement sections with RAP. Most agencies reported that HMA mixtures containing RAP demonstrated poorer cracking performance than pavements with no RAP, including fatigue and low-temperature cracking, but permanent deformation or rutting performance was improved (FHWA 2011).

Figure 1.2 illustrates the production process of RAP. Existing pavements typically are scraped by a milling machine with carbide teeth/cutting drums, transported to plants in order to be crushed into convenient sizes and gradations, and then transported to desired locations.

**Figure 1.2 Pavement milling**

## 1.2 Problem Statement

The Kansas Department of Transportation (KDOT) is increasingly allowing recycled materials in Superpave HMA mixtures. As materials and construction costs continue to increase, KDOT and the paving industry seek to include more RAPs in asphalt pavements. However, similar to many other state highway agencies in the United States, Kansas roads have experienced premature cracking and deterioration of pavements built with high-RAP mixtures, thereby affecting long-term durability of these pavements, as shown in Figure 1.3 for a 1-year old pavement in Kansas. In general, Hamburg Wheel Tracking Device (HWTD) test results for a virgin HMA mixture with no RAP have been consistent from sub-lot to sub-lot. However, test results for HMA mixtures with high RAP percentages vary significantly, as shown in Table 1, in which consecutive sub-lots/lots demonstrated unpredictably different results with only 24% RAP. Another mix with 35% RAP performed much satisfactorily than the mix with 24% RAP. This trend was also evident for high-RAP mixtures evaluated at Kansas State University. RAP variability is thought to be responsible for performance variability of HMA mixtures with high RAP content, including early cracking. In addition, RAP that is currently produced differs from previous generations because recycled Superpave pavements have better aggregates and binder. These RAP sources are expected to be less variable and highly valuable. However, durability of mixtures containing high RAP content still needs to be ensured.

**Figure 1.3 Low-severity transverse cracking on US-83 in Thomas County**

**Table 1.1 Summarized Hamburg Wheel test results of SR-12.5A with high RAP content**

| Mix No./Lot | RAP (%) | Average Number of Passes | Average Rut Depth (mm) |
|---|---|---|---|
| 1/LOT-6A | 24 | 16,070 | 11.2 |
| 1/LOT-6C | 24 | 20,000* | 19.38 |
| 2/LOT-1D | 35 | 20,000* | 3.36 |

* reached maximum number of passes

## 1.3 Objectives

The following objectives were pursued in this study:

1. Evaluate cracking resistance of Superpave mixtures with higher RAP Content.
2. Evaluate the effect of RAP source or RAP quality on the cracking potential of mixtures.
3. Establish minimum asphalt binder content and maximum RAP content to ensure satisfactory cracking resistance.

## 1.4 Organization of Thesis

This thesis contains a total of five chapters, including this Introduction. Chapter 2 provides literature review on RAP use, durability issues associated with pavements containing RAP, and cracking evaluation tests performed for this study. Chapter 3 presents laboratory mixture design and testing methods, and Chapter 4 presents test results and statistical analysis. The conclusion and recommendations for future study are summarized in Chapter 5.

# Chapter 2 - Literature Review

## 2.1 Introduction

Research of RAP materials in new construction and pavement rehabilitation continues to be a topic of interest for pavement industry. The amount of RAP that can be accepted to add in new HMA mixtures without compromising long-term pavement performance has been and continues to be extensively explored in many studies. A majority of states in the United States currently use 15% to 25% RAP in new HMA. This chapter presents a comprehensive literature review in order to assess the effects of RAP use on physical, chemical, and volumetric properties of HMA mixtures. Because RAP is a source of asphalt binder, it is expected to reduce the quantity of virgin binder used in a mixture. Benefits and challenges of using RAP as an aggregate source are also discussed in this chapter. Primary distresses on flexible pavement are rutting and cracking; this literature review also summarizes previous work associated with four cracking evaluation tests.

## 2.2 Reclaimed Asphalt Pavement

Reclaimed Asphalt Pavement (RAP) is the term given by the Federal Highway Administration (FHWA) to removed and/or reprocessed pavement materials those contains asphalt binder and aggregates. These materials are removed from existing road surface for reconstruction or resurfacing or to obtain access to buried utilities. To ensure better quality and stable gradation, proper crushing and screening of RAP is done. RAP is produced by removing existing asphalt pavement layers via milling or full-depth removal. Pavement milling machines typically remove up to 50-mm thicknesses in a single pass. For full-depth removal, pavements are broken into small, manageable segments and then ripped off using a rhino horn on a bulldozer or pneumatic pavement breakers. Scraped-off road segments are transferred to RAP plants in order to participate in a series

of operations, including crushing, screening, conveying, and stock piling. Hot-in-place and cold-in-place recycling are other popular methods of recycling and typically applied with required additives (Bonaquist 2007).

## 2.3 Why Use RAP?

The following factors contribute to increased RAP usage in new construction and rehabilitation projects of pavements:

- **Increased cost of virgin materials**: The cost of virgin asphalt binder has increased significantly since the oil crisis in the mid-1970s (Karlsson and Isacsson 2006). Binder costs increased more than 300% by 2008 (Brown et al. 2009). A typical asphalt mixture consists of 95% aggregate and 5% asphalt by weight, but aggregate accounts for only 30% of the total cost, while binder accounts for the other 70% (Brown et al. 2009). However, aggregates are becoming scarce and/or unevenly distributed over the country landscape, and costs associated with processing and transporting aggregates to project locations have increased significantly due to increased energy prices.
- **Recycling of Road Refuse:** Each year the United States produces huge volumes of RAPs. Traditionally, this refuse has been disposed of in landfills or left in stockpiles; however, chemical activity and leaching properties of RAP make it unsuitable for landfilling in large volume. Thus large piles of RAP are scattered around. In order to reuse this material, all states use up to 25% RAP in new HMA, and feasibility of higher RAP content is currently under study (Brown et al. 2009). According to FHWA, 80% of RAP removed during resurfacing, approximately 73 million tons, is reused each year. Maintaining the quality of RAP is expected to increase the quantity of RAP used in new pavement construction (Shen et al. 2007).

## 2.4 Changes in HMA Mixture Properties Due to RAP Usage

RAP materials before being removed from existing pavements were subjected to thousands of wheel passes and years of weathering. Most RAPs are from pavements those were originally constructed with penetration-graded asphalt binder, not performance grade. Performance Grade (PG) of the binder extracted from RAP is typically higher than the virgin binder required for relevant new project. Binder performance in ductility and cohesion is typically severely altered in RAPs as a result of oxidation, evaporation, exudation, and the physical hardening process (Karlsson and Isacsson 2006). Aggregates near the pavement surface sustain polishing effects of wheel passes, and binder films around aggregate particles can occasionally be worn off. Aggregates beyond the contact of wheel passes sustain changes caused by thermal gradient and variation in pressure. Chemically-active aggregates are suspected to be altered in their petrography, and a leaching effect may remove some constituents from HMA mixture that are soluble in motor oil or water. Aggregates in RAP are also suspected to be brittle and have less structural capacity than virgin aggregates. Interlocking of aggregates and inter-particle friction are keys to maintaining load-carrying capacity in flexible pavements; polished and rounded aggregates tend to degrade these properties. Typically, blending with virgin aggregates of dominant volume suppresses this change in performance (Daniel et al. 2005). However, these problems resurface if the virgin aggregate content decreases, as in the case of HMA mixtures with high RAP.

When aggregates and binder are mixed in order to obtain virgin HMA, some of the heated asphalt binder gets absorbed into the aggregate pores and the remainder of the binder creates a coating or film around the aggregates, resulting in mixture cohesion (Huang et al. 2005). RAP aggregates have absorption capacities and aggregate-to-binder interactions that are consistent with absorption and interaction observed in virgin mixtures. RAP typically changes volumetric and mechanistic properties of the mixture (Huang et al. 2005). The degree of blending between the

virgin binder and the RAP binder in mixture has dual contribution to mixture properties. Although this blending is not well-understood, many studies have concluded that the issue is insignificant below 25% RAP content (West et al. 2014).

Daniel et al. (2005) studied changes in volumetric properties of HMA mixtures with increasing RAP content and compared those to that for a control HMA mixture with no RAP. The addition of RAP increased the voids in mineral aggregate (VMA) and voids filled with asphalt (VFA) of the mixtures. Increase in RAP content increased mixture stiffness but decreased creep compliance, thereby showing that HMA mixtures with RAP are more resistant to permanent deformation and less resistant to fatigue cracking.

## 2.5 Issues Regarding RAP Use

HMA mixtures with RAP content up to 25% have demonstrated similar results according to several researchers (Kandhal et al. 1996, McDaniel et al. 2000, Shu et al. 2008, Li et al. 2008). Most transportation agencies have reported the following issues regarding placement and performance of HMA mixture containing high quantities of RAP:

- Difficulties in attaining desired air void content and density during construction
- Dry appearance of the mixture
- Early cracking and raveling of the pavement surface

Chemical agents commonly known as asphalt rejuvenating agents are currently in use or under study. Early cracking was the focus of this study.

## 2.6 Superpave Mixture Design System

Superpave mixture design is an outcome of the Strategic Highway Research Program (SHRP). SHRP research has focused on six areas related to the road network in the United States, including an asphalt research program. Research produced a performance-based specification (PG)

for the asphalt binder and a new mixture design system. In addition, a new compactor, Superpave Gyratory Compactor (SGC), was used in the Superpave mixture design. Design methodology was originally planned as a performance-based HMA mix design system, and initial methodology included three levels of mix designs with increasing difficulty: Level 1, Level 2, and Level 3. Level 1 was the entry-level mixture design, but Levels 2 and 3 required performance-based mixture evaluation tests. Due to lack of suitable performance tests and levels of complexity, Levels 2 and 3 are still under research. An entry-level mixture design is currently labelled as a Superpave mixture design (Huber et al. 2013).

Level 1 mixture design is based on mixture parameters that define fundamental properties of the mixture, such as optimum air void content, minimum asphalt binder content, and aggregate gradation. In order to prepare specimens for volumetric analysis and performance tests, surrogate material properties were established to evaluate the performance of Superpave. Mixture performance tests are still under research in order to provide an active guideline (Huber et al. 2013).

## 2.7 Asphalt Pavement Durability Issues

Durability is a definitive problem in asphalt pavement performance. Durability of a flexible pavement section indicates the ability of pavement layers to maintain structural integrity against detrimental or damaging effects caused by climate and traffic loading throughout the service life of the pavement (Nicholls et al. 2008). According to Bonaquist (2013), a durable pavement should possess four prime properties: structural adequacy (sufficiently thick to carry traffic loading), proper drainage, proper construction, and use of proper materials for construction. The addition of recycled materials such as RAP and RAS to HMA have not yet provided definitive evidence of improved durability; instead a decrease in performance has been prominently determined in

literature. As the practice of RAP material usage in HMA mixture becomes increasingly prevalent, however, uncertainties regarding durability of HMA pavements must be addressed.

### 2.7.1 Aggregate Properties

RAP in HMA mixtures works as aggregates too. To ensure pavement durability, the aggregates must have some desirable properties (Meininger and Nichols 1990), such as toughness and abrasion resistance in which aggregates should withstand mixing and compaction and maintain original gradation. Aggregates should also be sound and durable and resistant to degradation under traffic load during the service life of the pavement. Plastic fines interfere with the asphalt coating and potentially hamper mixture durability in regards to moisture resistance; therefore, clay content should be minimized. Aggregates with low clay content have demonstrated good performances (Brown et al. 2009).

### 2.7.2 Binder Properties

Appropriate Superpave PG binder selection depends on climatic conditions at the project location. Proper PG binder grade ensures mixture durability in terms of resistance to rutting, fatigue cracking, and low-temperature thermal cracking. When RAP is used in sufficient quantity, a virgin binder is selected depending on project location and effective grade of the RAP binder. The resultant binder grade (blend of virgin and aged binders) should guard against breaches in durability. NCHRP Project 9-12 and KDOT have established guidelines to compensate for the binder grade adding a stiff element (RAP) to the mixture. An RAP binder-to-virgin binder ratio of 0.25 to 0.35 is acceptable before the binder grade must be changed (Bonaquist 2011).

### 2.7.3 Volumetric Properties

An NCHRP project studied the effect of mixture volumetric properties on performance of HMA mixtures and concluded that in-place air void content and effective binder content of the mixture are two properties that most significantly affect pavement durability (Christensen et al. 2013). In-place air void content is controlled by construction practices. However, durability decreases with increased air void content. Pavements sections with lower air voids are less permeable, and low permeability helps reduce the rate of binder aging. Effective virgin binder content contains voids filled with mineral aggregate (VMA) minus the air void content. VMA is the controlling factor for HMA mixture durability. Christensen et al. (2013) also suggested that a 1% increase in VMA design will increase 1% of effective virgin binder content at 4% air voids. Several agencies have reduced the design number of gyrations in order to increase virgin binder content. Although only a passive relationship has been found between the number of gyrations and effective binder content, alteration of gradation is more appropriate (Shakiba et al. 2013).

## 2.8 Past Research Evaluating Cracking Potential

Cracking is one of the dominant distress types of flexible pavements. For performance-based specification, two approaches are frequently studied in order to evaluate cracking resistance. The first approach investigates the number of load cycles sustained at a certain temperature before crack initiation under various experimental setups. The second approach integrates the degree of damage that occurs from the original undamaged sample under repetitive loading. This section describes four cracking propensity tests.

### 2.8.1 Semi-Circular Bending (SCB) Test

The Semi-Circular bending (SCB) test provides information regarding mixture stiffness and the energy release associated with crack formation. Although the test method is simple, several

sequential steps are required in order to obtain usable parameters from the test output. Unfortunately, however, interpretation of output parameters is debatable. The test initially was designed to evaluate cracking potential and fracture mechanics of the mixture. Researchers currently tend to evaluate HMA mixture stiffness characteristics (Saadeh et al. 2011).

Chong and Kuruppu (1984) first used the SCB test to study fracture properties of rock materials. Loading configuration was strain-controlled, three-point flexural loading at a constant strain rate of 0.005 mm/s. A single-edged notch was made on the surface directly below the load line to provide a weak plane for controlled cracking. Test methods suggested by various studies to evaluate HMA mixture performance were nearly identical to Chong and Kuruppu's. However, the strain rate and sample thickness varied in many studies. A typical setup for the SCB test at Kansas State University is shown in Figure 2.1 (b).

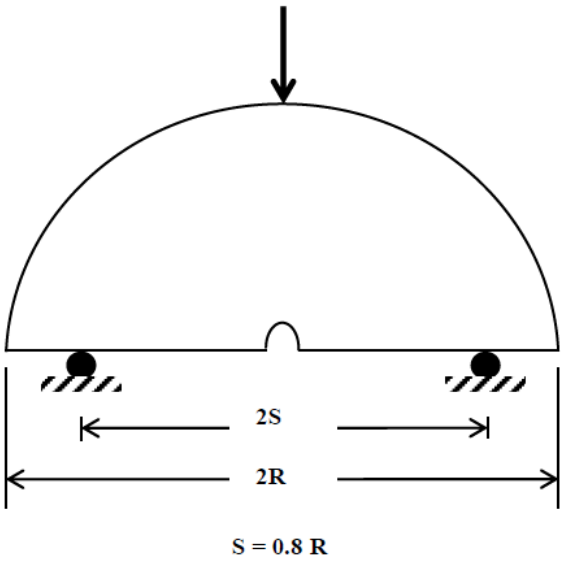


**(a)**

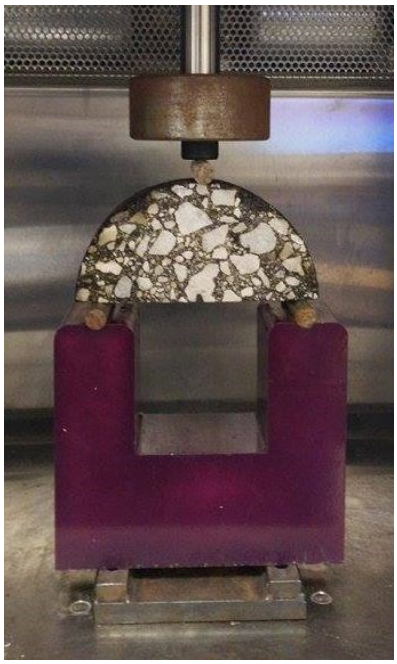

**(b)**

**Figure 2.1 (a) Schematic SCB test setup, (b) SCB test**

Disk-shaped samples with diameters of 100 or 150 mm. are used in the SCB test. Sample thickness is typically kept within 35 to 50 mm. at 7±1% for most test setups (Huang et al. 2009). Various loading rates in the stain-controlled test have been used, and strain rates vary from 0.01 to 0.001 mm/s in the literature (Walubita et al. 2002).

Notch depth affects peak load of the sample in the SCB test (Cooper et al. 2014). Some researchers prefer to place the notch along the thickness plane to ensure crack initiation at the notch location. Results have shown that the deeper the notch depth, lower the peak load. Cooper et al. (2014) correlated this phenomenon with a decrease in ligament area that resisted failure when depth increased.

Quality standards of mixtures with high RAP content were studied using the SCB test at the University of Iowa (2015). Samples were prepared with high RAP content (30%, 35%, and 40%), and tests were performed at two temperatures (-18 and -30 °C). Results showed that fracture energy (FE) decreased and stiffness increased as the test temperature decreased.

For this particular thesis, 25 °C was selected as the test temperature, similar to a study by Molenaar et al. (2002). Al-Qadi et al. (2015) also utilzed the SCB test for high-RAP HMA mixtures. Using the finite element method (FEM), they showed that the area that contributes to crack initiation reduces for HMA mixtures that contain increased amounts of RAP. Figure 2.2 (a) shows the resisting zone against cracking with 0% RAP compared to 30% RAP with a narrower contributory area, as shown in Figure 2.2 (b).

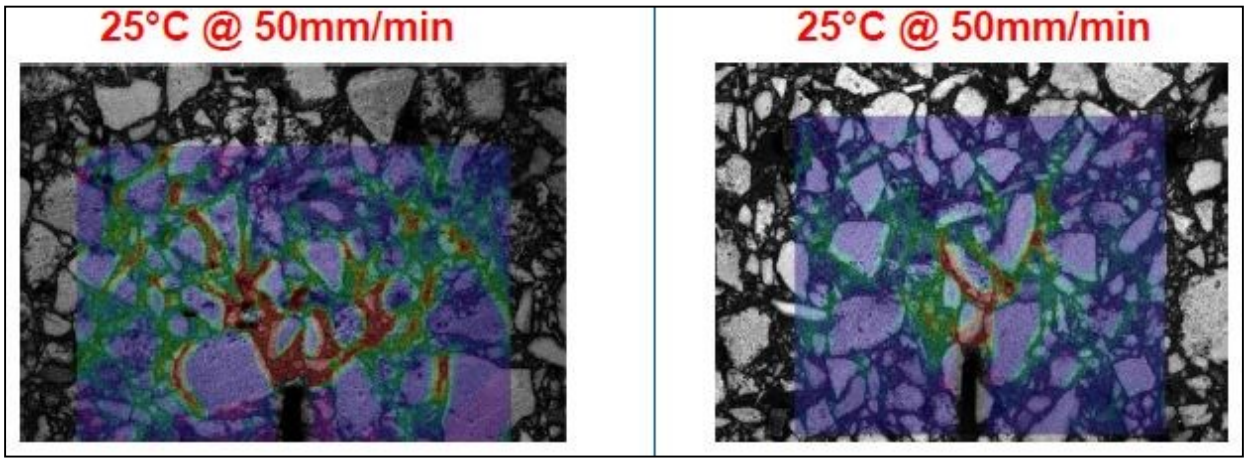


**Figure 2.2 FEM of SCB stress zone (Al-Qadi et al. 2015)**

Because stress distribution during SCB testing is not uniform and the HMA mixture is heterogeneous, simple geometry-based models cannot fully analyze SCB test output. Therefore, researchers have utilized a variety of methods in order to interpret test output. Molenaar et al. (2002) calculated tensile stress based on peak load and specimen diameter. Other output parameters, such as flexibility index, stiffness modulus and FE, can be calculated using the load versus displacement curve obtained during SCB testing. Buss et al. (2013) identified the load versus load line displacement curve (P-u) as typical output of the SCB test, shown in Figure 2.3. This research used test output (load versus displacement) data in order to construct Mode 1 shown

in the figure. Using curve setter in MATLAB, Mode 2 of the curve was extrapolated in order to evaluate rate of energy release.

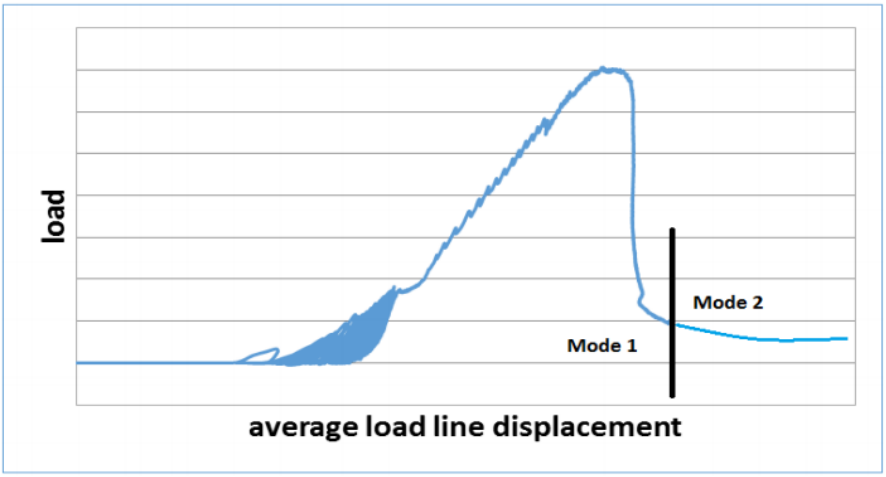


**Figure 2.3 SCB load versus load line displacement (P-u) curve (Buss et al. 2013)**

Podolsky et al. (2014) studied the effects of additives in HMA at low temperatures and evaluated mixture performance at low temperatures (-24, -12, and 0 °C) using the SCB test. Results showed that when the temperature increased from -24 °C to -12 °C, the FE increased, but when the temperature increased from -12 °C to 0 °C, FE decreased. Between these two temperatures, the sample became softer and less capable of withstanding load.

Huang et al. (2013) studied fatigue performance of HMA mixtures using the repetitive SCB (R-SCB) test. However, instead of constant strain, the sample was tested under constant sinusoidal load at a frequency of 5 Hz with minimum peak load as the input. The study revealed a relationship between resistance to fatigue cracking and asphalt binder properties. The SCB test was suggested as a valid test to evaluate fatigue performance of HMA mixtures with acceptable margin of error.

The SCB test has also been used to apply principles of fracture mechanics to asphalt pavement. Adamson et al. (1996) first considered asphalt mixtures as quasi-brittle materials.

Scullion et al. (2012) studied repeated loading SCB test instead of monotonic loading and evaluated mixtures in terms of number of load cycles until failure. However, the released energy could not be calculated for this test, and results were reported in number of load cycles until failure. Results displayed variability beyond acceptable limits.

Al-Qadi et al. (2014) analyzed samples with high RAP and no RAP, proving that increased percentages of RAP decrease the area that contributes to crack resistance, thereby increasing susceptibility to cracking.

### 2.8.2 Texas Overlay Test

The Texas Overlay OT) test, developed and standardized by the Texas Institute of Transportation (Tex-248-F), verifies cracking performance for HMA. The test determines the susceptibility of HMA mixtures to fatigue or reflective cracking. In the OT test, repeated direct tension is applied to the sample glued to a flat plate with a joint in the middle. The loading mechanism simulates cracking in the underlying layer of HMA overlays (TxDOT 2014). Schematics of a typical OT test setup and actual setup in the Asphalt Mixture Performance Tester (AMPT) at Kansas State University are illustrated in Figures 2.4 (c) and 2.4 (d), respectively.

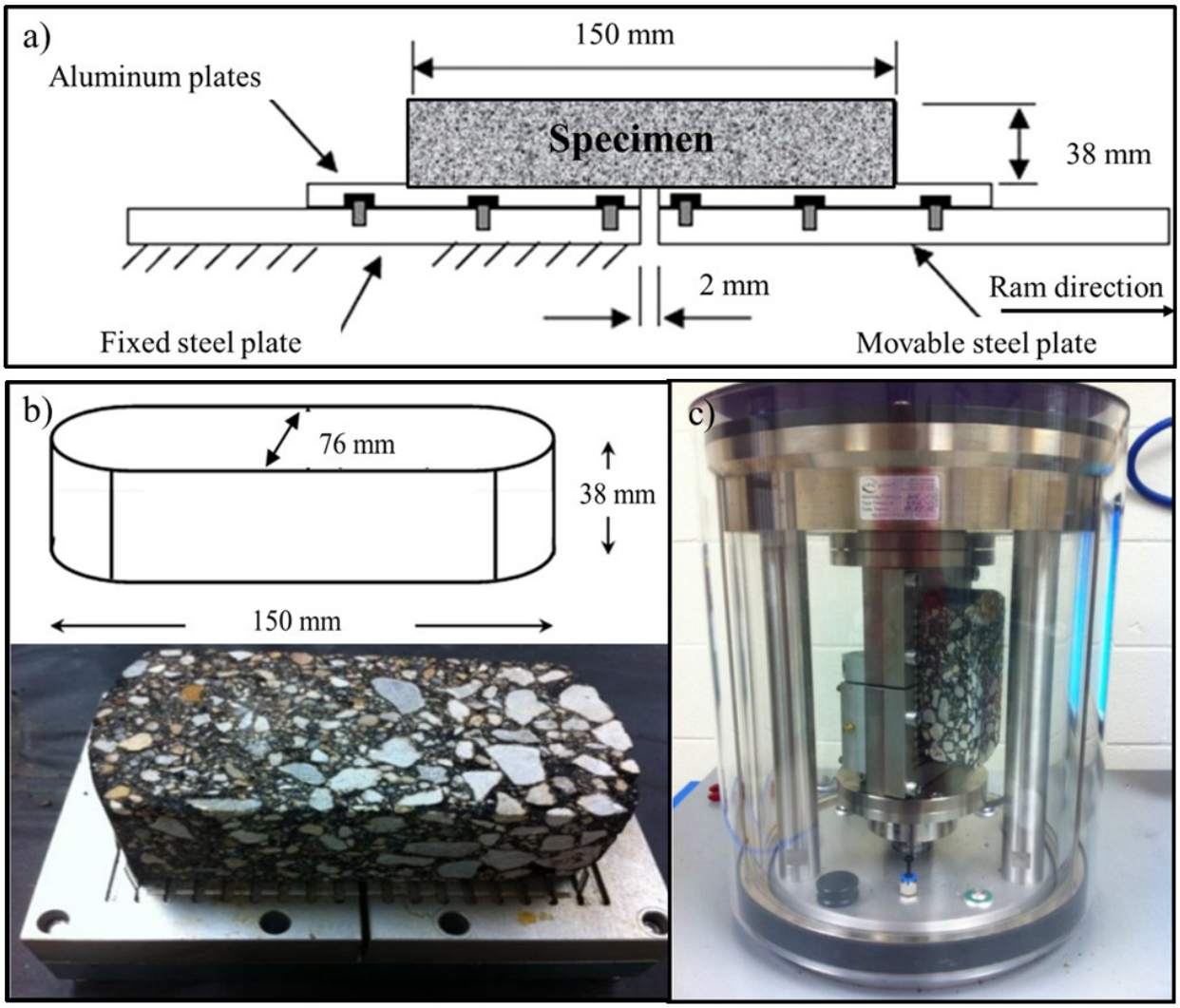


**Figure 2.4 Texas OT setup at Kansas State University**

The OT test is rapid and repeatable, allowing rapid identification of unsatisfactory samples. Because load is applied at a certain frequency in the test, crack initiation and crack propagation properties are able to be characterized (Zhou et al. 2004). Zhou et al. (2004) also discovered that the OT test evaluates reflective cracking potential of HMA mixtures, leading to the suggestion that the OT test is a promising fatigue cracking test for HMA. Theoretically, the higher the number of OT load cycles before the crack propagates through the thickness of the sample, the higher the

resistance to cracking. For dense-graded Texas HMA mixtures, Zhou et al. (2006) showed that HMA mixtures that sustained over 300 OT cycles demonstrated satisfactory crack resistance.

Li et al. (2014) studied the OT test in order to characterize cracking resistance potential of approximately 30 mixture designs with various material properties and aggregate gradations. They concluded that the OT test could be used to evaluate cracking resistance of HMA mixtures. The Washington state DOT performed the OT test on five mixture designs with five replicates of each design. Variability in test results was very high, and results were inconclusive (DeVol et al. 2008).

The OT test was also studied with monotonic tensile load in order to evaluate the rate of FE release (Walubita et al. 2012). The load-displacement (P-u) curve was generated at a constant loading rate and test temperature, and variability of test results was within the acceptable limit of 30%. Monotonic OT was considered to be a routine surrogate of repeated OT.

The OT test was compared to other cracking tests such as the monotonic and repeated indirect-tension test, the monotonic and repeated SCB test, the disk-shaped compaction tension test, and direct tension tests (Scullion et al. 2012). For repeated loading tests, variability was higher.

A technical report published by the Texas Transportation Institute (2012) listed sample drying method, glue quantity, number of replicates, air void content, sample age at the time of testing, and test temperature variation as key aspects of OT test repeatability and variability. As the tolerance level for variability of OT results increased up to 30% by the pavement community, the number of replicates for each type of sample decreased to 3 instead of 5. An ongoing project of the Texas Department of Transportation (TxDOT) focuses on modification of the current OT test in order to measure and characterize fatigue properties of HMA mixtures.

### 2.8.3 Dynamic Modulus Test

Dynamic modulus has been introduced as a key input parameter in the mechanistic-empirical design method of HMA pavements. AASHTO PP61-13 proposed a dynamic modulus test protocol that requires testing at 4, 20, and 40 °C and at loading frequencies from 0.01 Hz to 10 Hz. In AASHTO TP 62-07, five temperatures from -10 to 54 °C and six frequencies from 0.1 to 25 Hz were required. For this study, tests were performed at 4, 21, and 37 °C with six frequencies 0.1, 0.5, 1, 5, 10, and 25 Hz in order from the lowest temperature to the highest temperature and from the highest to lowest frequencies, as is typical for these tests. Typical test setup of the dynamic modulus test is presented in Figure 2.5. The test was conducted in Universal Testing Machine (UTM) and AMPT at Kansas State University.

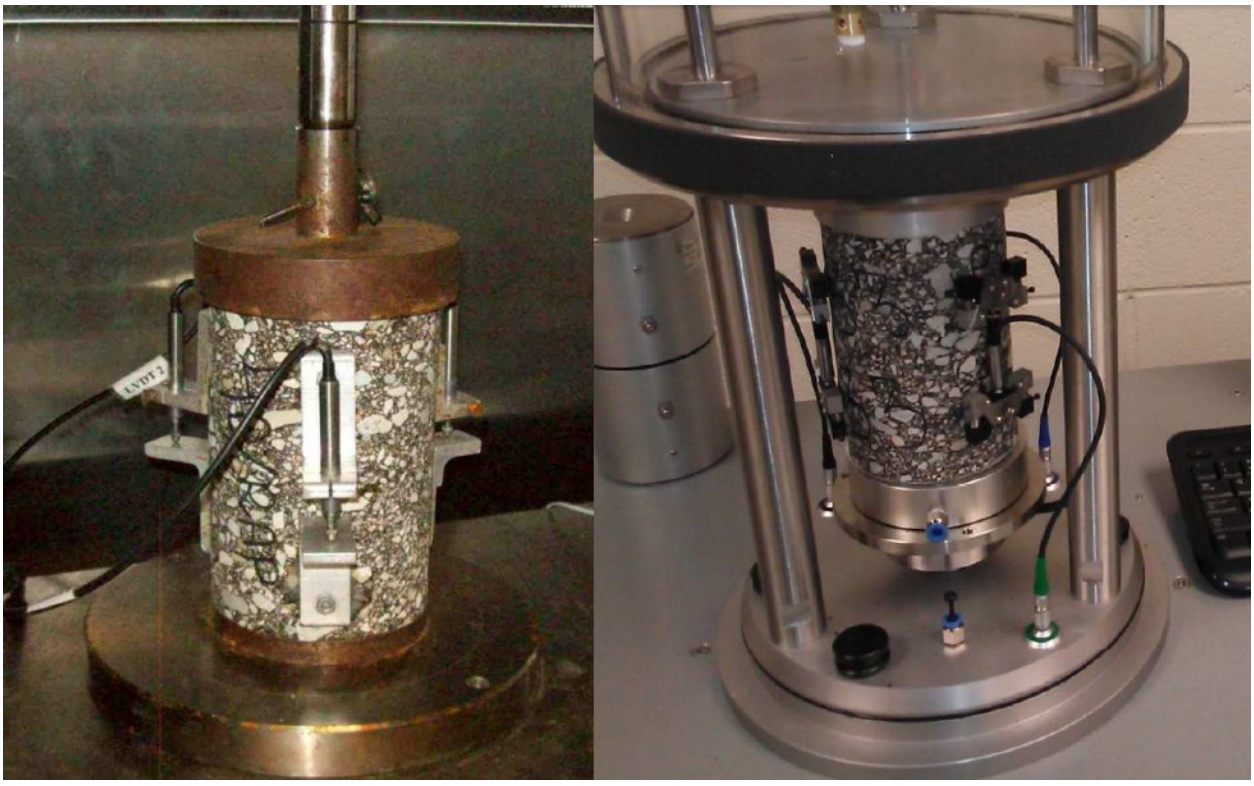

**Figure 2.5 Dynamic modulus test setup (Sabahfar 2012)**

Dynamic modulus values represent stiffness of the HMA mixture. Ghabchi et al. (2015) used dynamic modulus to compare warm-mix asphalt (WMA) and HMA stiffness in order to assess cracking performance. Most state DOTs that implement AASHTOware Pavement ME design have also accepted dynamic modulus as the HMA characteristic with which design analysis can be conducted (West et al. 2014).

Dynamic modulus test outputs over a range of temperatures and frequencies are superposed in order to formulate dynamic modulus master curves. These master curves are used to predict dynamic modulus values at various points (i.e., temperature and frequency) of interest. Dynamic modulus master curves used in the AASHTOware Pavement ME design are typically constructed using symmetric sigmoidal function. Studies have shown that lab-tested samples display a non-symmetric trend in dynamic modulus values, particularly at high temperatures when unconfined stiffness of HMA approaches zero. However, a nonsymmetric sigmoidal function is more appropriate for explaining such phenomenon (Khosravifar et al. 2015). A schematic of the dynamic modulus master curve is presented in Figure 2.6.

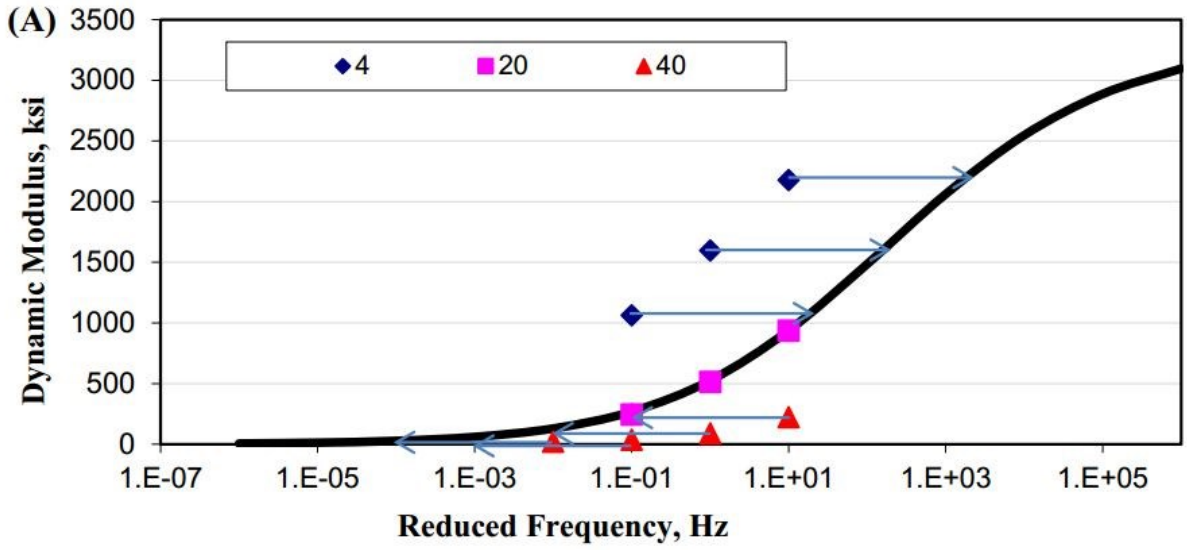


**Figure 2.6 Dynamic modulus master curve (Khosravifar et al. 2015)**

Yao et al. (2013) showed that the dynamic modulus can be used to classify asphaltic materials. This study tested samples at five temperatures (5, 20, 30, 40, and 60 °C) and at six frequencies (0.1, 0.5, 1, 5, 10, and 25 Hz). Master curves were formed using the symmetric sigmoid function, and coefficients of master curve (a, b, c, and d) were used to compare materials.

Cho et al. (2010) conducted rigorous laboratory testing in order to develop predictive equations for the dynamic modulus of HMA mixtures. Results showed that dynamic modulus of a mixture increased with increased loading frequency and decreased test temperature. They also concluded that air void did not significantly influence dynamic modulus. Large nominal maximum aggregate size in the mixture resulted in higher modulus other mixtures.

Yu et al. (2012) studied the effect of aggregate gradation and particle angularity on dynamic modulus of HMA mixtures. They discovered that the more the aggregates are packed, the greater the increase in dynamic modulus. Particle angularity also was found to have positive correlation.

In order to determine test temperature, researchers have selected temperature ranges suitable for the study area depending on geographic locations of projects. Sakhaeifar et al. (2015) used a temperature range of -10 to 54 °C. Their study proposed a model to predict in-place dynamic modulus with a satisfactory level of accuracy.

### 2.8.4 Evaluation of Fatigue Performance

Fatigue performance of HMA pavements has been studied using various test setups and loading patterns. Two types of loading patterns are presented in the literature: repeated direct tension loading and repeated tension-compression loading. Tong et al. (2014) used repeated direct tension loading to study fatigue crack growth in HMA samples in a dynamic mechanical analyzer. The fatigue law was verified using test results. Kim et al. (2009) used the tension-compression

loading pattern to study fatigue performance of HMA mixtures. In order to study fatigue performance of HMA mixtures, Ren et al. (2015) designed a repeated uniaxial penetrating test based on composite modification of the Flow Number test and Uniaxial Penetrating test that simulates repeated vehicle load. Daniel et al. (2002) studied fatigue characteristics of HMA samples at various strain amplitudes and frequencies at different test temperatures.

In HMA mixtures, resistance against fatigue cracking is primarily controlled by the asphalt binder; aggregate contribution to fatigue cracking resistance is low (Tan et al. 2011). Their study concluded that laboratory tests typically underestimate fatigue resistance of mixtures by not considering the healing effect of binder under real-time loading during the rest period. Extended rest periods between loading cycles could simulate real-time loading, but no index has been developed in order to quantify the amount of healing by the binder. Therefore, this issue has been addressed by the Viscoelastic Continuum Damage (VECD) theory. In order to model damage, the work potential theory takes healing effect into account. Various sample shapes and sizes for fatigue evaluation are also under experimentation. Figure 2.7 shows a cylindrical sample and a prismatic sample (for field sampling) (Martin et al. 2013).

Several models have been developed in order to evaluate fatigue characteristics of HMA pavements. Modelling approaches can be broadly classified as mechanistic material models and micromechanical models. Mechanistic material models can be further classified as empirical and derived. Monismith et al. (1961) and Pell et al. (1975) proposed an empirical model called fatigue law. Three categories of theory-derived models are presented in the literature: dissipated creep stain energy model (Roque et al. 2010), VECD theory (Roque et al. 2010, Underwood et al. 2012), and viscodamage model. Numerical models have been primarily studied for micromechanical models in order to evaluate fatigue characteristics of HMA mixtures. The lattice model (Guddati

et al. 2002), the discrete element-based method, and two-way coupled approaches are examples of micromechanical modelling (Underwood 2014).

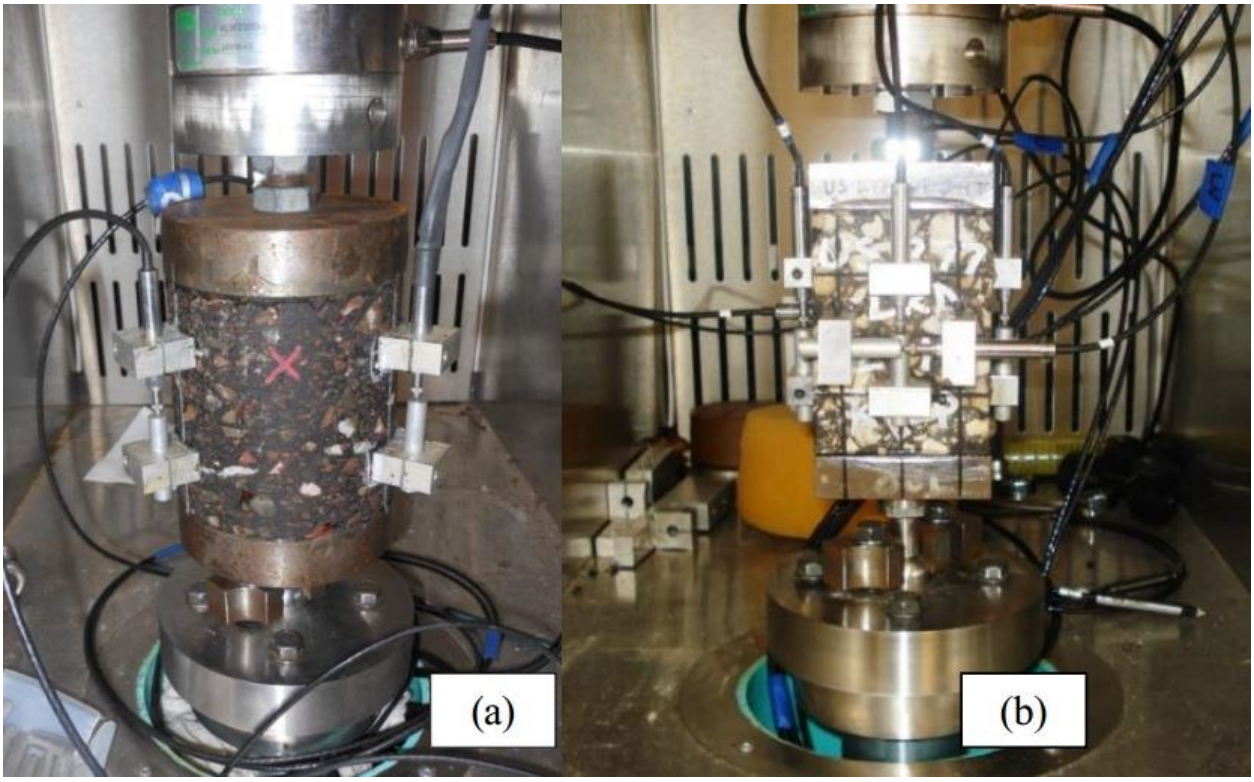


**Figure 2.7 Push-pull fatigue test samples: (a) cylindrical, (b) prismatic field sample (Martin et al. 2013)**

The VECD test (VECD FEP++) evaluates pavement performance using FEM-based analysis and the viscoelastic continuum theory. The test was developed by North Carolina State University under the NCHRP 1-42A effort. The combination of the VECD test and FEM allows fracture mechanics of the compacted sample and continuum damage mechanics of the mixture to be simultaneously captured while deals with the microcracking phenomenon (Underwood 2014).

The S-VECD model was developed based on the elastic-viscoelastic correspondence principle, the temperature-time superposition principle (for dynamic modulus properties), and the work potential theory (Xie et al. 2014). The elastic-viscoelastic principle was used to explain viscoelastic behavior of HMA mixtures in the model in order to convert strain to equivalent pseudo

strain. The temperature-time superposition principle was used to merge the effect of these two strains at different temperatures to certain reference temperature, and then the work potential theory (Schapery 1990) was used to model damage growth. Equation 2.1 was derived in order to calculate pseudo strain at time step *t*.

$$\varepsilon^R = \frac{1}{E_R}\int_0^t E(t-\tau)\frac{d\varepsilon}{d\tau}d\tau \qquad \textbf{(2.1)}$$

where $\varepsilon^R$ is the pseudo strain and $\varepsilon$ is the actual strain. $E^R$ is the reference modulus, and $E(t)$ is the relaxation modulus at time step *t*. In the next step, damage growth is modeled. Damage parameter $S$ is defined as the structural change in stiffness as a result of repetitive loading in terms of pseudo stiffness, $C$ (Equation 2.2) (Kim et al. 2009).

$$C = \frac{\sigma}{\varepsilon^R * I} \qquad \textbf{(2.2)}$$

The work potential theory has three fundamental functions:

a. Pseudo strain energy density function

$$W^R = f(\varepsilon^R, S) = \frac{1}{2}\sigma\varepsilon^R = \frac{1}{2}(\varepsilon^R)^2 C \qquad \textbf{(2.3)}$$

b. Stress-pseudo strain relationship

$$\sigma = \frac{\partial W^R}{\partial \varepsilon^R} = C(S)\varepsilon^R \qquad \textbf{(2.4)}$$

c. Damage evolution law

$$\frac{dS}{dt} = \left(-\frac{\partial W^R}{\partial \varepsilon^R}\right)^{\alpha} \qquad \textbf{(2.5)}$$

where $W^R$ is pseudo strain energy density and $\alpha$ is the damage evolution rate. Cumulative damage accumulated due to loading for each time step can be evaluated using Equation 2.6, resulting in development of damage characteristics curves (C-S) for each mixture.

$$S_{N+1} = S_N + \left[-\frac{DMR}{2}(C_N - C_{N-1})(\varepsilon^R)^2\right]^{\frac{\alpha}{\alpha+1}} \Delta\xi^{\frac{1}{\alpha+1}} (K_1)^{\frac{1}{\alpha+1}} \qquad \textbf{(2.6)}$$

$$C = 1 - C_{11}S^{C_{12}} \qquad \textbf{(2.7)}$$

where *DMR* is dynamic modulus ratio, $\Delta\xi$ is the reduced time interval, and $K_1$ is constant accounted for cyclic data.

$$DMR = \frac{|E^*|_{Fingerprint}}{|E^*|_{LVE}} \qquad \textbf{(2.8)}$$

Depending on predicted damage characteristics, fatigue life prediction can be done for mixtures.

In this study, a simplified VECD test was utilized in order to evaluate fatigue performance of HMA mixture with RAP. Because prediction of effective stress versus strain equations and growth of macrostrain are typically the bases for evaluating viscoelastic properties of HMA mixtures (Lee et al. 2011), dynamic modulus and damage characteristics were used for the VECD model in this study. The VECD model considered stiffness of a damaged body as a body with lower stiffness; the amount of associated damage was related to the effective area. Damage characteristic curves were direct indications of fatigue resistance of a material at each time step.

Increase in RAP content has been reported to lead to low fatigue resistance, but a decrease in fatigue life has not been found to decrease significantly. Hossein et al. (2013) concluded that HMA mixtures with up to 50% RAP can perform well. Evaluation of crack initiation in the fatigue test is typically considered to be the stopping point of the test. However, researchers have had difficulty identifying microcracks as soon as they appear. Therefore, Hossein et al. (2013) conducted a study to detect cracks using laser technology in order to provide an automated stopping point.

## 2.9 Summary

Many agencies have reported that the addition of recycling materials decreases levels of cracking performance and durability. Ongoing studies seek to identify acceptable levels of decrease in performance. Rutting performance has been proven to improve with the addition of recycle materials. Researchers are attempting to suggest specifications based on mixture performance and mixture recipe. Various tests have been used to characterize cracking resistance of HMA mixtures, and various fatigue models have been proposed in order to define cracking resistance of these mixtures.

# Chapter 3 - Methodology

## 3.1 Experimental Design

Three RAP sources were used for this project in order to study the effect of RAP source and increasing RAP content on HMA mixtures. The sources were Shilling Construction Company, Konza Construction Company, and a KDOT project on US 73 near Kansas City. For each RAP source, three Superpave mixture designs with increasing RAP content (20, 30, and 40%) were prepared. Sabahfar (2012) developed the mixture designs for the first two RAP sources (Shilling and Konza RAP). Mix designs for the project on US 73 were developed in this study. All mixtures had 12.5-mm nominal maximum aggregate size (NMAS). These mixtures when contain RAP is known as SR-12.5 in KDOT mix design specifications. Virgin aggregates used in all mix designs were kept same, and cracking potential tests were performed on all mixtures. Sabahfar (2012) previously used the dynamic modulus test to study fatigue cracking and permanent deformation of mixes containing Shilling and Konza RAP. Aziz (2013) evaluated the cracking potential of those mixtures using the SCB test and OT test. In this study, the VECD test was used to test mixtures with all three RAP sources in order to evaluate fatigue cracking potential. Mixtures with RAP from US 73 were also tested for cracking potential using the SCB, OT, and dynamic modulus tests.

## 3.2 Aggregate and RAP Gradation

Mixture aggregate gradations for this study were done by blending five virgin aggregates and the RAP. The following virgin aggregates were obtained from Shilling Construction Company: CS-1 (crushed limestone with coarse gradation), CS-1A (crushed limestone with fine gradation), MSD-1 (manufactured sand), CG-5 (crushed gravel), and SSG (natural/river sand). Table 3.1 lists gradations of each aggregate and RAP sources, and Figure 3.1 shows gradations on semi-log scale and Figure 3.2 shows blending of nine mixtures on 0.45-power chart. Although all

RAP sources demonstrated substantial amounts of fines, some mixtures were deficient in the dust-to-binder ratio. Therefore, in order to meet specifications, 1% limestone dust was added to the aggregate blend. Table 3.2 summarizes aggregate proportions for each SR-12.5A mixture.

**Table 3.1 Aggregates and RAP gradations**

| Material | CS-1 | CS-1A | MSD-1 | CG-5 | SSG | Shilling RAP (1) | Konza RAP (2) | US 73 RAP (3) |
|---|---|---|---|---|---|---|---|---|
| **Sieve Size** | **% Passing** | | | | | | | |
| ¾ | 100 | 100 | 100 | 100 | 100 | 100 | 100 | 100 |
| ½ | 59 | 100 | 100 | 100 | 100 | 98 | 96 | 99 |
| ⅜ | 20 | 100 | 100 | 100 | 100 | 94 | 92 | 96 |
| **#4** | 2 | 29 | 99 | 96 | 95 | 80 | 78 | 80 |
| **#8** | 2 | 6 | 63 | 77 | 77 | 64 | 64 | 57 |
| **#16** | 2 | 2 | 36 | 49 | 53 | 47 | 48 | 39 |
| **#30** | 2 | 1 | 22 | 30 | 31 | 33 | 35 | 28 |
| **#50** | 2 | 1 | 13 | 18 | 12 | 20 | 21 | 19 |
| **#100** | 2 | 1 | 9 | 11 | 4 | 13 | 15 | 15 |
| **#200** | 2 | 1 | 8 | 9 | 4 | 10 | 12 | 12 |

**Table 3.2 Proportion of individual aggregates in the mix design**

| Aggregate Type | Aggregate Proportion (%) | | | | | | | | |
|---|---|---|---|---|---|---|---|---|---|
| | Shilling RAP (1) | | | Konza RAP (2) | | | US 73 (3) | | |
| **RAP** | 20 | 30 | 40 | 20 | 30 | 40 | 20 | 30 | 40 |
| **CS-1** | 20 | 16 | 12 | 20 | 16 | 12 | 15 | 14 | 12 |
| **CS-1A** | 12 | 15 | 13 | 12 | 15 | 13 | 17 | 15 | 13 |
| **MSD-1** | 12 | 13 | 13 | 12 | 13 | 13 | 18 | 15 | 13 |
| **CG-5** | 16 | 12 | 12 | 16 | 12 | 12 | 12 | 10 | 9 |
| **SSG** | 20 | 14 | 10 | 20 | 14 | 10 | 18 | 16 | 13 |

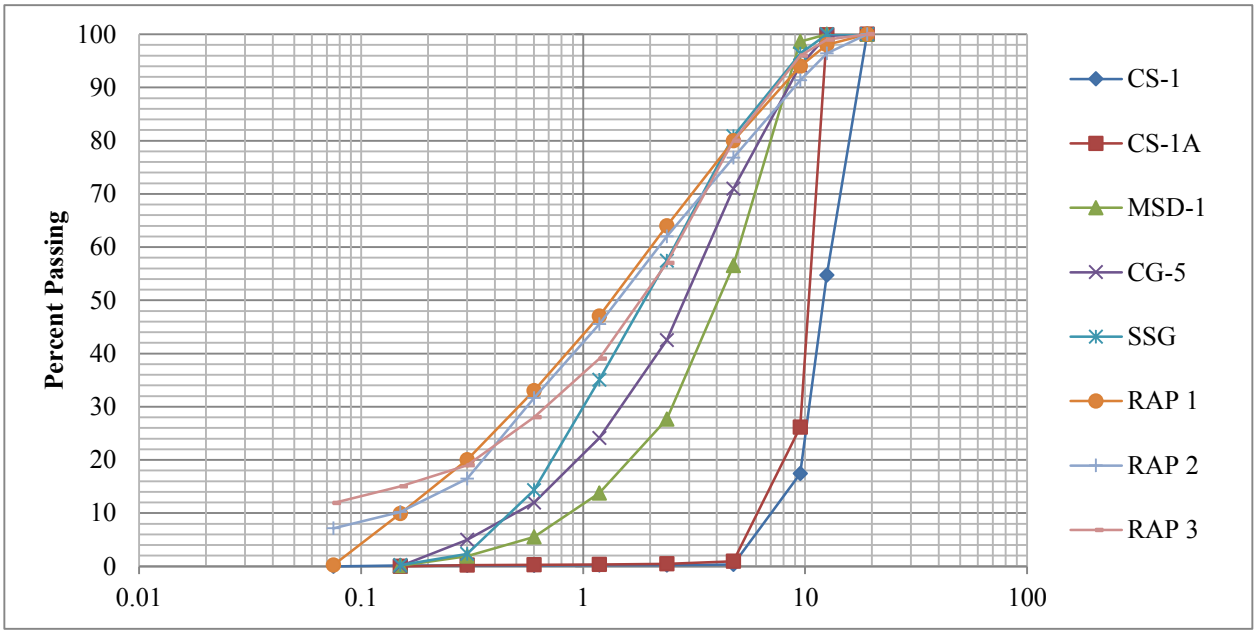


**Figure 3.1 Aggregate gradations**

**Table 3.3 Aggregate blending of mixtures**

| Sieve Size (mm) | 20% RAP | | | 30% RAP | | | 40% RAP | | | KDOT Requirements |
|---|---|---|---|---|---|---|---|---|---|---|
| | Shilling RAP | Konza RAP | US 73 RAP | Shilling RAP | Konza RAP | US 73 RAP | Shilling RAP | Konza RAP | US 73 RAP | |
| **19** | 0 | 0 | 0 | 0 | 0 | 0 | 0 | 0 | 0 | 0 |
| **12.5** | 8 | 7 | 7 | 6 | 9 | 7 | 8 | 6 | 6 | 0-10 |
| **9.5** | 17 | 15 | 13 | 12 | 18 | 12 | 15 | 13 | 11 | 10 Min |
| **4.75** | 34 | 34 | 34 | 30 | 34 | 33 | 34 | 31 | 31 | |
| **2.36** | 51 | 51 | 52 | 48 | 51 | 52 | 51 | 48 | 51 | 42-61 |
| **1.18** | 67 | 67 | 67 | 65 | 67 | 67 | 67 | 64 | 66 | |
| **0.6** | 79 | 79 | 80 | 77 | 79 | 79 | 78 | 76 | 78 | |
| **0.3** | 89 | 88 | 91 | 87 | 88 | 90 | 88 | 86 | 89 | |
| **0.15** | 93 | 93 | 96 | 92 | 93 | 94 | 92 | 91 | 93 | |
| **0.075** | 95 | 94 | 97 | 93 | 94 | 96 | 93 | 92 | 95 | 90-98 |

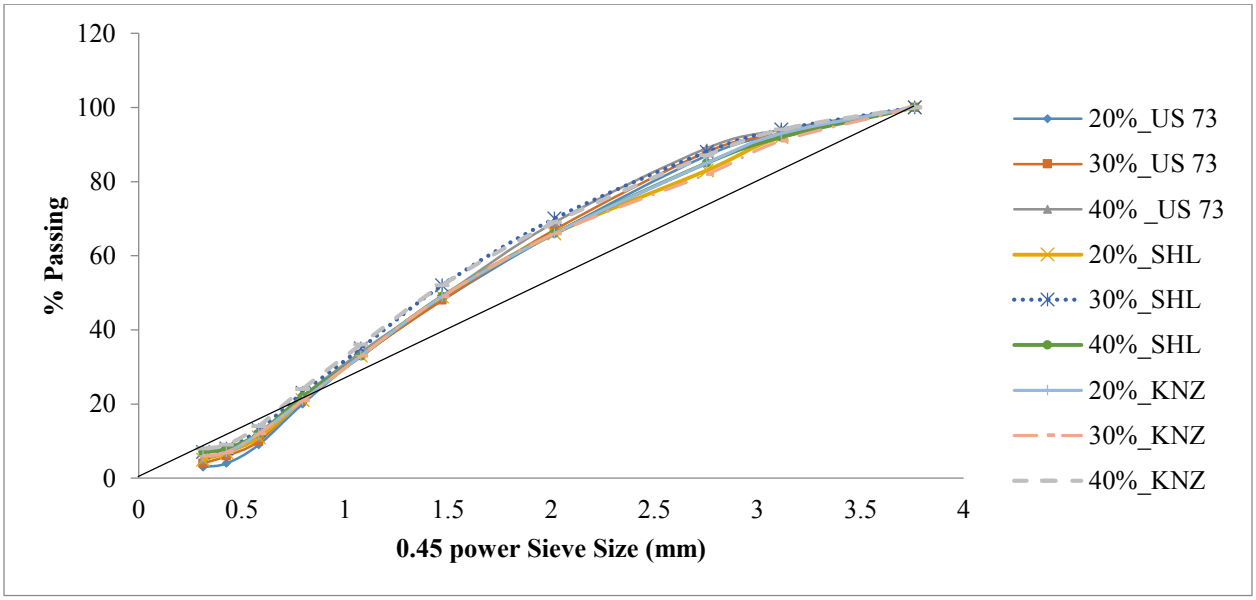


**Figure 3.2 0.45-power sieve size distribution curve**

## 3.3 RAP and Virgin Binder Grade

Performance Grade (PG) of the virgin binder was selected in accordance with AASHTO M 323 guidelines. Binder in the RAP typically becomes stiff due to years of weathering. Therefore, if RAP is used in a mixture, the virgin binder grade must account for the aged binder contribution. According to current guidelines (AASHTO M 323), no adjustment in virgin binder grade is required for mixtures with less than 15% RAP. Because this study utilized mixtures with higher percentages of RAP, softer binder had to be used. Guidelines for binder modification are summarized in Table 3.4.

**Table 3.4 Binder grade modification recommendations for RAP additions**

| Recommended virgin asphalt binder grade | %RAP |
|---|---|
| No change in binder selection | <15 |
| Select virgin binder one grade softer than normal | 15-25 |
| Follow recommendations from blending chart | >25 |

For the first two sources of RAP, virgin binder PG was selected as 70-28 by Sabahfar (2012). For the third RAP source, US 73, PG 70-28 was also selected. KDOT determined effective PG of the RAP binder to be 86-14. Based on the KDOT blending chart, the low sides of PG limits were -26 and -24, and upper limits were 74 and 76 for 20% and 40% RAP content, respectively, as shown in Figure 3.3. Therefore, a high side of 70 and a low side of -28 were selected for mixtures containing US 73 RAP.

KDOT BLENDING CHART CALCULATION

LowSideofTheBinder

| Project Number | | |
|---|---|---|
| RAP & Virgin Binder Inputs | | |
| Temperatures | $PG_{upper}$ | $PG_{lower}$ |
| $PG_{RAP}$ | 86 | -14 |
| $PG_{virgin}$ | 70 | -28 |

| RAP Percent in Mix Design* | | 20.0 |
|---|---|---|
| Blended Low Grade of Binder: | | -26 |

HighSideofTheBinder

| Project Number | | |
|---|---|---|
| RAP & Virgin Binder Inputs | | |
| Temperatures | $PG_{upper}$ | $PG_{lower}$ |
| $PG_{RAP}$ | 86 | -14 |
| $PG_{virgin}$ | 70 | -28 |

| RAP Percent in Mix Design* | | 40.0 |
|---|---|---|
| Blended High Grade of Binder: | | 74 |

* If utilizing FRAP insert total FRAP percent (coarse and fine) in Mix Design

Blending Chart Calculations

| %RAP | $PG_{blend}$ = |
|---|---|
| 0.00 | -28 |
| 5.00 | -27 |
| 10.00 | -27 |
| 15.00 | -26 |
| 20.00 | -26 |
| 25.00 | -25 |
| 30.00 | -24 |
| 35.00 | -24 |
| 40.00 | -24 |
| 45.00 | -23 |
| 50.00 | -22 |
| 55.00 | -21 |
| 60.00 | -21 |

Blending Chart Calculations

| %RAP | $PG_{blend}$ = |
|---|---|
| 0 | 70 |
| 5 | 71 |
| 10 | 71 |
| 15 | 72 |
| 20 | 74 |
| 25 | 74 |
| 30 | 74 |
| 35 | 75 |
| 40 | 76 |
| 45 | 76 |
| 50 | 77 |
| 55 | 78 |
| 60 | 78 |

**Figure 3.3 PG virgin binder selection using KDOT blending chart**

## 3.4 Laboratory Mix Design

As mentioned, in this study, nine SR-12.5A mixture designs were established for three RAP sources (Shilling, Konza, and US 73) and three RAP contents (20%, 30%, and 40%). Sabahfar (2012)

performed the first six mixture designs, and the other three designs were developed in this study. Mixture designations used throughout this document are shown in Table 3.5.

**Table 3.5 Identification of mixture designs**

| Mixture Identification | RAP Source | RAP Content (%) | Comment |
|---|---|---|---|
| **1** | Shilling Co. | 20 | Sabahfar (2012) |
| **2** | | 30 | |
| **3** | | 40 | |
| **4** | Konza Construction | 20 | |
| **5** | | 30 | |
| **6** | | 40 | |
| **7** | US 73 | 20 | This study |
| **8** | | 30 | |
| **9** | | 40 | |

All mixtures met the volumetric property and other requirements for SR-12.5A mixture specifications in Kansas. The design asphalt content was selected based on volumetric property criteria at 4 percent air voids at the design level number of gyrations ($N_{des}$) of 75. Steps followed for the mix design process are described in the following sections.

### 3.4.1 Mixing

Before mixing the aggregates, RAP, and virgin binder, all aggregates were dried on individual trays overnight at 110±5 °C in order to remove excess moisture. Aggregates, RAP, and virgin binder were heated separately before mixing. The aggregates and virgin binder were heated in order to attain recommended mixing temperatures of 153 to 160 °C. RAP was heated to 48 °C in order to avoid

further aging of the accompanying binder. Mixing was done using a lab-scale paddle mixer, as shown in Figure 3.4.

**Figure 3.4 Paddle mixer used in this study**

### 3.4.2 Sample Preparation for Volumetric Analysis

#### 3.4.2.1 Samples for $G_{mm}$

Theoretical maximum specific gravity ($G_{mm}$) of mixtures was determined using Kansas Test Method KT-39. Loose mixture was separated into small pieces in a way that no lump was greater than 5 to 6 mm. They were then aged in a temperature-controlled oven for 2 hours at 130 to 138 °C (compaction temperature range). Mixtures were stirred after 1 hour for homogenous conditioning. The required sample size for this test for the 12.5-mm NMAS mixture was 1500 gm.

#### 3.4.2.2 Samples for $G_{mb}$

The Kansas test method, KT-15, Procedure III, was used to prepare compacted samples to measure the bulk specific gravity of the compacted mixture. Mixtures were heated at recommended compaction temperatures (130 to 138 °C) for 2 hours. The mold and the top and bottom plates of the

SGC were also heated at the same temperature for approximately 45 min. Samples were compacted using SGC at 4±0.2% air voids at $N_{des}$ of 75 to 115 mm height.

### 3.4.3 Test Procedures

#### 3.4.3.1 $G_{mm}$ Test Procedure

Once the loose mixture cooled after mixing, it was broken into small pieces, weighed, and poured into a calibrated flask in order to determine $G_{mm}$. Weights of the flask with and without the sample were also taken in the air. The flask was half-filled with water at 25±0.5 °C, and a vacuum of 3.6±0.4 kPa was applied in order to remove excess air trapped inside the loose mixture. Full vacuum was applied in 30 seconds and maintained for 14±0.5 min. A vibrator plate under the flask agitated the sample to remove air, and then the flask was suspended in a water bath at 25±0.5 °C for 10±1 min. The weight of the flask with sample under water was measured. Figure 3.5 shows the steps for measuring $G_{mm}$.

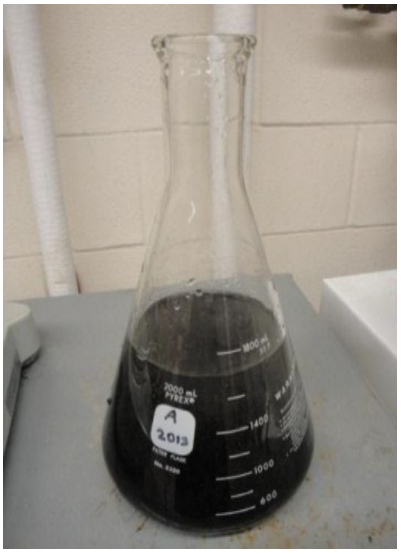

**(a)**


**(b)**

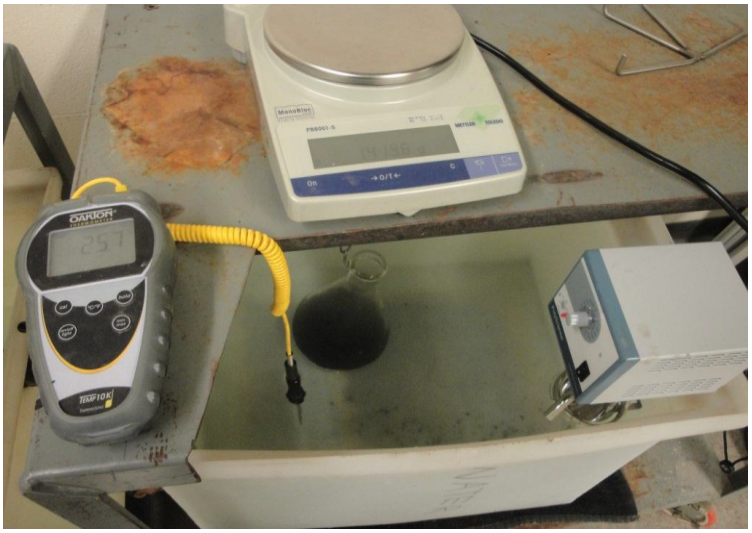

**(c)**

Equation 3.1 was used to calculate the theoretical maximum specific gravity ($G_{mm}$).

**Figure 3.5 (a) Loose HMA mixture in calibrated conical flask, (b) vacuum application on loose mixture to remove air, and (c) submerged mass measurement of loose mix (Aziz 2013)**

where *A* is mass of dry sample in air (gm) and *C* is mass of sample in water at 25°C (gm).

#### 3.4.3.2 $G_{mb}$ Test Procedure

In this test, the dry mass of the sample in air was measured first, and then the sample was submerged in water for 4±1 min in order to measure the mass in water. Water temperature was maintained at 25±0.5 °C. The sample was removed from the water, rolled in a damp towel, and the mass of the sample at the saturated surface dry (SSD) condition was determined. $G_{mb}$ was calculated using Equation 3.2.

$$G_{mb} = \frac{A}{(B-C)} \qquad \textbf{(3.2)}$$

where A is mass of dry sample in air (gm), B is mass of SSD sample (gm), and C is mass of saturated sample in water at 25 °C.

### 3.4.4 Volumetric Properties

Using $G_{mm}$ and $G_{mb}$ values and specimen heights at the initial, final, and design number of gyrations, volumetric properties were calculated for the mixtures, as presented in Table 3.6. As shown in the table, the mixtures met all volumetric and other KDOT requirements for 12.5-mm NMAS Superpave mixture.

**Table 3.6 Volumetric properties of mixtures**

| Mix Design | % Air Voids at Ndes | | | %VMA | | | %VFA | | | Dust-to-binder Ratio | | | %Gmm at Nini | | | %Gmm at Ndes | | |
|---|---|---|---|---|---|---|---|---|---|---|---|---|---|---|---|---|---|---|
| | R1 | R2 | R3 | R1 | R2 | R3 | R1 | R2 | R3 | R1 | R2 | R3 | R1 | R2 | R3 | R1 | R2 | R3 |
| 20% RAP | 3.9 | 4.0 | 3.9 | 14.1 | 14.0 | 16.2 | 71.6 | 71.5 | 68.4 | 0.60 | 0.61 | 0.65 | 88.5 | 88.5 | 83.5 | 96.0 | 96.0 | 95.0 |
| 30% RAP | 4.0 | 3.9 | 3.9 | 14.0 | 14.1 | 15.9 | 71.3 | 71.3 | 67.3 | 0.60 | 0.62 | 0.65 | 88.0 | 88.0 | 84.8 | 96.0 | 96.0 | 94.0 |
| 40% RAP | 4.0 | 4.0 | 4.1 | 14.2 | 14.1 | 14.8 | 71.9 | 71.9 | 71.5 | 0.70 | 0.61 | 0.68 | 87.8 | 87.8 | 87.6 | 96.0 | 96.0 | 95.0 |
| KDOT Superpave volumetric mix design specifications | | | | Minimum 14 | | | 65-78 | | | 0.6-1.2 | | | Maximum 90.5 | | | Maximum 98.0 | | |

Note: R1 = Shilling RAP; R2 = Konza RAP; R3 = US 73 RAP

### 3.4.5 Design Asphalt Binder Content

When the trial mixture satisfied the volumetric properties, the corresponding binder content was taken as the design binder content. However, several trials were necessary before this design binder content was obtained. Table 3.7 lists total binder content, virgin binder content, and RAP binder contents for each mixture.

**Table 3.7 Binder proportions (total binder, virgin binder, and RAP binder content)**

| Mix Design | Shilling RAP | | | Konza RAP | | | US 73 RAP | | |
|---|---|---|---|---|---|---|---|---|---|
| | Total Asphalt Content (%) | Virgin Asphalt added (%) | Asphalt Content from RAP (%) | Total Asphalt Content (%) | Virgin Asphalt added (%) | Asphalt Content from RAP (%) | Total Asphalt Content (%) | Virgin Asphalt added (%) | Asphalt Content from RAP (%) |
| **20% RAP** | 4.7 | 3.6 | 1.1 | 4.3 | 3.5 | 0.8 | 4.8 | 3.5 | 1.3 |
| **30% RAP** | 4.8 | 3.1 | 1.7 | 4.4 | 3.2 | 1.2 | 4.6 | 3.2 | 1.4 |
| **40% RAP** | 4.3 | 2.1 | 2.2 | 4.1 | 2.5 | 1.6 | 4.5 | 2.7 | 1.8 |

## 3.5 Moisture Susceptibility Test

The moisture susceptibility test was performed according to the Kansas test method, KT-56: Resistance of Compacted Asphalt Mixtures to Moisture-induced Damage, which measures changes in tensile strength resulting from effects of saturation, freezing, and accelerated water conditioning of SGC-compacted mixtures. KT-56 is a slightly modified version of AASHTO T 283 and is also known as the modified Lottman test in Kansas. Samples were compacted to 7±0.5% air voids using SGC. Diameters of the compacted samples were 150 mm and heights of the samples were 95±5 mm six specimens were compacted and tested for each mixture design. After compaction and air void determination, three specimens of comparable air voids were selected for testing in dry conditions, and three specimens were selected for testing after being exposed to one full freeze-thaw cycle and hot-water soak. The later set of samples was also subjected to partial vacuum saturation between 70 to 80% of the volume of air before freezing. This was done by immersing the samples in a vacuum container filled with water pressurized at 33 to 87 kPa pressure in order to remove air and partially saturate the sample. After correct saturation level was attained,

three samples were wrapped in plastic film and sealed in an airtight bag with 10 mL free water. Samples were then placed in a freezer for at least 16 hours at -18±3 °C temperature. After completion of the freezing cycle, the samples were thawed in a hot water bath for 24±1 hours at 60±1 °C. The samples were cooled to room temperature in a water bath of 25±1 °C temperature for 2 hours and then tested for indirect tensile strength. Figure 3.6 shows test stages.


**Figure 3.6 Moisture susceptibility test steps (Sabahfar 2012)**

The first set of samples was stored sealed in plastic wrap in dry conditions. Before testing, these samples were also kept in the water bath for 2 hours at 25±1 °C. Both samples were tested

at a loading rate of 50mm/min until failure. Peak loads were recorded, and tensile strength of each sample was calculated using Equation 3.3 (Hossain et al. 2010).

$$S = \frac{2P}{\pi t D} \qquad \textbf{(3.3)}$$

where *S* is tensile strength (kPa), *P* is maximum load (N), *t* is specimen thickness (mm), and *D* is specimen diameter (mm). Tensile strength ratio (TSR) was calculated according to Equation 3.4.

$$TSR = \frac{S_2}{S_1} x100\ (\%) \qquad \textbf{(3.4)}$$

where $S_1$ is average tensile strength of unconditioned samples and $S_2$ is average tensile strength of conditioned samples.

## 3.6 Semi-Circular Bending Test

The SCB test was performed in two modes for this study: static and repetitive. The static mode evaluated cracking resistance of HMA mixtures under monotonic load. The R-SCB test was performed in order to investigate fatigue cracking behavior of mixtures using strength parameters of mixtures derived from static SCB (S-SCB) tests. Both tests were performed in the Universal Testing Machine (UTM-25).

### 3.6.1 Static Semi-Circular Bending Test

The S-SCB test uses a three-point bending load. The test was performed under a monotonic load at a static load rate of 30mm/min at 25 °C. Samples were compacted using SGC in order to produce 150 mm diameter and 100±5 mm high cylindrical samples with 7±1% air voids. Test samples were sawn into two 50 mm thick disks and then cut into halves in order to produce semicircular samples of 150 mm length of the bottom surface and 50±5 mm width. A triangular notch of 2.5 to 5 mm depth was fabricated at the middle of the base of the sample. Three replicates

were tested for each mixture. Samples were conditioned at the test temperature for 2 hours in a temperature-controlled chamber. The test setup is shown in Figure 3.7.

**Figure 3.7 SCB test setup**

The three-point bending setup was custom-made for the test. Roller supports were cleaned with lubricant oil before each test in order to avoid stress concentration near the support. The load line of the sample was aligned with the top of the notch for controlled crack initiation, and loading rate of 30 mm/min was determined based on previous researchers (Walubita et al. 2010). Once a crack appeared and a rapid change in the stress-strain curve occurred, the test was stopped manually.

After completion of the test, peak load, and load-load line deflection (P-u) curve were obtained. From the P-u curve, Mode I of the fracture process (Figure 3.8) was obtained. In order to identify Mode II, MATLAB was used to simulate the trend in the curve. The area under the entire curve was obtained by MATLAB and taken as the FE (Equation 3.5). Fracture stiffness parameter was also calculated using Equation 3.6.

$$G_f = \frac{W_f}{A_{lig}} \qquad \textbf{(3.5)}$$

where $G_f$ is FE (J/m$^2$) and $A_{lig}$ is area under the load-line (m$^2$).

$$S = c\left(\frac{L}{D}\right)\frac{P}{td} \qquad \textbf{(3.6)}$$

where *S* is stiffness modulus, *c* is dimensionless function of relative spacing between supports, *L/D* is length-to-diameter ratio, *P* is load (KN), and *t* is thickness of the sample (mm).

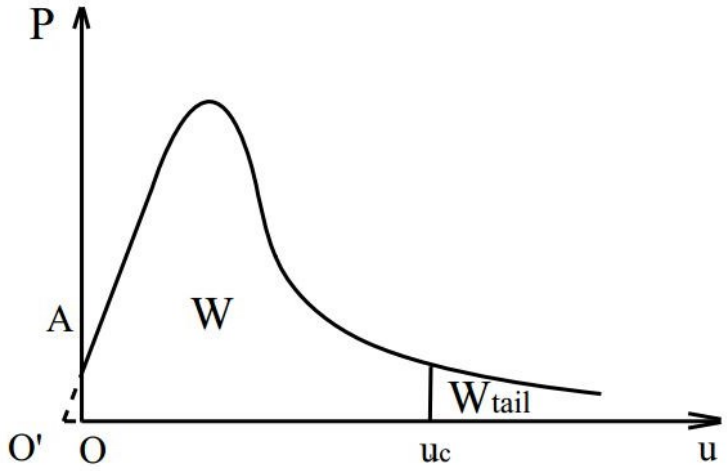


**Figure 3.8 Typical load-displacement curve for SCB test (Cooper 2014)**

### 3.6.2 Repetitive Semicircular Bending Test

The R-SCB test, performed in order to evaluate fatigue cracking potential of the mixtures, used the average peak load obtained from the S-SCB test. For each mix, four percentages of peak loads (30, 40, 50, and 60%) were used as input values. For each load percentage, three samples were tested under repetitive loading. R-SCB test procedures were similar to the S-SCB test in terms of sample preparation and test temperature, but the test mode was switched from the stain-controlled mode to the stress-controlled mode. A loading frequency of 10 Hz was used with no rest period, as suggested by Walubita et al. (2010). Walubita et al. (2010) also suggested that 50% of the peak load should be used to evaluate fatigue performance of HMA mixtures. Therefore, test results from the 50% peak load were used for further analysis.

The R-SCB test was stopped manually after full propagation of a crack along the load-line, and the number of cycles before failure was recorded. A flow chart of the test is shown in Figure 3.9. The crack mouth opening was also monitored during this test using an Epsilon clip-on gauge attached on the bottom surface of the specimen (as shown in Figure 3.7). This device measured the gradual increase in crack dimensions in order to provide a guideline for test standardization.

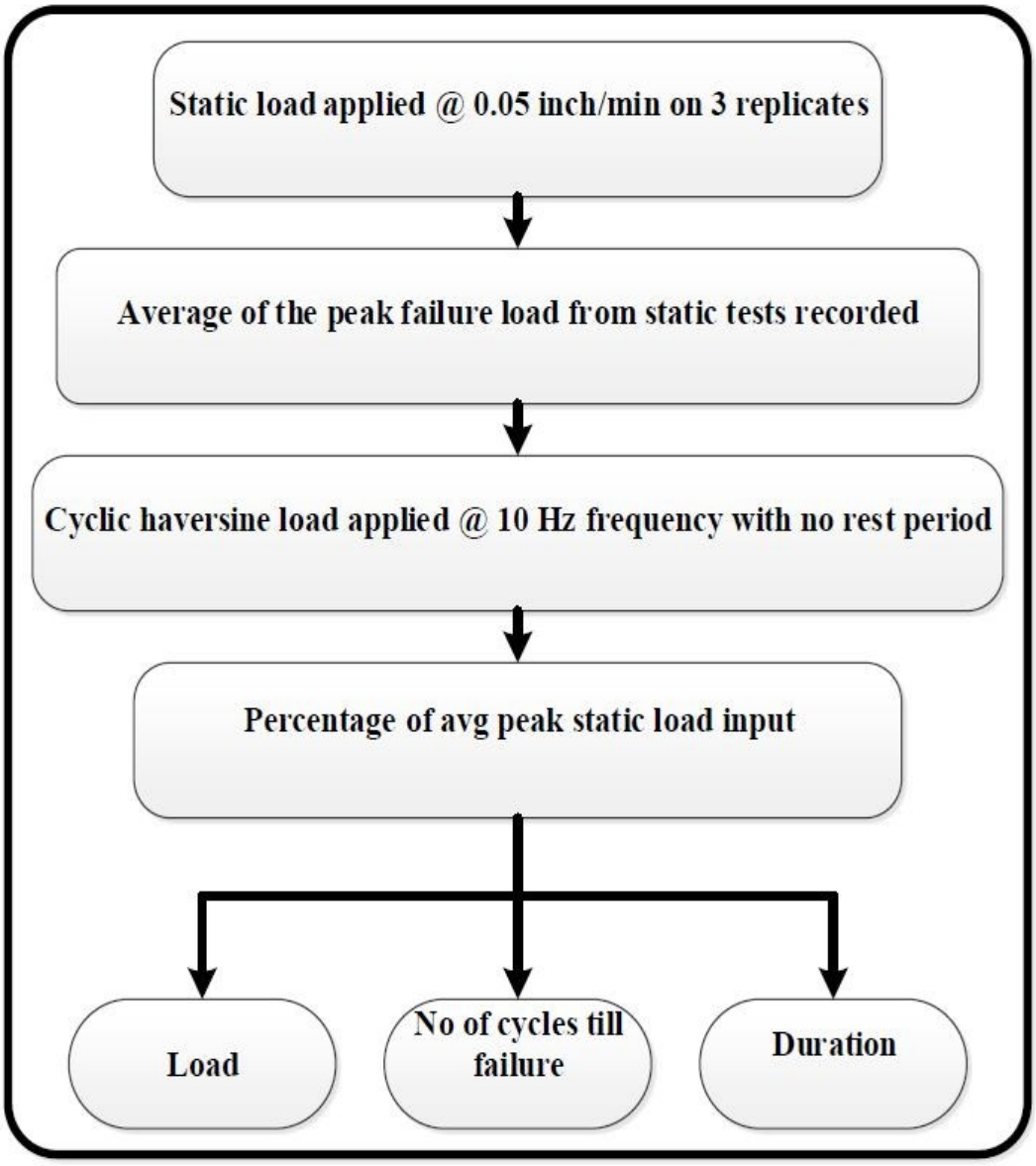


**Figure 3.9 Flow chart of R-SCB test**

## 3.7 Texas Overlay Test

The Texas Overlay test is performed on the HMA mixtures to evaluate the reflective cracking resistance. The test was developed by the Texas Department of Transportation (TxDOT) and is covered by the TxDOT standard test procedure TEX-248-F.

Test samples for the OT test required fabrication of cylindrical compacted samples with diameters of 150 mm. and heights of 115±5 mm. at 7±1% air voids using an SGC. OT test samples were trimmed, as shown in Figure 3.10. Final test samples were 150 mm long, 76 mm wide and 3.8 mm high. Three replicates of each mix were tested.

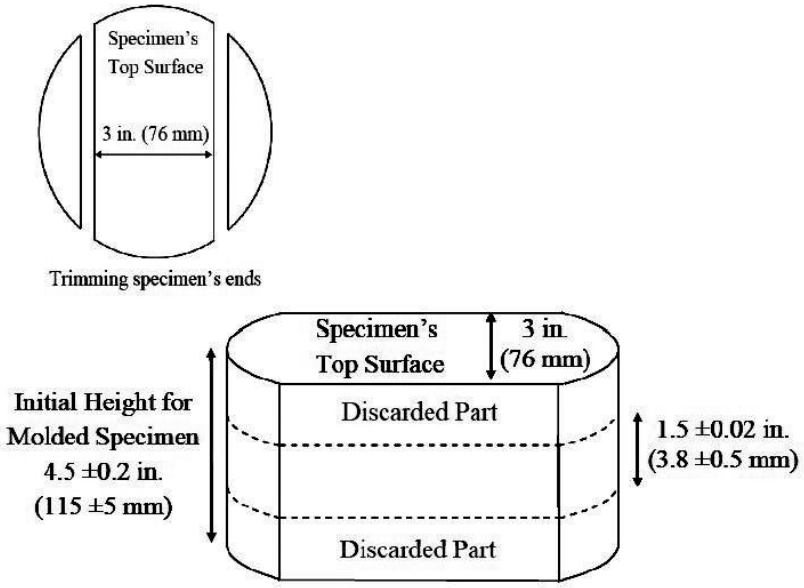


**Figure 3.10 Sample fabrication (TEX-248-F)**

Epoxy glue was used to affix trimmed samples to two metal plates which had gaps between them. Figure 3.11 showed a glued sample to the OT test plates that had gap of 4.2 mm between the plates. A heavy weight rested over the newly glued sample, and the glue was allowed to cure for 24 hours. The test was then performed using the AMPT in which the sample was attached to the base plate. One Linear Variable Differential Transformer (LVDT) was also attached to the sample. Figure 3.12 shows the test in the AMPT environment.

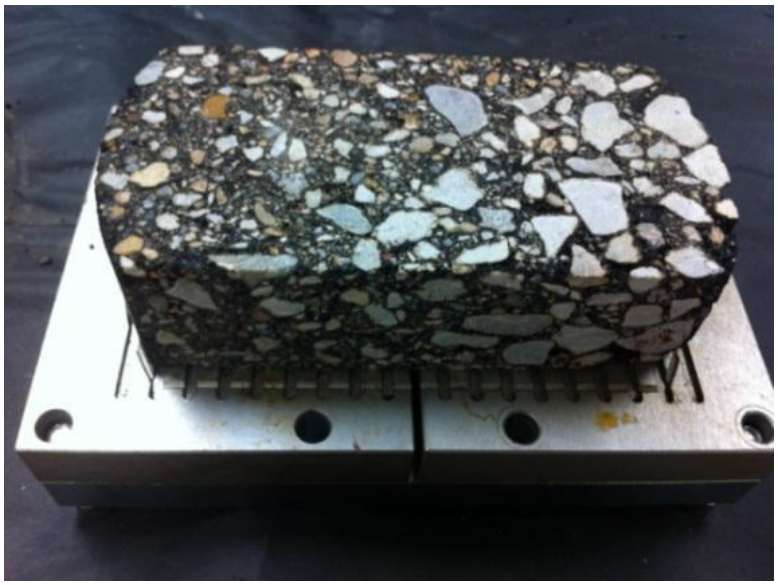

**Figure 3.11 Glued OT sample**

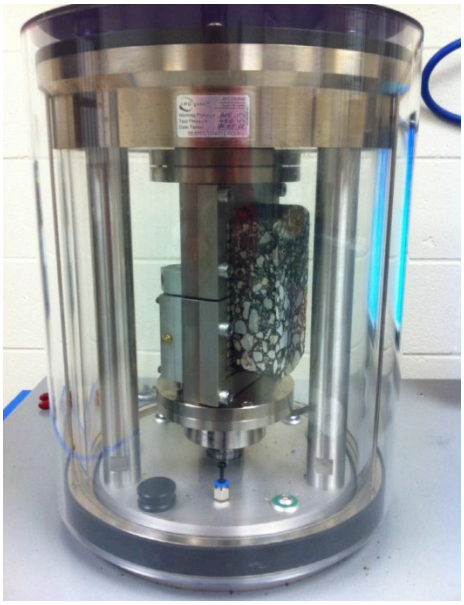

**Figure 3.12 Sample mounted inside AMPT**

The test temperature was 25 °C according to TEX-248-F test procedure. Samples were preconditioned in a temperature-controlled chamber for 2 hours at that temperature. The loading rate was 10 seconds per cycle (5 seconds loading and 5 seconds unloading). The load pulse configuration was cyclic triangular displacement-controlled waveform at the standard maximum

opening of 4.2 mm. During loading, repetitive movement of only one plate along the length of the sample resulted in tensile stress directly at the center of the sample. The test was terminated when the sample passed 1,000 OT cycles or at a load reduction of 93%, whichever came first. TxDOT has set a minimum of 300 OT cycles in order for an HMA mixture to be acceptable. Recorded parameters at the completion of the test were the number of OT cycles, applied load, and displacement along the load line. Figure 3.13 shows a flow chart of the OT test process.

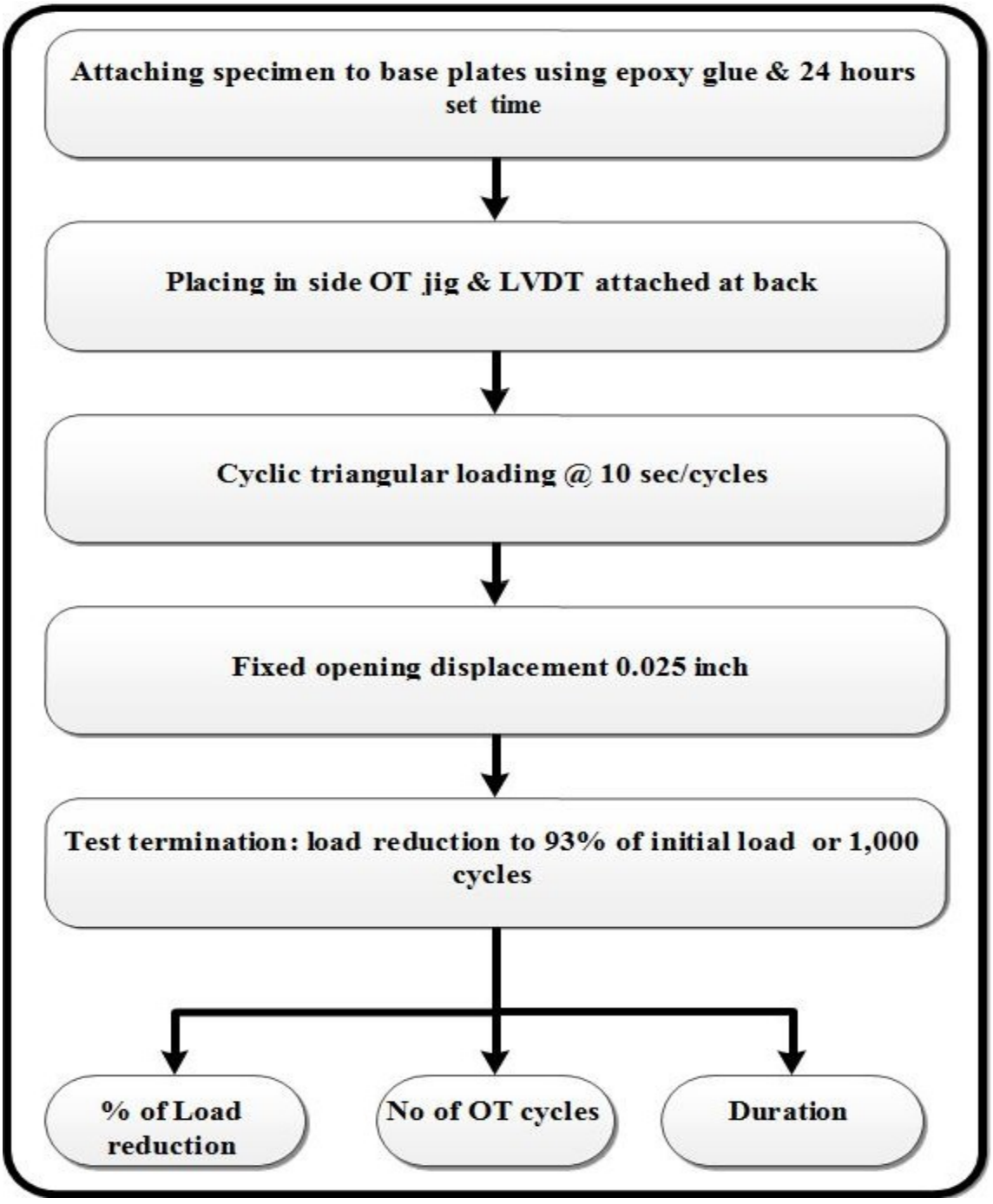


**Figure 3.13 Flow chart of the OT test (Aziz 2013)**

## 3.8 Dynamic Modulus Test

The dynamic modulus test is typically performed on HMA mixtures in order to measure stiffness. In this study, dynamic modulus tests were conducted according to AASHTO TP 62-07. Cylindrical samples with diameters of 150 mm and heights of 172±5 mm were compacted in an SGC to an appropriate level of air voids to ensure 7±1% air voids in the cored test sample. According to AASHTO TP 62-07, cored samples for the test must have diameters of 100 to 104 mm and heights of 150 mm. Three LVDTs were used to measure deformation at three locations, as shown in Figure 3.14

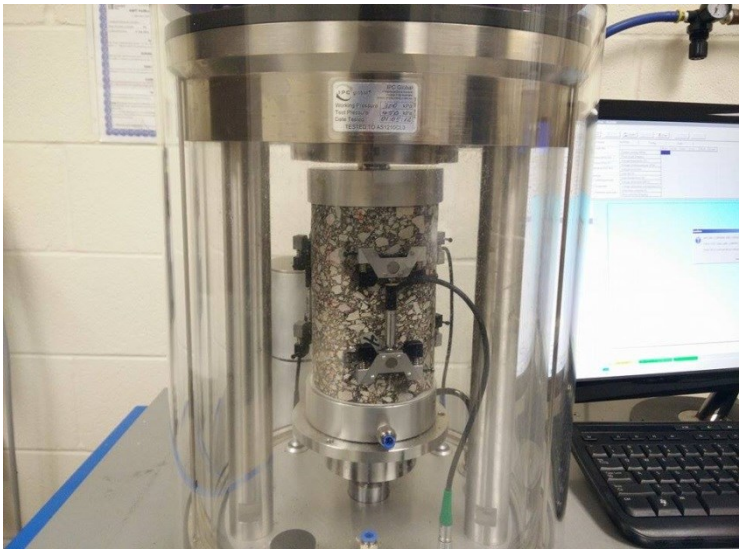

**Figure 3.14 Dynamic modulus test sample inside AMPT**

In this test a compressive sinusoidal load, shown in Figure 3.15, was applied at various temperatures and loading frequencies. Dynamic modulus was calculated by dividing peak-to-peak stress by peak-to-peak strain according to stress-strain developed from this test.

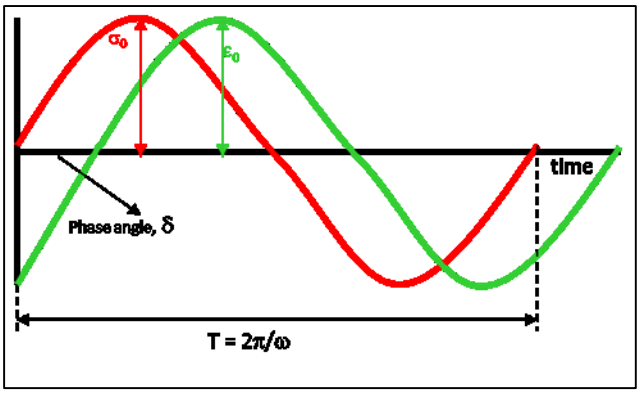


**Figure 3.15 Sinusoidal stress-strain response curve in the dynamic modulus test**

Dynamic Modulus e test was performed at three temperatures: 4 °C, 21 °C, and 37 °C. Temperatures of -10 °C and 54 °C were also suggested in the guideline, but they could not be used because LVDTs did not perform accurately at temperatures lower than zero and epoxy began melting at temperatures higher than zero (Sabahfar 2012). The test was performed for six frequencies (0.1, 0.5, 1, 5, 10, and 25 Hz) between axial strains of 50 to 150 microstrains. Samples were preconditioned at 4 °C overnight and tested for six frequencies. Then the same sample was conditioned at 21 °C for 1 hour and tested at six frequencies. The same sample was again conditioned for 2 hours at 37 °C and tested. Three replicates of each mix were tested.

After conditioning at the desired temperature, the sample was placed inside the AMPT. Because the loading mode was compression, screws were not necessary for mounting. Proper alignment of the loading head with the sample was achieved, and thin Neoprene pads were used to avoid end friction. The test was terminated after testing the sample at each frequency, beginning from the lowest one. Figure 3.16 shows a flow chart of the test process.

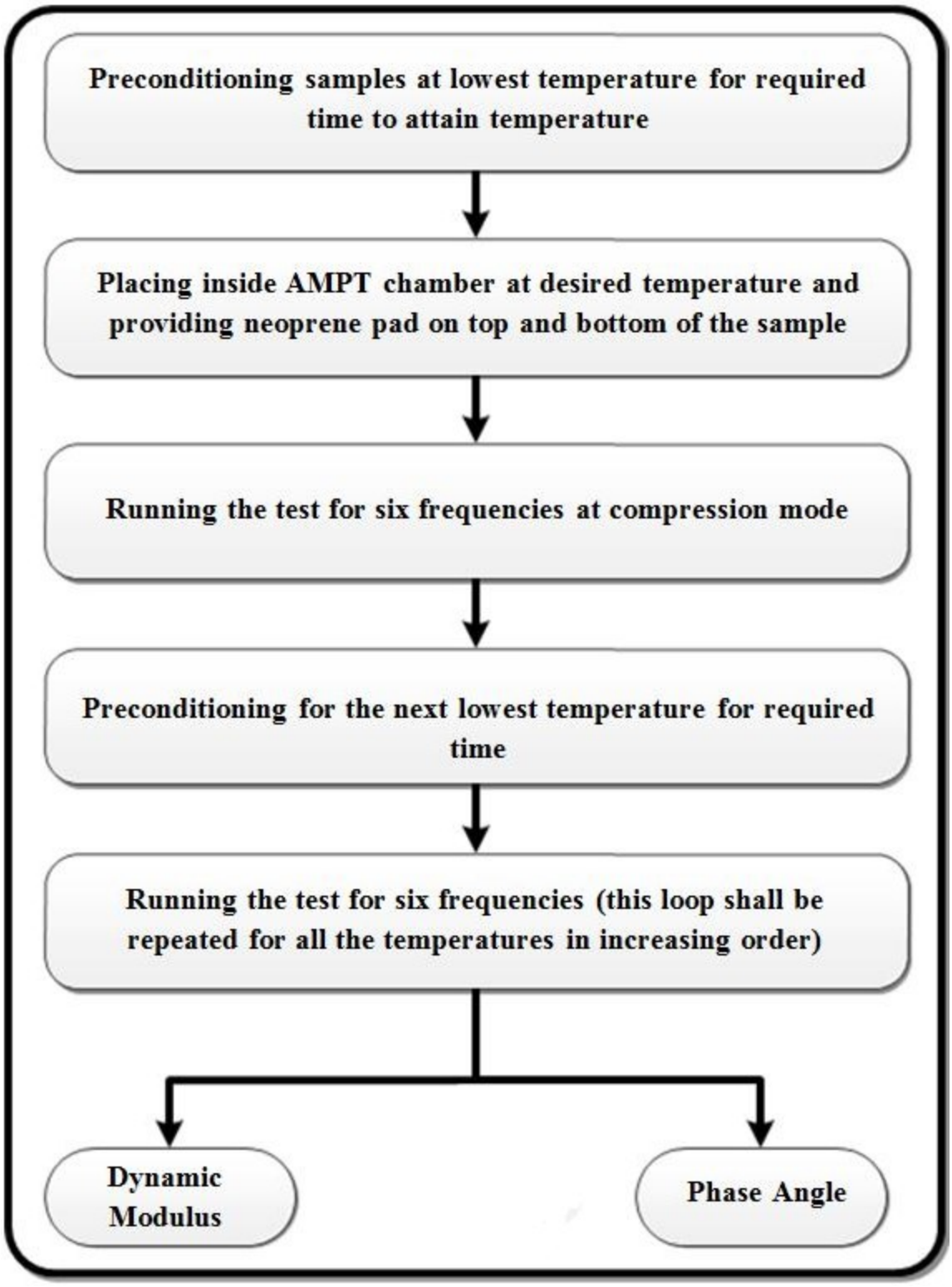


**Figure 3.16 Flow chart of the dynamic modulus test**

## 3.9 Simplified Viscoelastic Continuum Damage Test

VECD theory, a mechanistic approach to study fatigue performance of HMA mixture, depends more on theoretical considerations than phenomenological approaches like in the beam fatigue test. Phenomenological approaches tend to show large margin of errors, but the Simplified Viscoelastic Continuum Damage (S-VECD) approach is gaining gradual acceptance because it is capable of predicting fatigue performance of HMA mixes with errors in tolerable limits.

Sample preparation in the S-VECD test was similar to sample preparation for the dynamic modulus test. Samples were compacted in a SGC to heights of 180 mm and diameters of 150 mm at the predetermined air voids to ensure 7±0.5% air voids in the trimmed samples that were cored out of the compacted samples. The trimmed test samples had diameters of 100 to 104 mm and heights of 127 to 132 mm. Figure 3.17 shows a cored sample. Height and diameter measurement were taken at five places for each sample.

Because the sample is loaded repeatedly in pull-pull mode during the test, strong glue was required to ensure that failure did not occur along the glue or near the end. A customized gluing jig was used to apply Devcon 10110, also known as steel putty, in order to attach the top and bottom plates to the sample, as illustrated in Figure 3.18. However, the steel putty had to cure for at least 4 hours in order to achieve appropriate adherence.

Three LVDTs were attached to the specimen in order to measure deformation. Epoxy was used to attach the sample to three sets of clips with 75 mm gauge length located 120° from each other.

**Figure 3.17 VECD sample coring**

**Figure 3.18 VECD sample gluing**

The applicable test temperature for these tests was suggested in AASHTO TP 107-14. The temperature for the test in this study was selected based on 98% reliability, and the PG was

determined from the LTPPBind at the location of interest. The PG was PG 64-22 for this project. AASHTO TP 107-14 required that the lower end of the binder grade in absolute value to be subtracted from the upper grade and to be divided by 2. Then 3°C had to be subtracted from this result. Maximum value is suggested not to exceeding 21°C. If the value after calculation comes higher than $21^0$C, $21^0$C should be used. In this study, the test temperature was selected as 18°C depending on binder grade PG 64-22. Test samples were conditioned for two to four hours in a temperature-conditioning chamber to achieve the test temperature.

In this study, the S-VECD test was performed using AMPT. The sample was tightly attached to the top and bottom platen of the machine using screws, as shown in Figure 3.19. The test was performed with three sequential steps described in the following paragraphs.

**Figure 3.19 VECD sample mounted inside AMPT**

- Application of zero loads: After the sample was glued to the top and bottom plates and placed in AMPT, the temperature-controlled chamber was activated. Application of zero loads and proper attachment of the sample ensured that no confining pressure and no torsional stress occurred.
- Dynamic modulus fingerprint test: This test step, performed for 55 tension-compression loading cycles at 10 Hz frequency, provided an initial estimation of dynamic modulus of the sample. After completion of the fingerprint test, a 20-min rest period was provided so the samples could recover from the loading effect.
- Direct tension fatigue test: After the rest period, a repeated-load fatigue test was performed using the direct tension mode. The test evaluated deterioration in dynamic modulus of the sample due to fatigue loading cycles. The test was conducted for 50 to 70 peak-to-peak microstrains at 10 Hz frequency. AASHTO TP 107-14 suggested 300 microstrains as the strain level for the initial sample. Strain levels of next two samples were decided based on the number of fatigue cycles found for the first sample. Table 3.8 presents guidelines for deciding consecutive initial microstrains for two other replicates of the same mixture. Figure 3.20 shows a diagram of a typical dynamic modulus versus number of fatigue cycles.

**Table 3.8 Microstrain level selections for Replicates 2 and 3 in VECD test**

| Case | $\varepsilon_2$ | $\varepsilon_3$ |
|---|---|---|
| $500<N_{f1}<1000$ | $\varepsilon_1$-100 | $\varepsilon_1$-150 |
| $1{,}000<N_{f1}<5{,}000$ | $\varepsilon_1$-50 | $\varepsilon_1$-100 |
| $5{,}000<N_{f1}<20{,}000$ | $\varepsilon_1$+50 | $\varepsilon_1$-50 |
| $20{,}000<N_{f1}<100{,}000$ | $\varepsilon_1$+100 | $\varepsilon_1$+50 |
| $100{,}000<N_{f1}$ | $\varepsilon_1$+150 | $\varepsilon_1$+100 |

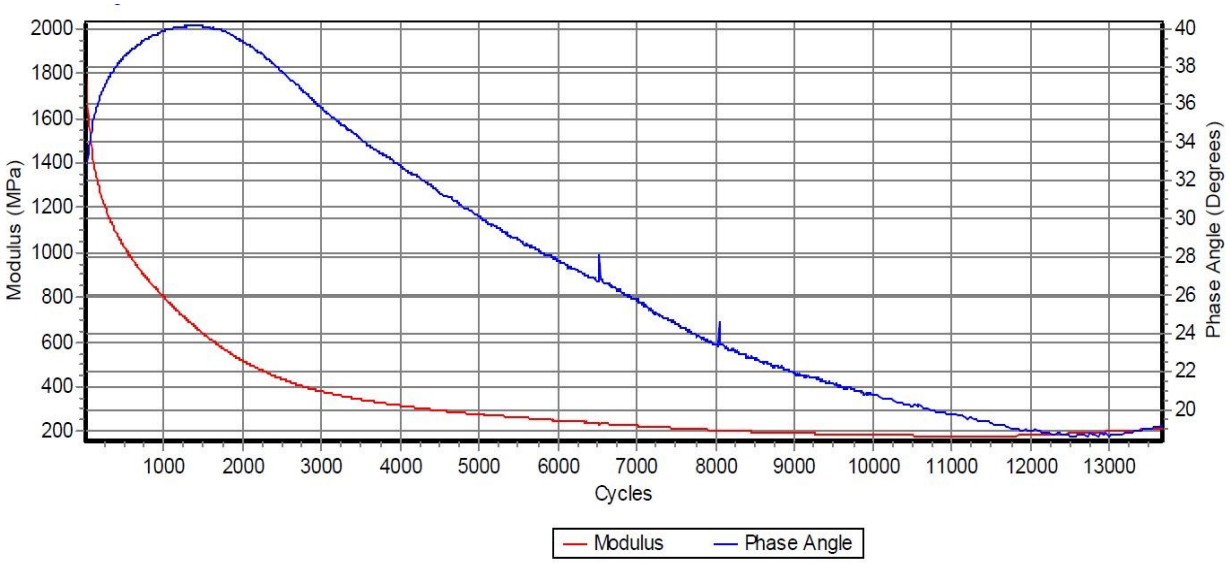


**Figure 3.20 Typical numbers of fatigue cycles in S-VECD test**

The test was stopped when microcracks began to appear. Change in the pattern of diminishing dynamic modulus curve was also an indication of sample failure. Figure 3.21 shows a completely-cracked sample and a sample after appearance of microcracks. A flow chart for this step is presented in Figure 3.22.

**(a)** **(b)**

**Figure 3.21 (a) Fully-cracked S-VECD sample, (b) S-VECD sample with microcracks**

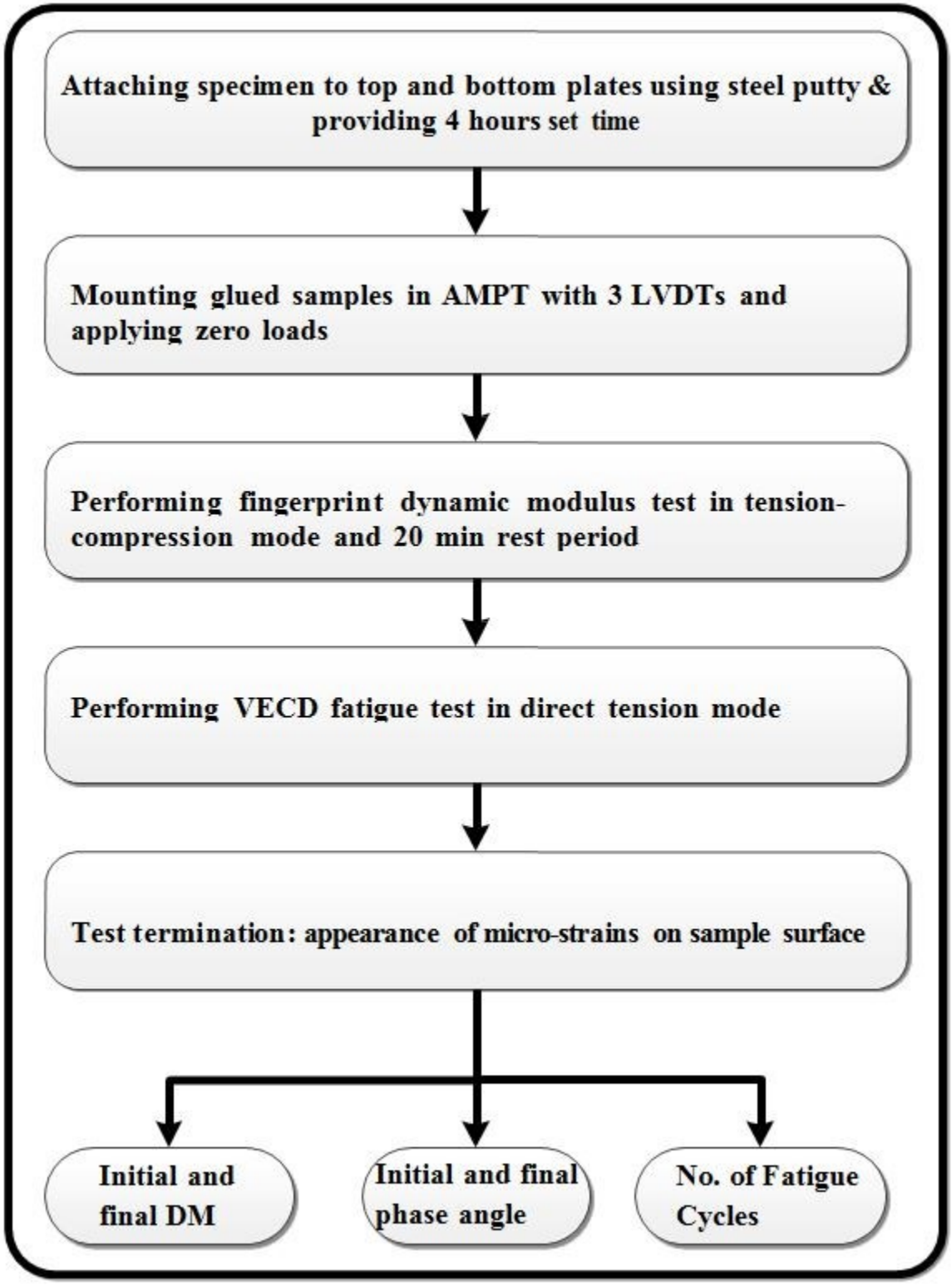


**Figure 3.22 Step-by-step operations of VECD test**

Fatigue performance prediction was done using the software Alpha-F. Test results were used to simulate the condition of a damaged sample and its changes in dynamic modulus properties in order to attain final level of damage. Equation 3.7 (exponential model) and Equation 3.8 (power model) were calibrated for each mix using results from three replicates, and mixtures were compared to each other based on parameter values in these equations.

$$C = e^{aS^b} \qquad \textbf{(3.7)}$$

$$\text{or, } C = 1 - yS^z \qquad \textbf{(3.8)}$$

where *S* is cumulative damage to attain first fatigue crack-line; *C* is pseudo secant modulus at the time of crack initiation; *a, b* are fitting coefficients for exponential model; and *y, z* are fitting coefficients for the power model. In this study, the power model was used to compare fatigue performance of various mixtures. The average number of cycles to fatigue failure in this test was also determined using the software.

# Chapter 4 - Results and Analysis

## 4.1 Moisture Susceptibility Test Results

The moisture susceptibility test was performed according to the Kansas standard test method KT-56 in order to assess moisture susceptibility of HMA mixtures with high RAP content. Table 4.1 tabulates results of the test. Three replicates for each conditioned and unconditioned state were tested in indirect tension. The table also shows the TSR of the conditioned samples to the unconditioned samples. Sabahfar (2012) performed tests for the Shilling and Konza RAP sources, and tests for the US 73 RAP source were conducted in this study.

**Table 4.1 Moisture susceptibility test results**

| RAP Source | RAP Content (%) | Air Voids (%) | | Average Tensile Strength (lbs.) | | Tensile Strength Ratio (%) |
|---|---|---|---|---|---|---|
| | | Conditioned | Unconditioned | Conditioned | Unconditioned | |
| Shilling | 20 | 7.2 | 7.2 | 3,390 | 4,430 | 90 |
| | 30 | 6.8 | 6.7 | 4,257 | 4,964 | 86 |
| | 40 | 6.6 | 6.6 | 4,425 | 5,391 | 82 |
| Konza | 20 | 6.9 | 6.9 | 3,249 | 4,473 | 73 |
| | 30 | 6.8 | 6.8 | 3,307 | 4,906 | 67 |
| | 40 | 7.0 | 6.9 | 3,255 | 6,235 | 52 |
| US 73 | 20 | 7.1 | 7.1 | 4,289 | 4,766 | 90 |
| | 30 | 7.3 | 7.2 | 4,101 | 4,825 | 85 |
| | 40 | 7.0 | 7.1 | 4,007 | 4,887 | 82 |

Figure 4.1 illustrates TSR values for mixtures in this study. For all sources, TSR values decreased as the RAP content in the mixture increased. Mixtures with Shilling and US 73 RAP met minimum TSR requirements of KDOT (80%) even at the highest RAP content (40%), but mixtures with the Konza RAP did not meet minimum requirements of KDOT. Data in Table 4.1 show that these mixtures had very indirect tensile strength in the unconditioned state. Conditioning

led to very low indirect tensile strength of these mixtures; consequently, TSR values were lower. The binder in the Konza RAP was highly aged. The freeze cycle in KT-56 was presumed to have ruptured the asphalt films during the freeze cycle of conditioning, leading to low indirect tensile strength after conditioning.

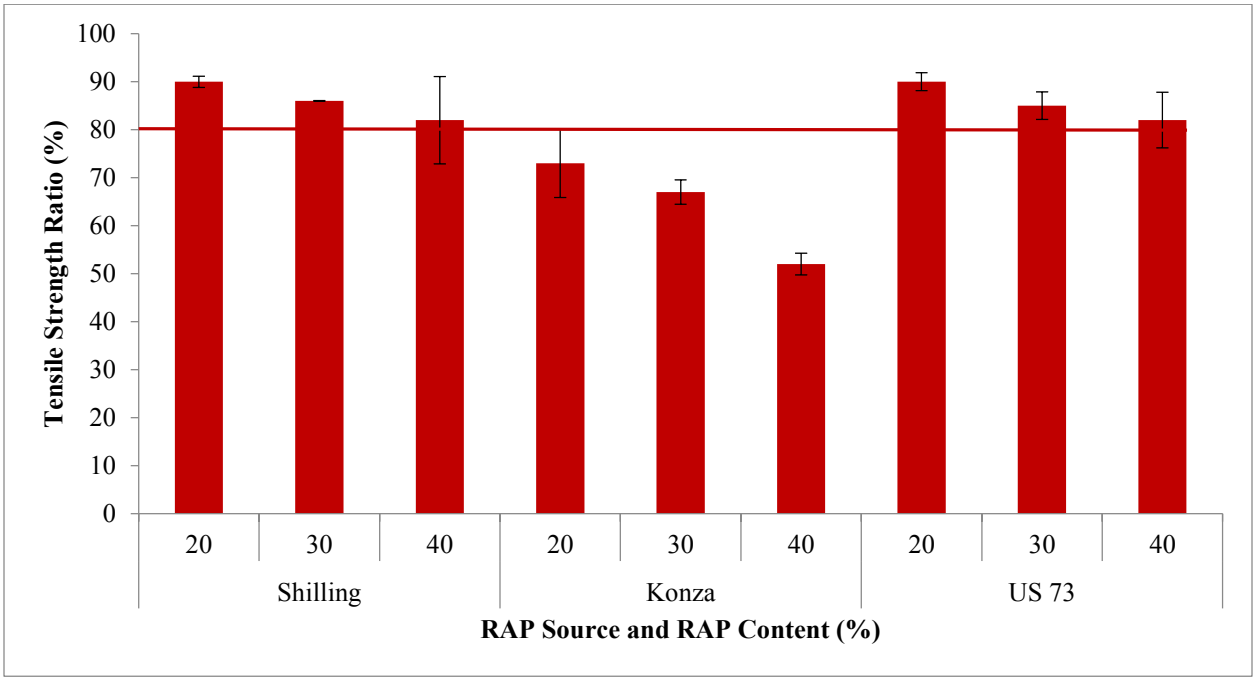


**Figure 4.1 TSR test results**

## 4.2 Semi-Circular Bending Test Results

The SCB test was performed in order to investigate cracking resistance of Superpave mixtures with varying RAP content. The S-SCB test was performed to evaluate the rate of energy release in order to initiate fracture under increasing load. In the R-SCB test, repeated load was applied on the samples in order to simulate recurring wheel load. Aziz (2013) performed S-SCB and R-SCB tests for mixtures with Shilling and Konza RAP. In this study, these tests were repeated for the US 73 RAP source.

### 4.2.1 Static SCB Test Results

Average FE and stiffness value of each Superpave mixture are tabulated in Table 4.2. For each mixture, three replicates were tested. Bending strain and stress represented by displacement and load, respectively, at the termination of the test somewhat indicated ductility of HMA mixtures (Aziz 2013). The coefficient of variation (COV) of test results for each mixture is indicated in parentheses under the corresponding FE values in Table 4.2. These values indicate fairly good repeatability of the test.

**Table 4.2 SCB test results**

| RAP Source | RAP Content (%) | Air Voids (%) | Peak Load (KN) | Average Fracture Energy ($J/m^2$)* | Average Stiffness (MPa) |
|---|---|---|---|---|---|
| Shilling | 20 | 7.3 | 2.55 | 2,098.7 (8.6) | 20,491 |
| | 30 | 7.2 | 3.15 | 2,064.9 (10.4) | 29,440 |
| | 40 | 7.3 | 3.88 | 2,173.8 (8.1) | 58,594 |
| Konza | 20 | 7.2 | 2.48 | 1,632.2 (6.0) | 26,804 |
| | 30 | 7.1 | 1.72 | 1,769.4 (5.2) | 27,407 |
| | 40 | 7.2 | 3.12 | 1,884.0 (18.6) | 33,843 |
| US 73 | 20 | 7.3 | 1.51 | 1,161.2 (15.2) | 11,124 |
| | 30 | 7.1 | 1.87 | 1,098.6 (8.2) | 18,313 |
| | 40 | 7.2 | 2.04 | 1,701.1 (15.6) | 18,466 |

*COV shown in parentheses.

According to Table 4.2, mixtures with Shilling RAP, FE for mixtures with 20% RAP and 30% RAP are not numerically similar values but for 40% RAP, FE value is abruptly higher. Area under the load-deflection curve at a strain-controlled monotonic loading setup is an indication of material stiffness (Roylance 2001). As mentioned, a mixture containing 40% RAP is expected to

have a higher stiffness value. Using only this FE value, no definitive conclusion regarding cracking performance of viscoelastic HMA mixtures could be reached. Cracking performance is associated with ductility of a mixture under loading before initiating the crack. For viscoelastic materials, fracture mode is cup-and-cone fracture. If a material releases energy in a higher rate in order to reach fracture, the material is comparatively brittle and thus weaker in cracking (Anderson 1995).

Stiffness values of mixtures presented in Table 4.2 also increased as RAP content increased. Again, mixtures containing 20% and 30% RAP did not show a large difference in stiffness values, but the mixture with 40% RAP had much higher stiffness value, as shown in Figure 4.2. As illustrated in the figure, this trend in FE values in which increased RAP content increased the FE was also observed for mixtures with other RAP sources, leading to the release of energy at a higher rate. Stiffness values also increased with increasing RAP content, as shown in Figure 4.3. Mixtures containing RAP from US 73 had the lowest FE and stiffness values. Figure 4.3 also shows that mixtures with Shilling RAP had the highest stiffness values.

In Figure 4.4, rates of energy released per minute for mixtures are compared. For Shilling and US 73 RAP sources, an increasing trend of energy release rate was observed, indicating that the mixtures became brittle with increasing RAP content. As from unit ligament area, per minute energy release rate was higher for mixtures containing 40% Shilling RAP or 40% US 73 RAP. The samples failed at much faster rates and were more susceptible to cracking than mixtures containing 20% and 30% RAP.

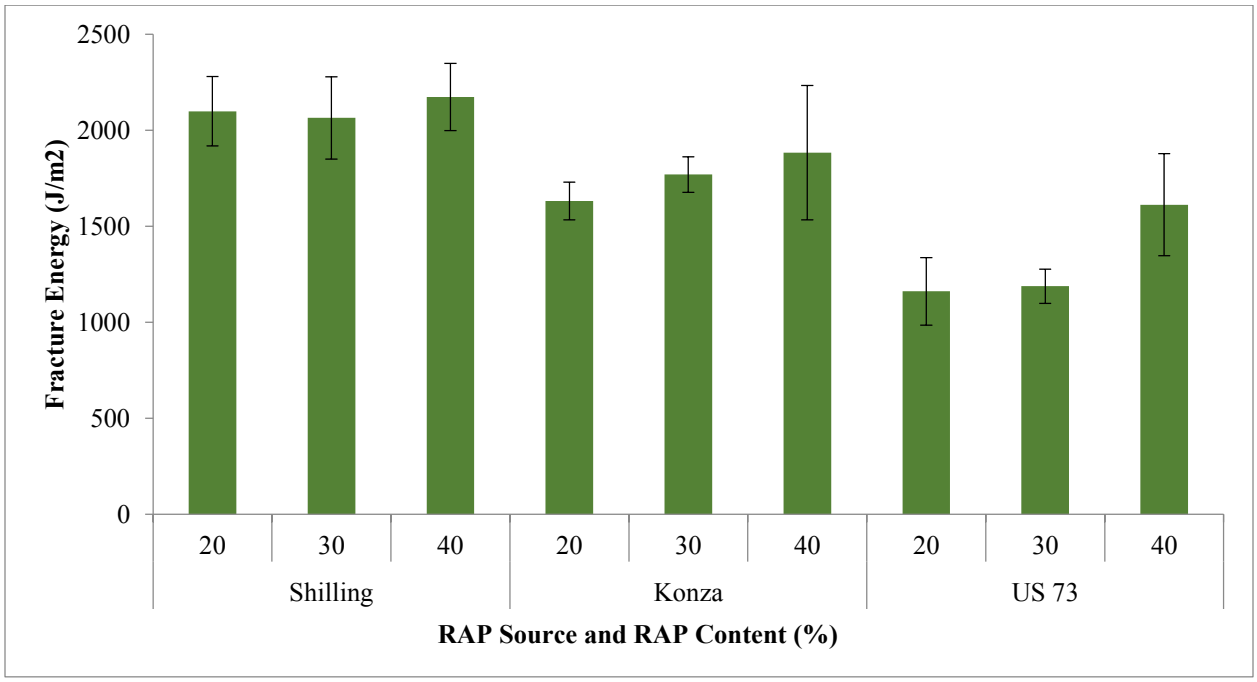


**Figure 4.2 S-SCB test FE results**

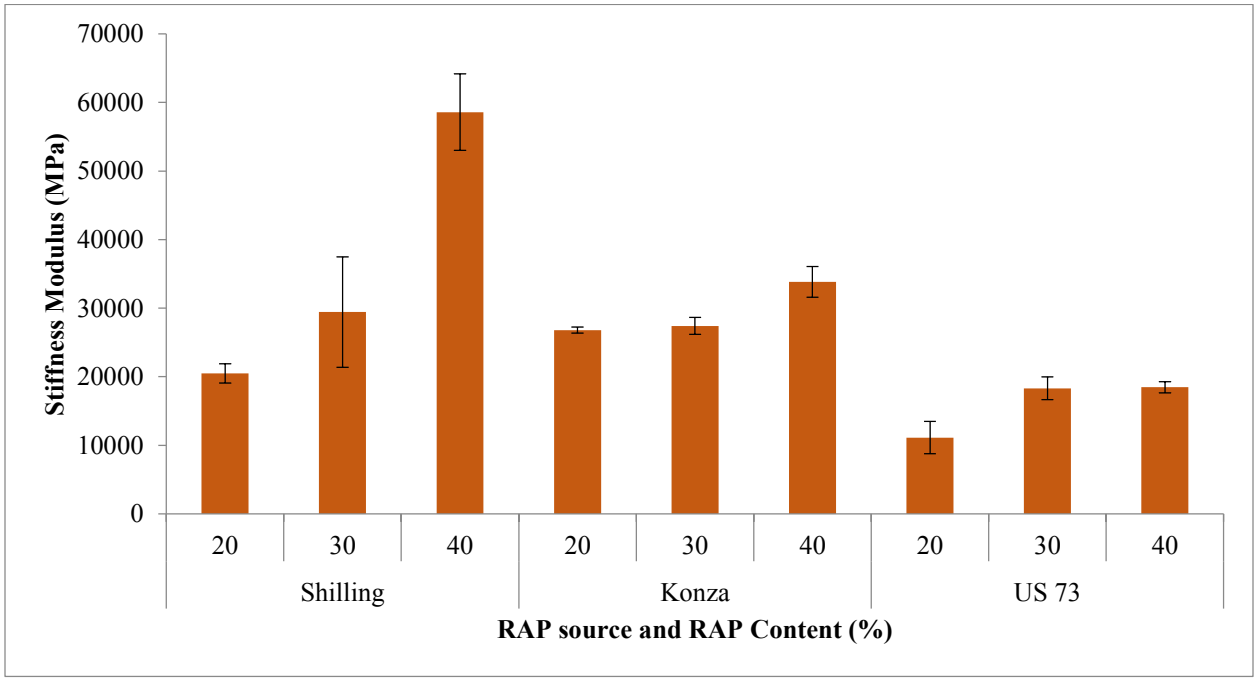


**Figure 4.3 S-SCB stiffness results**

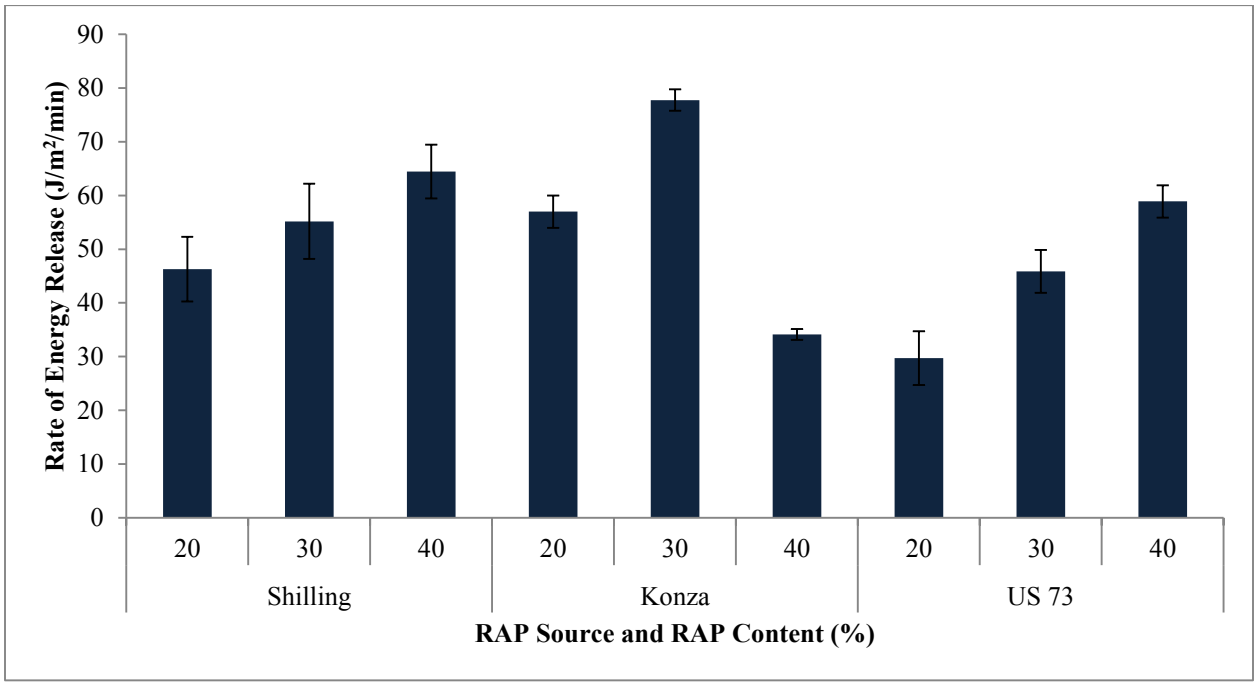


**Figure 4.4 Rate of energy release comparison**

However, according to the rate of FE release, cracking resistance of this mixture was the lowest. Mixtures containing RAP from US 73 had the lowest stiffness values and the highest cracking resistance. Therefore, high stiffness of HMA is not necessarily a safeguard against cracking.

### 4.2.2 Repetitive SCB Test

The R-SCB test was performed using four input loads (30, 40, 50, and 60%) derived from the initial peak load obtained in the S-SCB test. Previous research has indicated that a load value of 50% peak load most appropriately simulates fatigue performance; therefore, R-SCB Test was used for this study. Table 4.3 lists the average number of load cycles for each mixture for 50% of the peak load input in the R-SCB test. Figure 4.5 shows the results graphically. The number of load cycles was measured until cracks propagated throughout the total thickness of the specimen

under repetitive loading. Therefore, the higher the number of load cycles until failure, the higher the cracking resistance.

**Table 4.3 R-SCB test results**

| RAP Source | RAP Content (%) | Initial Peak Load (kN) | Input Load (kN) | Average No. of Load Cycles | COV (%) |
|---|---|---|---|---|---|
| Shilling | 20 | 2.55 | 1.28 | 13,607 | 8.2 |
| | 30 | 3.15 | 1.58 | 11,227 | 5.1 |
| | 40 | 3.88 | 1.94 | 10,113 | 2.5 |
| Konza | 20 | 2.48 | 1.24 | 8,593 | 10.4 |
| | 30 | 1.72 | 0.86 | 6,830 | 10.6 |
| | 40 | 3.12 | 1.56 | 16,567 | 10.5 |
| US 73 | 20 | 1.51 | 0.76 | 22,170 | 9.2 |
| | 30 | 1.87 | 0.94 | 17,568 | 3.7 |
| | 40 | 2.04 | 1.02 | 2,680 | 3.0 |

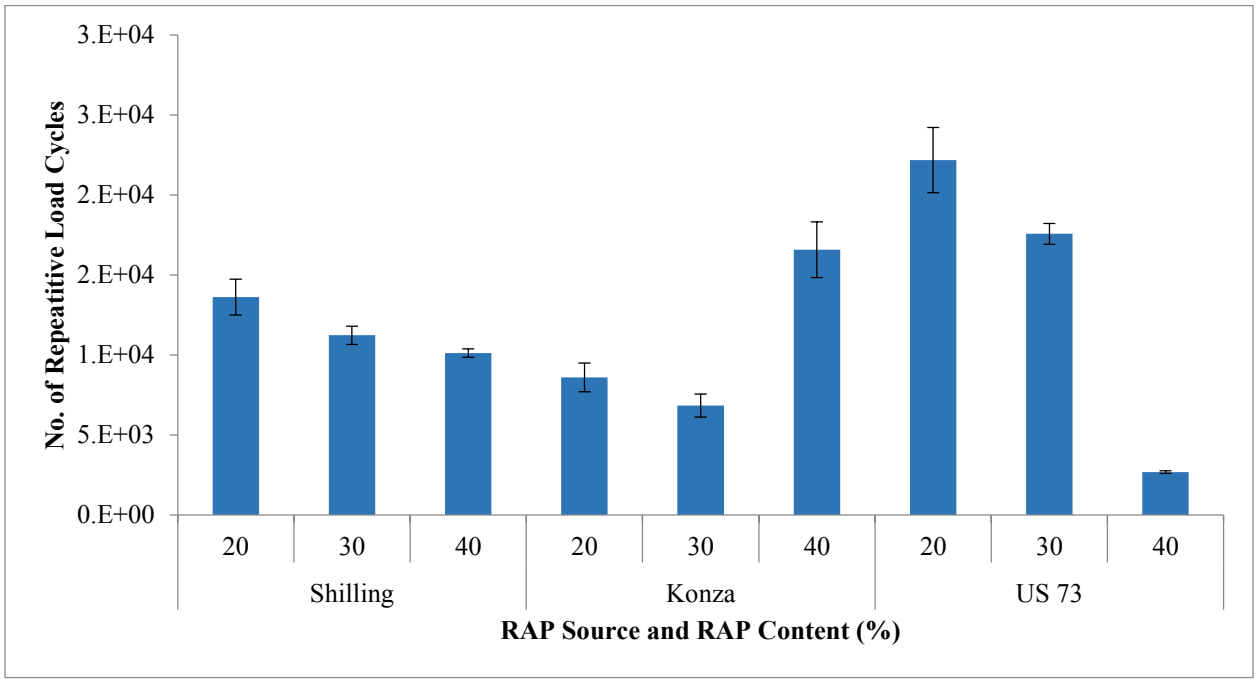


**Figure 4.5 Number of load cycles of R-SCB test**

Results in Table 4.3 and Figure 4.5 indicate that increasing RAP content reduced cracking resistance of mixtures with Shilling and US 73 RAP. However, an anomaly was observed for the Konza RAP source: mixtures containing 20% and 30% RAP from this source showed almost an equal number of load cycles to fracture, but the mixture with 40% RAP displayed the maximum number of load cycles. According to Figure 4.5, the inference can be made that the mixtures with US 73 RAP showed better cracking resistance than the other two sources. However, the US 73 source was from a highway project, whereas the other two RAPs were obtained from the processed stockpile of contractors at RAP plants.

## 4.3 Texas Overlay Tester Test Results

The Texas OT test was performed in order to evaluate reflective cracking resistance of HMA mixtures with high RAP content. Triplicate specimens of mixtures with three RAP contents from three RAP sources were tested according to TEX-248F test method. Table 4.4lists peak loads in the load-displacement curve. The basis of performance comparison of mixtures is the number of OT load cycles before failure. Results for the nine mixtures are summarized in Table 4.4 and presented in Figure 4.6 Samples were compacted to 7±1% air voids. Peak load in the load-displacement curve were also recorded for corresponding mixtures. The COV among each replicate block of the test is presented in parentheses for the respective mixture data. This test showed much higher COVs than the R-SCB tests.

**Table 4.4 Texas OT test results**

| RAP Source | RAP Content (%) | Air Void (%) | Average Initial Peak Load (KN) | Average No. of OT Cycles to Failure ($N_{OT}$)* | Duration (min) |
|---|---|---|---|---|---|
| **Shilling** | 20 | 7.2 | 2.35 | 805 (17.4) | 134 |
| | 30 | 7.3 | 2.9 | 477 (24.5) | 80 |
| | 40 | 7.1 | 3.28 | 128 (16.9) | 21 |
| **Konza** | 20 | 7.1 | 2.66 | 296 (25.2) | 49 |
| | 30 | 7.3 | 2.1 | 71 (22.7) | 12 |
| | 40 | 7.1 | 3.09 | 435 (14.9) | 73 |
| **US 73** | 20 | 7.2 | 1.5 | 939 (21.3) | 97.7 |
| | 30 | 6.9 | 0.7 | 561 (18.7) | 93 |
| | 40 | 7.1 | 0.5 | 529 (19.0) | 47.3 |

*COV shown in parentheses.

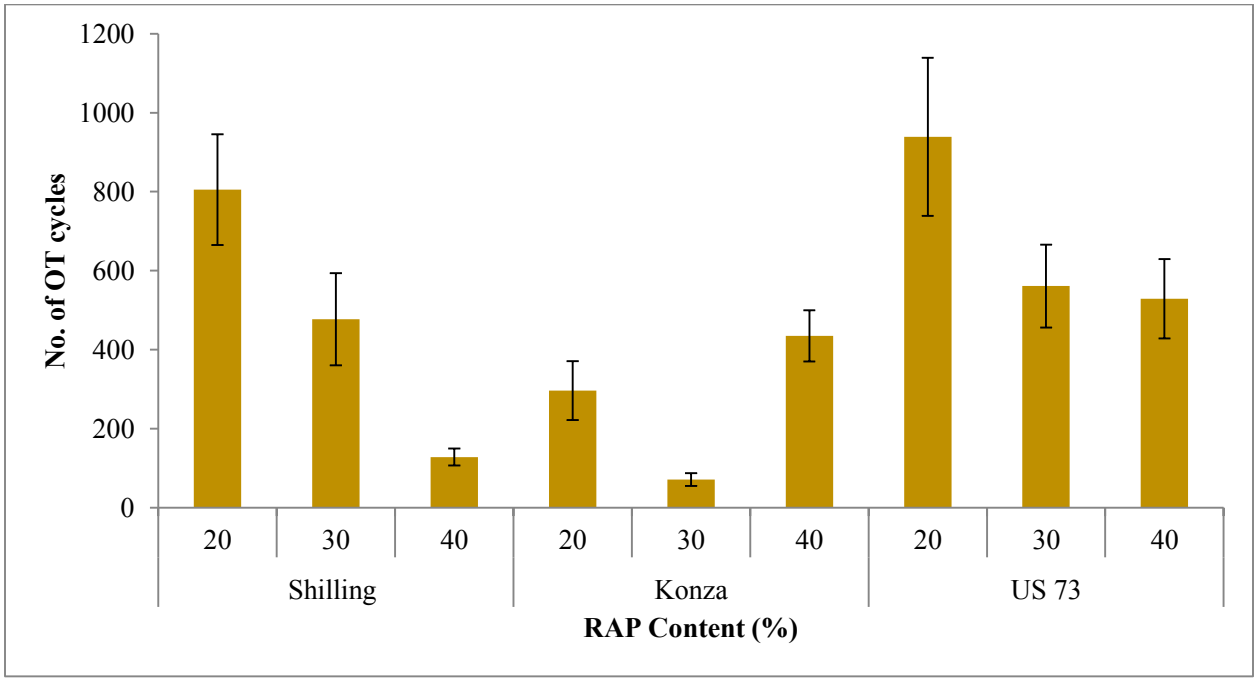


**Figure 4.6 Number of cycles in Texas OT test**

OT results confirmed findings from R-SCB tests. Mixtures with RAP from Shilling and US 73 performed the best. In both cases, the number of load cycles to failure (attainment of 1,000 OT cycles or 93% reduction of initial peak load) declined with increasing percentages of RAP. For both sources, mixtures with 40% RAP showed significantly lower cracking resistance. Therefore, high RAP content appears to make HMA mixtures more susceptible to reflective cracking. TxDOT requires a minimum number of 300 OT cycles for an acceptable HMA mixture. In this study, the mixture with 40% RAP from Shilling did not meet that requirement. This was also observed for mixtures with 20% and 30% RAP from Konza, with the exception of the mixture with 40% RAP from Konza which showed acceptable OT load cycles.

## 4.4 Dynamic Modulus Test Results

Dynamic modulus test results described stress-strain behavior of nonlinear viscoelastic materials such as HMA. The dynamic modulus test was performed at three temperatures (4, 21, and 37 °C) and six loading frequencies (0.1, 0.5, 1, 5, 10, and 25 Hz) in compression loading mode in an Asphalt Mixture Performance Tester (AMPT) according to AASHTO TP62-07. After completion of the test, AMPT provided outputs for the dynamic modulus and phase angle for six frequencies at constant temperature. A typical AMPT output file is presented in Figures 4.7 and 4.8.

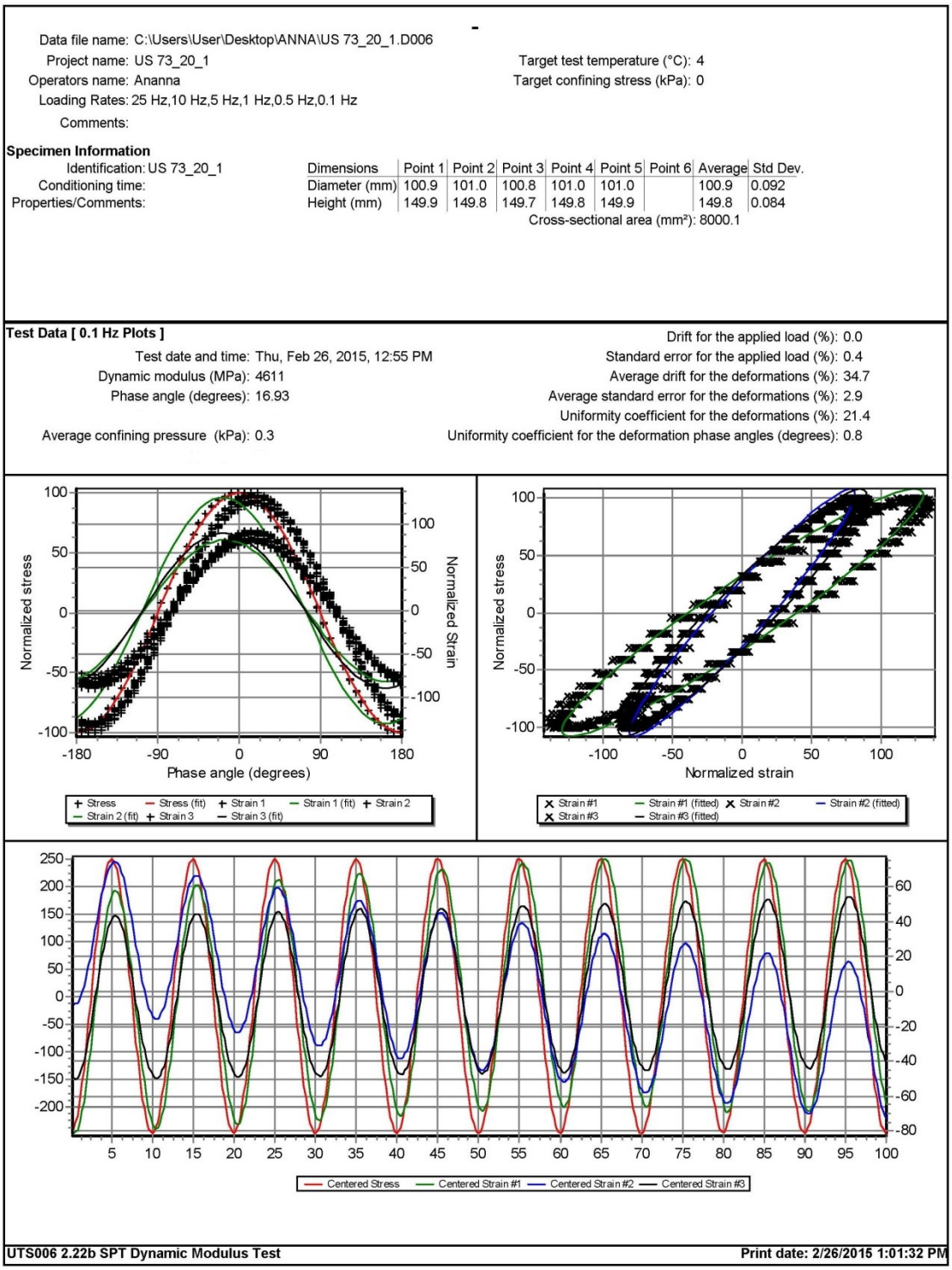


**Figure 4.7 Typical dynamic modulus test output (continued)**

-

Data file name: C:\Users\User\Desktop\ANNA\US 73_20_1.D006
Project name: US 73_20_1
Target test temperature (°C): 4
Operators name: Ananna
Target confining stress (kPa): 0
Loading Rates: 25 Hz,10 Hz,5 Hz,1 Hz,0.5 Hz,0.1 Hz
Comments:

**Specimen Information**

Identification: US 73_20_1
Conditioning time:
Properties/Comments:

| Dimensions | Point 1 | Point 2 | Point 3 | Point 4 | Point 5 | Point 6 | Average | Std Dev. |
|---|---|---|---|---|---|---|---|---|
| Diameter (mm) | 100.9 | 101.0 | 100.8 | 101.0 | 101.0 | | 100.9 | 0.092 |
| Height (mm) | 149.9 | 149.8 | 149.7 | 149.8 | 149.9 | | 149.8 | 0.084 |

Cross-sectional area (mm²): 8000.1

**Tabulated Results Summary**

| | 25 Hz | 10 Hz | 5 Hz | 1 Hz | 0.5 Hz | 0.1 Hz |
|---|---|---|---|---|---|---|
| Dynamic modulus (MPa) | 9337 | 8286 | 8636 | 7049 | 6323 | 4611 |
| Phase angle (Degrees) | 15.90 | 12.74 | 10.91 | 12.66 | 13.66 | 16.93 |
| Average temperature (°C) | 17.5 | 17.1 | 16.8 | 16.0 | 14.8 | 12.2 |
| Average confining pressure (kPa) | 0.1 | 0.1 | 0.1 | 0.2 | 0.2 | 0.3 |
| Average micro-strain | 113 | 112 | 99 | 101 | 102 | 108 |
| Load drift (%) | -0.2 | 0.3 | 0.7 | 0.0 | 0.0 | 0.0 |
| Load standard error (%) | 2.7 | 1.1 | 0.8 | 0.4 | 0.2 | 0.4 |
| Average deformation drift (%) | -4.6 | 10.4 | -25.1 | -3.2 | 16.6 | 34.7 |
| Average deformation standard error (%) | 8.7 | 4.7 | 1.7 | 1.5 | 1.2 | 2.9 |
| Deformation uniformity (%) | 28.6 | 34.6 | 20.8 | 20.7 | 20.6 | 21.4 |
| Phase uniformity (Degrees) | 6.0 | 3.2 | 0.4 | 0.5 | 0.6 | 0.8 |

**Figure 4.8 Typical dynamic modulus test output**

HMA mixture performance (rutting and fatigue cracking) can be compared based on dynamic modulus $|E^*|$ and phase angle ($\varphi$) values (Bhasin et al 2004). As loading frequency increases, the dynamic modulus value typically increases. At low temperatures, dynamic modulus of the same mixture is usually greater than that at high temperatures. In this study, dynamic modulus value at 10 Hz frequency was used to compare mixtures. This frequency was selected because it most closely corresponded to highway speeds of approximately 64 km per hour. Figure 4.9 illustrates dynamic modulus values of mixtures at 4 °C. The figure shows that dynamic modulus decreased with increasing RAP content; however, the rate of decrease was not identical for all RAP sources. Although the rates were similar for mixtures with Shilling and US 73 RAP, the mixture with Konza RAP showed a much lower rate of change of dynamic modulus with RAP content.

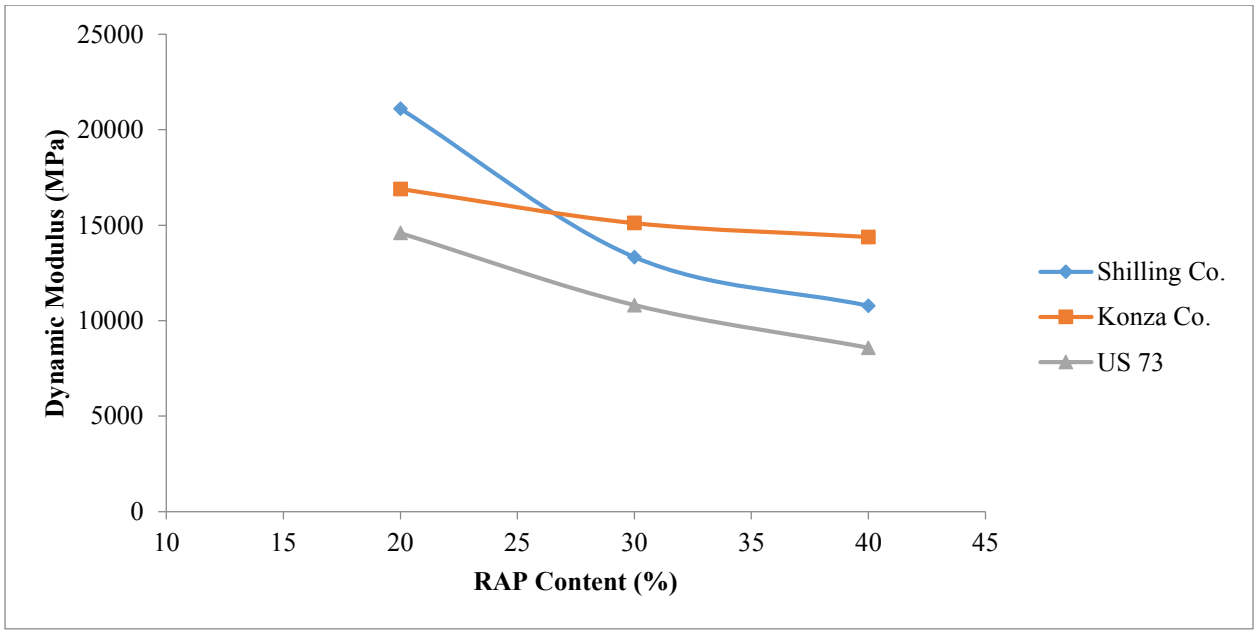


**Figure 4.9 Dynamic modulus value comparison of RAP sources**

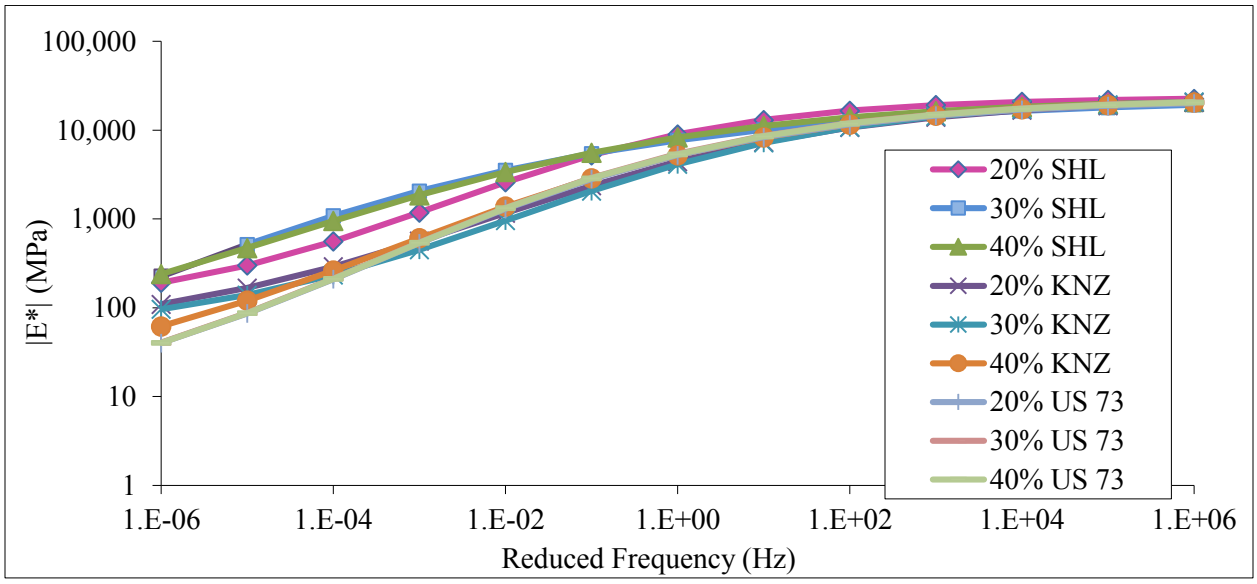


**Figure 4.10 Dynamic modulus master curves**

Dynamic modulus master curves were drawn for all temperatures and frequencies, as shown in Figure 4.10. The figure indicates that dynamic modulus values increased with increasing loading frequency. Master curves are helpful in predicting dynamic modulus values at the project's design temperature and vehicle classification associated with the project during the analysis period.

Figure 4.11 illustrates dynamic modulus values at 10 Hz loading frequency as compared to dynamic modulus values with changing temperatures. For most mixtures, dynamic modulus values decreased with increasing temperature, except for two mixtures: the mixture with 20% Shilling RAP and the mixture with 20% US 73 RAP. The source of this discrepancy is unknown.

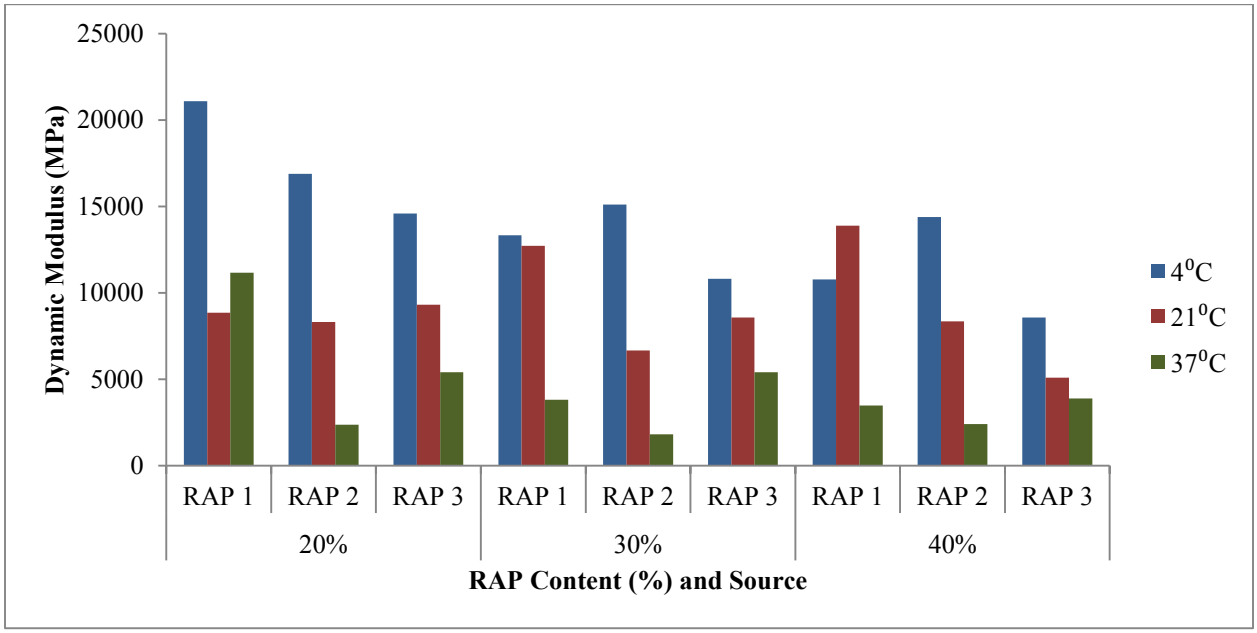


**Figure 4.11 Comparison of dynamic modulus values at various temperatures**

The cracking factor ( $|E^*|\sin\varphi$) is an indication of improved fatigue performance (Figured 4.12). The lower the cracking factor, the better the fatigue cracking performance. Results of this test tended to contradict results observed from R-SCB and OT tests. Mixtures with Konza RAP tended to show higher fatigue cracking resistance than the other mixtures.

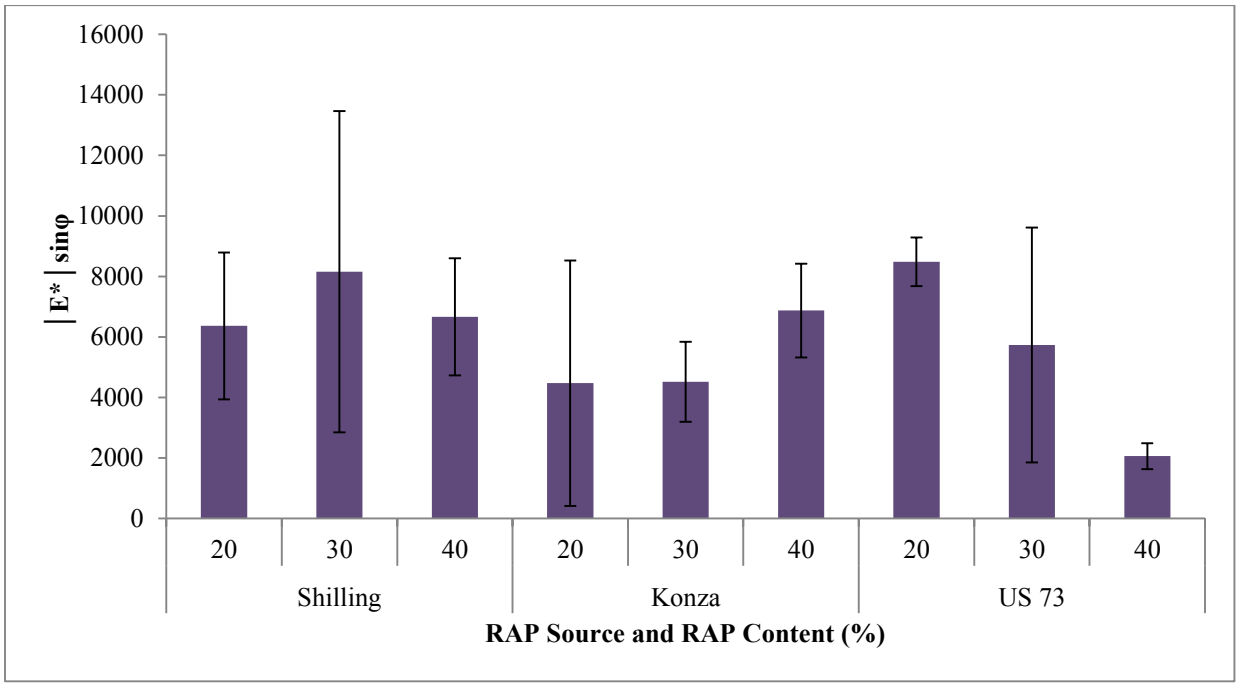


**Figure 4.12 Cracking factors comparison for RAP percentages**

## 4.5 Viscoelastic Continuum Damage Test Results

The VECD test was performed in order to evaluate fatigue performance of HMA mixtures. SGC-compacted samples were cored and cut in order to produce samples according to AASHTO TP-104-14. Triplicate samples were then subjected to the pull-pull or direct tension fatigue test. Initial output was the number of fatigue cycles before failure of the specimen, as presented in Table 4.5. VECD results showed that fatigue cracking resistance of mixtures with RAP decreased with increasing RAP for all RAP sources, including the Konza RAP.

**Table 4.5 VECD test results**

| RAP Source | RAP Content (%) | Air Void (%) | No. of Fatigue Cycles | COV (%) |
|---|---|---|---|---|
| Shilling | 20 | 7.0 | 7,567 | 14.2 |
| | 30 | 6.7 | 3,619 | 5.3 |
| | 40 | 7.0 | 1,771 | 5.2 |
| Konza | 20 | 7.1 | 6,788 | 4.6 |
| | 30 | 7.3 | 4,705 | 14.8 |
| | 40 | 7.4 | 960 | 7.9 |
| US 73 | 20 | 7.1 | 13,705 | 4.4 |
| | 30 | 6.6 | 1,1281 | 3.0 |
| | 40 | 7.0 | 5,598 | 7.4 |

### 4.5.1 Damage Characteristic Curve

A damage characteristic curve using test results from the VECD test for an HMA mixture is generally developed in order to study mixture resistance to damage. Mixtures are then compared based on parameter values. In this study, the following power model was investigated in order to compare fatigue performance of various mixtures:

$$C = 1 - yS^{z}$$

where *S* is cumulative damage to attain first fatigue crack line, *C* is pseudo secant modulus at the time of crack initiation, and *y, z* are the fitting coefficients. For a given normalized stiffness (*C*), a high damage parameter (*S*) value is indicative of increased resistance to damage (AASHTO TP 107-14). Results of three replicate tests for each mixture were used to fit the power model (Equation 3.8) of fatigue characteristics using the software Alpha-Fatigue in order to produce damage characteristic curves. Table 4.6 lists the fitting coefficients; *y* and *z* and pseudo strains at the failure are also listed.

**Table 4.6 VECD calibration equation coefficient values**

| RAP Source | RAP Content (%) | y | z | Pseudo Strain at Failure (με) |
|---|---|---|---|---|
| Shilling | 20 | 7.74E-03 | 5.00E-01 | 0.12 |
| | 30 | 6.58E-03 | 5.24E-01 | 0.13 |
| | 40 | 5.23E-03 | 6.18E-01 | 0.17 |
| Konza | 20 | 8.72E-03 | 4.19E-01 | 0.18 |
| | 30 | 1.12E-02 | 4.76E-01 | 0.20 |
| | 40 | 9.63E-03 | 5.22E-01 | 0.22 |
| US 73 | 20 | 5.85E-03 | 4.89E-01 | 0.10 |
| | 30 | 5.19E-03 | 4.81E-01 | 0.12 |
| | 40 | 5.47E-03 | 4.78E-01 | 0.15 |

Damage characteristic curves were developed using pseudo stiffness values at failure for the range of 1 to the end value (Xie et al. 2015). Figure 4.13 illustrates damage characteristic curves for mixtures containing Shilling RAP.

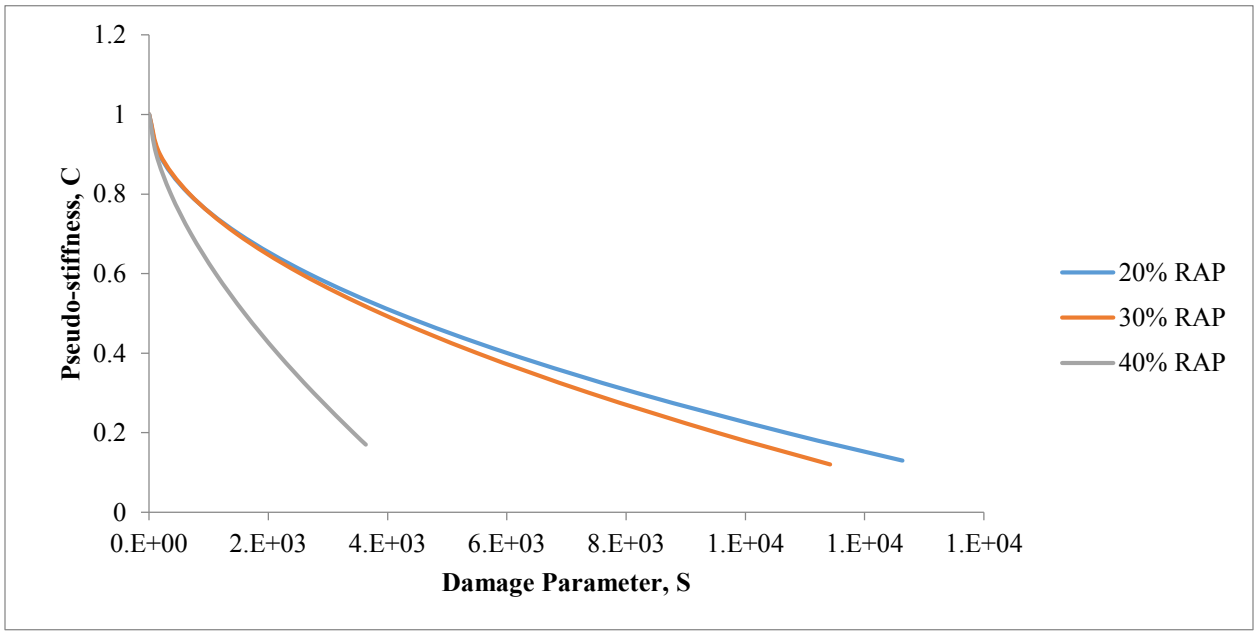


**Figure 4.13 Stiffness versus damage curves (Shilling RAP)**

Figure 4.13 demonstrates that mixtures containing 20% RAP showed damage value at any given normalized value of pseudo strain as compared to mixtures containing 30% and 40% RAP.

However, the mixture with 30% RAP showed a higher damage parameter value than the mixture containing 40% RAP. Although mixtures with 20% and 30% RAP displayed almost similar fatigue characteristics, the mixture with 40% RAP failed abruptly with a large difference in damage compared to the other mixtures. According to Table 4.5, Shilling RAP samples with low resistance to fatigue cracking had high values of end stiffness, indicating that stiff samples are less satisfactory for fatigue performance.

Figure 4.14 illustrates fatigue characteristic curves for mixtures containing RAPs from the Konza Company. The mixture containing 20% RAP showed a substantially higher value of the damage parameter than the other two mixtures. Mixtures with 30% and 40% RAP also demonstrated that increased RAP content decreased fatigue performance of the mixture. However, mixtures with US 73 RAP showed consistent fatigue behavior, as illustrated in Figure 4.15. Mixture performance did not change substantially in terms of damage parameter values for 20% and 30% RAP; however, the mixture with 40% RAP showed different damage parameter values.

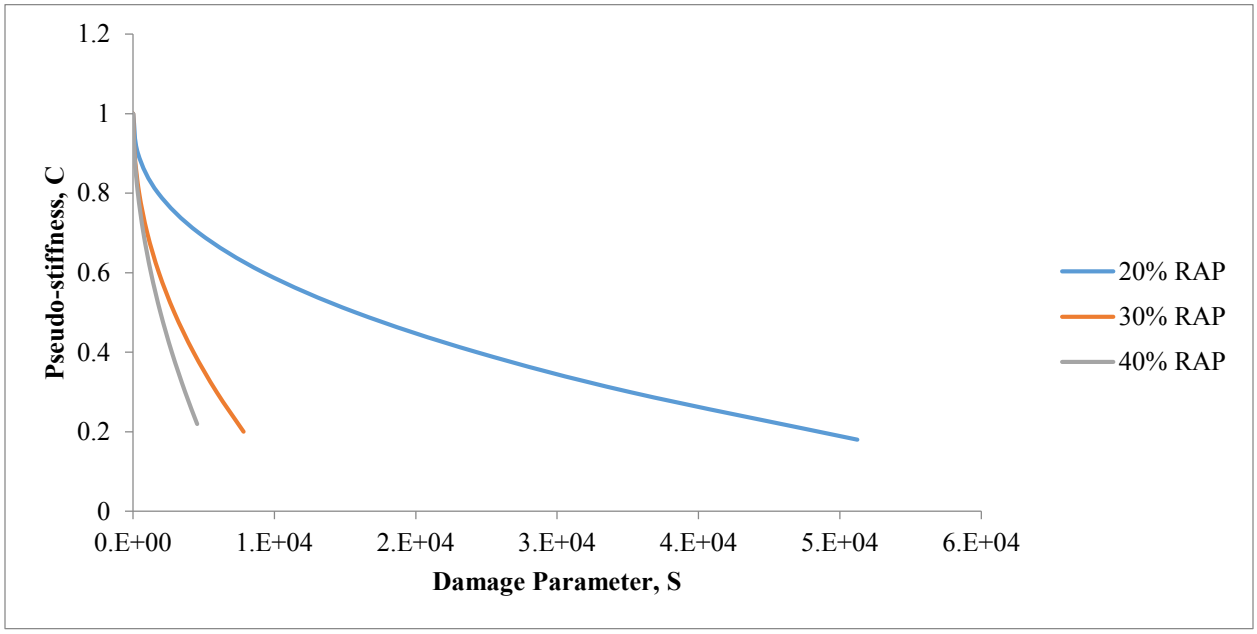


**Figure 4.14 Stiffness versus damage curves (Konza RAP)**

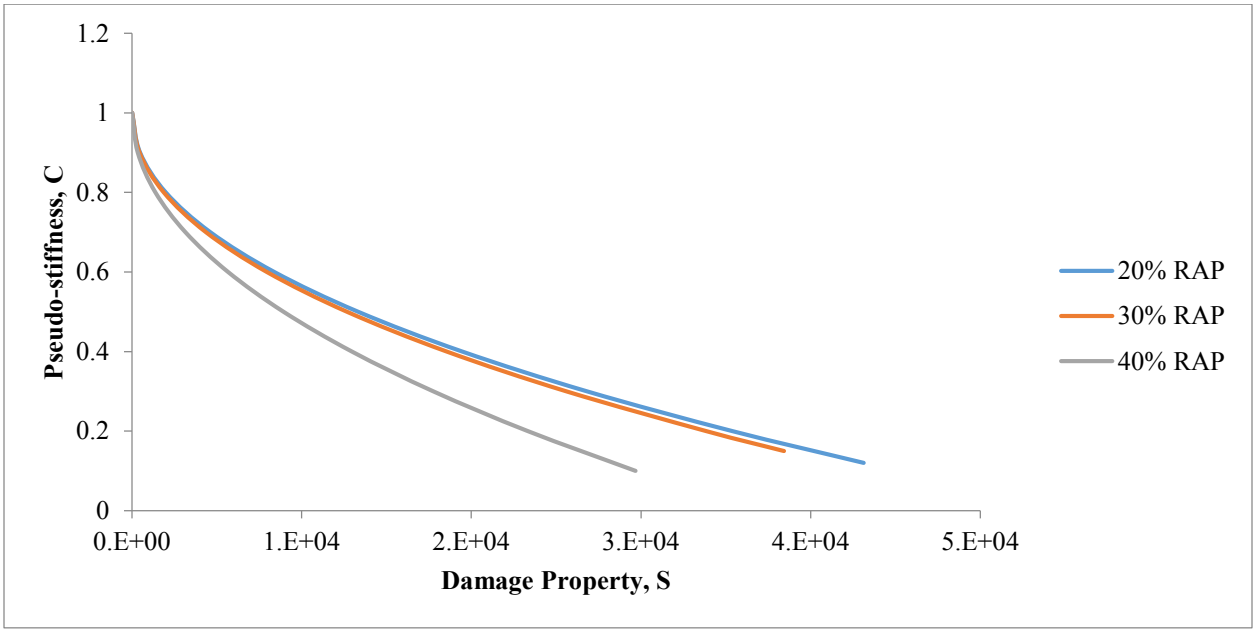


**Figure 4.15 Stiffness versus damage curves (US 73 RAP)**

### 4.5.2 Fatigue Life Prediction

Damage characteristic curves are essential for evaluation of damage resistance and resistance to fatigue cracking. In order to interpret characteristics for real-time constructed pavement, life prediction of HMA mixture is necessary. Using the same software, fatigue life of the mixture can be determined using Equation 4.1 for known strain level. The test was performed for three replicates. The first replicate was subjected to 300 microstrains (με), and other two were decided according to the AASHTO guideline but never exceeding 450 με.

$$N_f = K_1 \left(\frac{1}{\varepsilon_t}\right)^{K_2} (|E^*|)^{K_3} \qquad \textbf{(4.1)}$$

where $N_f$ is number of wheel passes, $\varepsilon_t$ is strain level (με), $|E^*|$ $is$ dynamic modulus of the mixture at any given temperature and 10 Hz load frequency (MPa), and $K_1$, $K_2$, $K_3$ are fitting coefficients. Equation 4.1 was calibrated using the least-squared distance method from data of three replicates. Using coefficient values, certain dynamic modulus, and associated strain level, remaining fatigue life of the mixture was predicted in terms of number of wheel passes.

In Figure 4.16, remaining fatigue life versus strain level is plotted for mixtures with Shilling RAP. Fatigue life is plotted on the log axis. At any strain level, the mixture with 20% RAP content showed highest fatigue life, but fatigue life decreased as the proportion of RAP increased in the mixture. With the increase in strain level, for the same mixture, fatigue life decreased for all three mixtures.

For mixtures containing Konza RAP and US 73 RAP, the hypothesis that mixtures with increasing amounts of RAP reduces fatigue life was verified. Fatigue life prediction curves are presented in Figures 4.17 and 4.18.

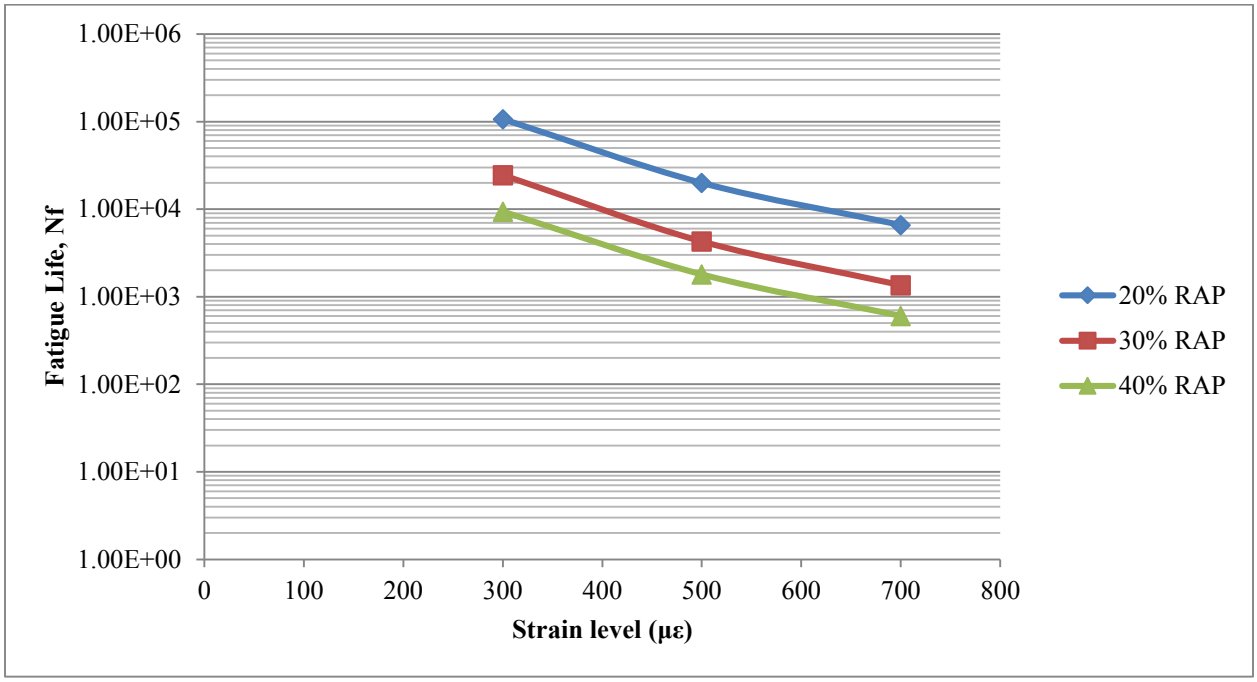


**Figure 4.16 Fatigue life prediction curves (Shilling RAP)**

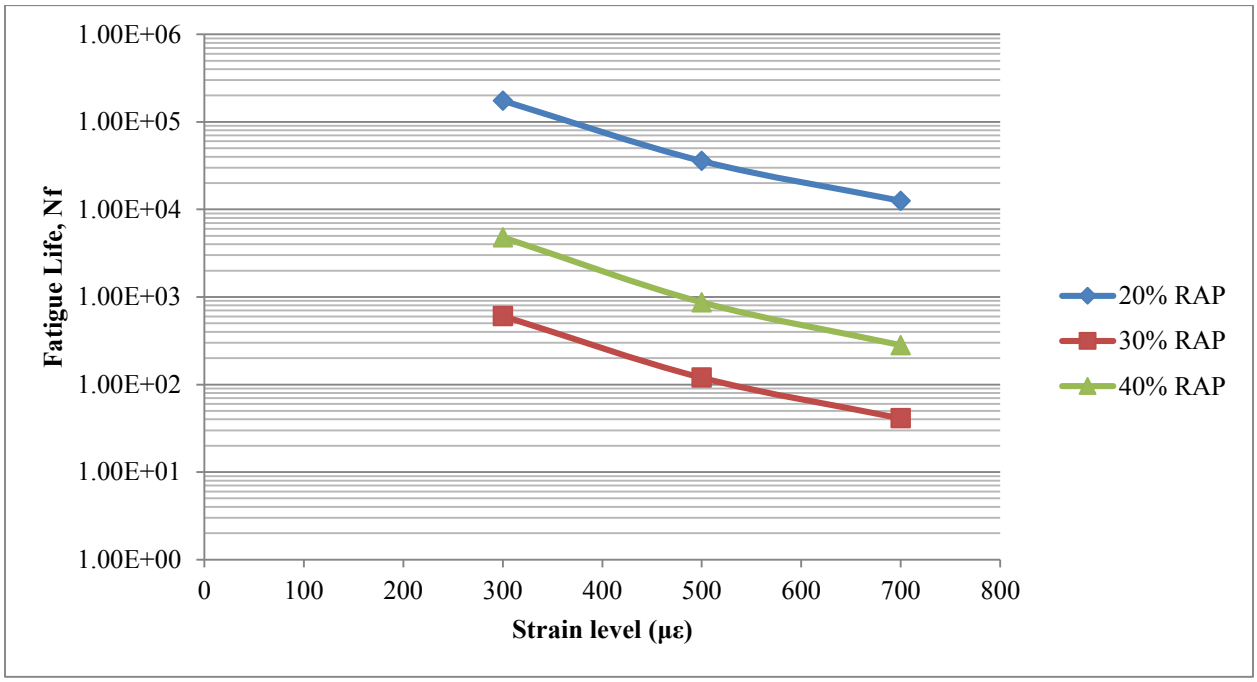


**Figure 4.17 Fatigue life prediction curves (Konza RAP)**

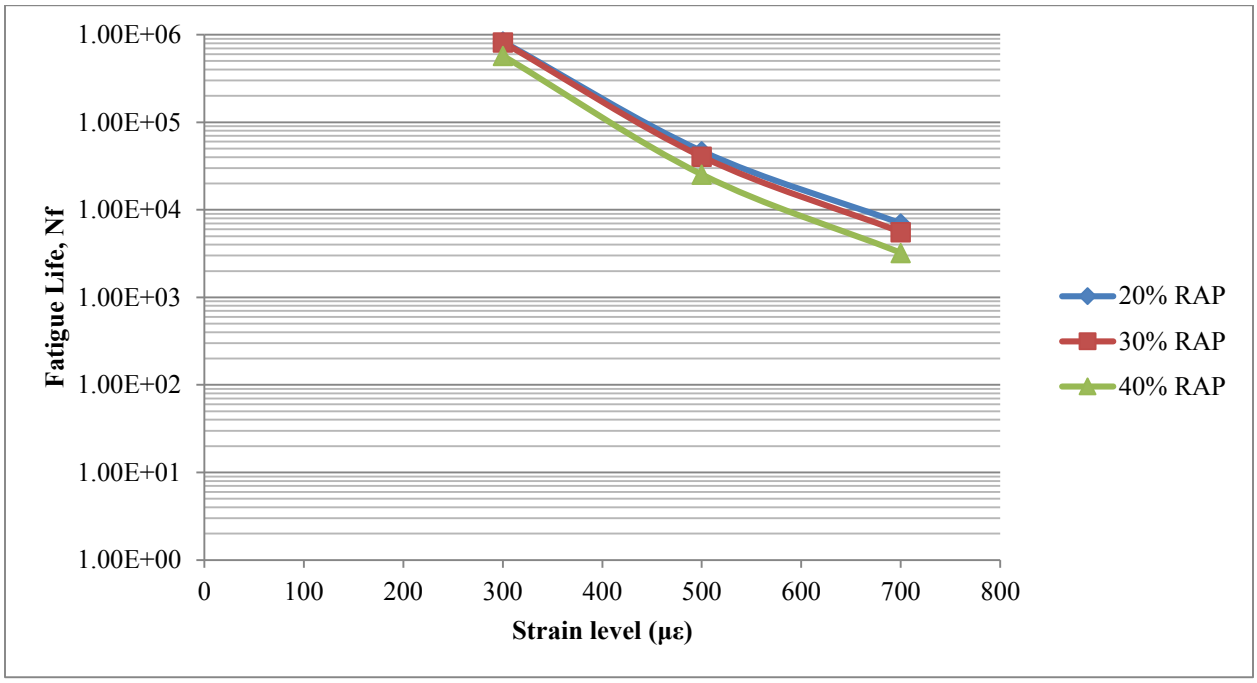


**Figure 4.18 Fatigue life prediction curves (Shilling RAP)**

## 4.6 Statistical Analysis

In this study, statistical analysis was performed using the software package Statistical Analysis System (SAS) (SAS 2011). The objective of this study was to determine the effect of RAP sources and high RAP contents on cracking performance of Superpave mixtures. Statistical analysis of test results was conducted in order to ascertain the significance of these factors.

### 4.6.1 Fitness of the Cracking Test

Results of all cracking tests were analyzed using a two-way, full-factorial model of Analysis of variance (ANOVA) in order to determine if the cracking test was sufficient to identify variation caused by two factors: RAP source and RAP content. The objective was to verify that the model used to analyze the results fit the outcomes of the cracking test. Therefore, the model p-value and F-value found by SAS were used at 95% confidence level. Table 4.7 lists p-values for various test results.

**Table 4.7 p-value and F-statistic values for cracking tests**

| Tests | p-value | F-Statistic |
|---|---|---|
| Semicircular Bending | <0.0001 | 11.28 |
| Texas Overlay | <0.0001 | 16.28 |
| Dynamic Modulus | 0.0325 | 2.82 |
| Viscoelastic Continuum Damage | <0.0001 | 196.05 |

At 95% level of confidence, p-values lower than 0.05 were considered to be significant. For all tests, p-values presented in Table 4.7 were lower than the level of significance, indicating that the model was accurate for determining variations caused by various levels of the factor RAP source (Shilling, Konza, and US 73) as well as the factor RAP content (20, 30, and 40%).

F-statistics values obtained during ANOVA were compared to the F-critical value found from the right-skewed F-distribution. For degrees of freedom of the model as 8 (3 x 3 -1) and

degrees of freedom of the error associated with the model as 18 {3x3(3-1)}, $F_{critical}$ at 5% significance level was found to be 2.51. When the F-value of the model for each test as presented in Table 4.7 was compared to this $F_{critical}$, all test results captured variations caused by the two factors in this study.

### 4.6.2 Significance of Factors

Table 4.8 lists p-values for the ANOVA performed for a full-factored model that used all levels of two factors, RAP source and RAP content, as well as factor interactions. The hypothesis that average results obtained from a certain test have no relationship to the factor(s) was tested in order to evaluate the significance of a factor. If the hypothesis was rejected, the factor contributes to the variation of mean results of the test at 5% level of significance. Results in Table 4.8 indicate that, for the SCB test, RAP source and RAP content significantly affect the FE outcome at various levels of the factor(s). However, the interaction between factors is not significant.

**Table 4.8 Significance of factors**

| Tests | p-value of RAP Source | p-value of RAP Content | p-value of Interaction |
|---|---|---|---|
| Semi-Circular Bending | <0.0001 | 0.0102 | 0.1655 |
| Texas Overlay | <0.0001 | 0.0004 | <0.0001 |
| Dynamic Modulus | 0.012 | 0.9816 | 0.0595 |
| Viscoelastic Continuum Damage | <0.0001 | <0.0001 | <0.0001 |

For the OT and VECD tests, all three aspects were found to be significant at 5% level of significance. Various RAP sources uniquely affected OT cycles and VECD fatigue cycles of the same mixture. RAP content significantly contributed to outcome variations of these two tests. In addition, the conclusion was made that RAP source and RAP content together significantly

contribute to OT cycles and VECD fatigue cycle numbers. This observation was justified by the drastic behavior of the mixture containing 40% Konza RAP. For the dynamic modulus test, analysis results were somewhat inconclusive. Although the RAP source was significant, the RAP content was not significant, thereby defying the traditional belief that increasing RAP content increases mixture stiffness. However, the high COV associated with the test results may have contributed to this outcome. Although a low cracking factor ($|E^*|\sin\varphi$), where $|E^*|$ is the dynamic modulus and $\varphi$ is the phase angle, has been used as an indicator of improved fatigue performance, results in this study did not indicate the high potential of using dynamic modulus test as a cracking evaluation test.

### 4.6.3 Sources of Variation

Statistical analysis results obtained in this study showed that the tests were sufficient to varying degrees in capturing variation caused by different factor levels and interactions. Results summarized in Table 4.9 indicate the contribution of each factor. Figure 4.19 shows these results graphically.

**Table 4.9 Sources of variability**

| Test | Contribution in Variation (%) | | | |
|---|---|---|---|---|
| | RAP Source | RAP Content | Interaction | Error |
| Semi-Circular Bending | 66 | 11 | 7 | 17 |
| Texas Overlay | 28 | 17 | 42 | 12 |
| Dynamic Modulus | 28 | 0 | 27 | 44 |
| Viscoelastic Continuum Damage | 50 | 46 | 3 | 1 |

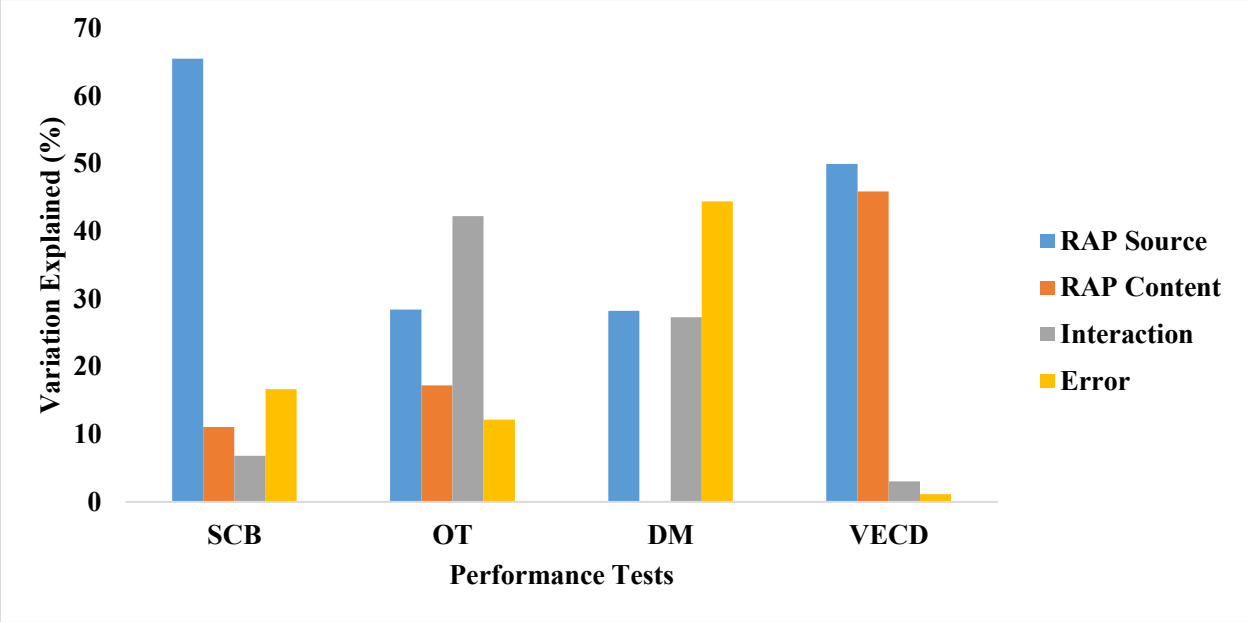


**Figure 4.19 Distribution of variation among sources**

For the SCB test, the largest source of variation in the test results occurred from the RAP source. RAP content was also significant, but the amount of resulting variation was small compared to RAP source. For the OT test, the primary source of variation was interaction, a combined effect of both factors. The test captured differentiation in the number of OT cycles caused by varying RAP content for individual RAP sources. Test results associated the dynamic modulus test with high error. The combined effect of RAP source and RAP content played role in determining dynamic modulus values. The VECD test consistently predicted results for individual effect of RAP source and RAP content on fatigue cycles as well as evaluation of the combined effect of factors. Error associated with the VECD test was also minimal.

### 4.6.4 Confidence Interval Analysis

Confidence interval analysis was conducted in order to thoroughly study factors. For the SCB test, interaction effect was not significant, so confidence interval prediction was performed for both factors individually. The OT and VECD tests demonstrated significant interaction effects,

therefore, prediction based on each individual factor was not justified, and their combined effect was studied for prediction purposes. In Figures 4.20 and 4.21, predicted ranges of FE for each RAP source and RAP content at 95% confidence level are presented.

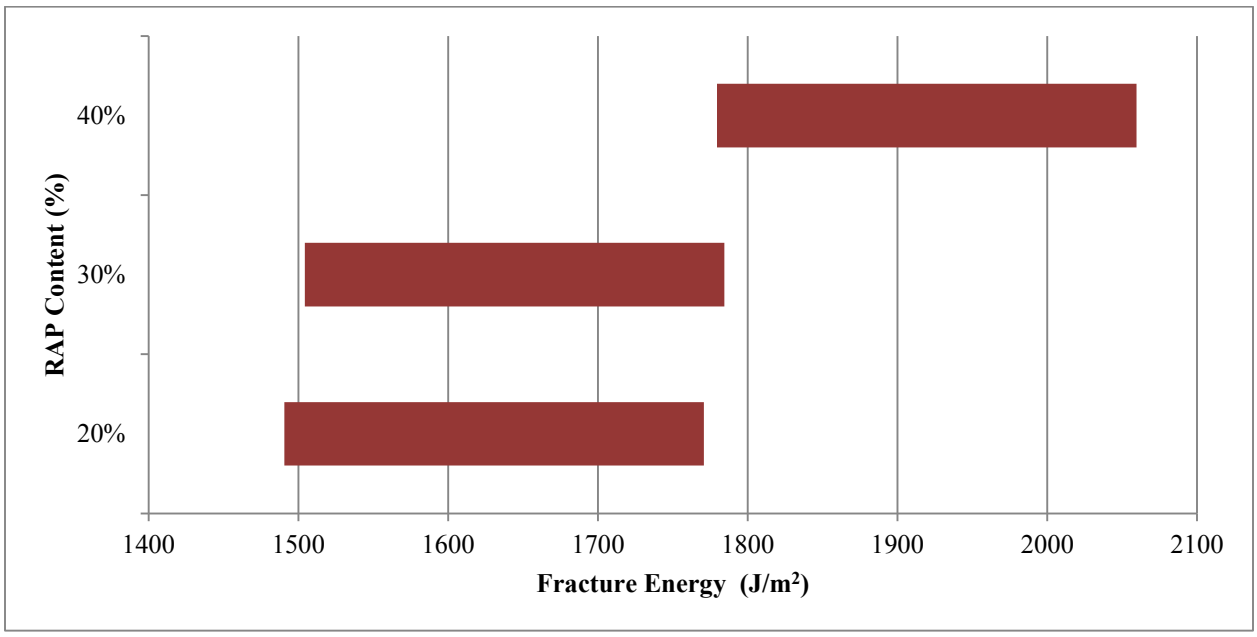


**Figure 4.20 95% confidence interval of RAP content in SCB test results**

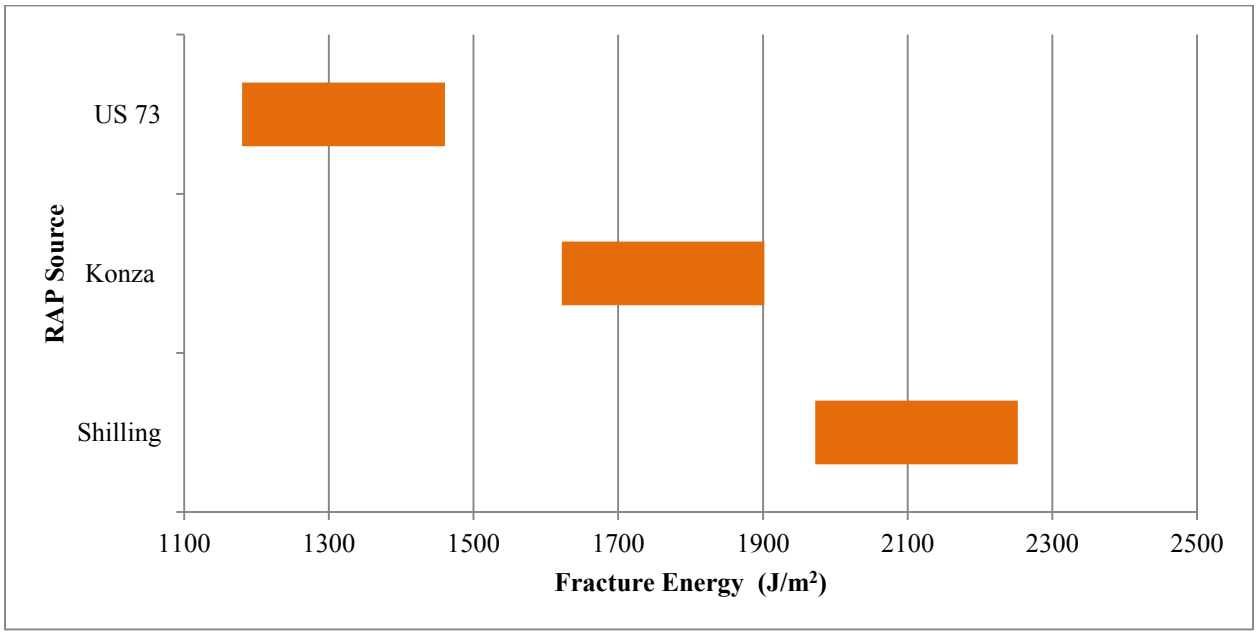


**Figure 4.21 95% confidence interval of RAP sources in SCB test results**

Confidence intervals for varying RAP content showed significant overlaps, but it was discrete for the factor RAP source. Calculated confidence intervals are suggestive of expected FE values if different quantities of RAPs are added to the mixtures.

Figure 4.20 represents the range of expected FE values for a particular source of RAP. From Figure 4.20 and 4.21 the conclusion can be made that mixtures containing 20% to 30% RAP from US 73 RAP performed the best. In Figure 4.22 confidence intervals for combined effects for OT test results are presented. The mixture with 20% Shilling RAP had the highest number of OT cycles, but the US 73 mixture behaved consistently for all three RAP contents. At 95% confidence level, US 73 mixtures with RAP content as high as 40% demonstrated satisfactory performance. Interaction effect was more justified by performance of the mixture with 40% Konza RAP. The mixture performed significantly better than the other two mixtures with varying RAP contents from the same source.

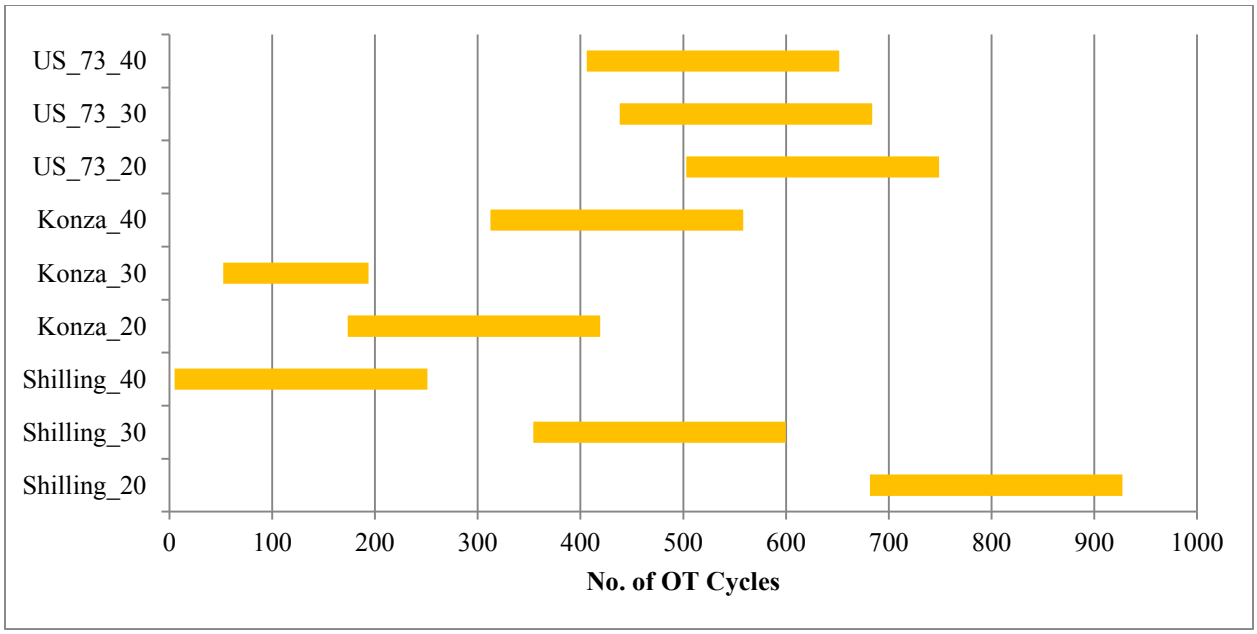


**Figure 4.22 95% confidence interval of OT test results**

Confidence Interval analysis results for the VECD test are presented in Figure 4.23 which shows the range of expected numbers of fatigue cycles for three RAP contents for each source of RAP. Mixtures containing 20% to 30% RAP from US 73 had the highest predicted fatigue cycles compared to the other mixtures. The mixture with 40% US 73 RAP was also satisfactory. Mixtures with 20% Shilling and Konza RAP demonstrated high expected values as well.

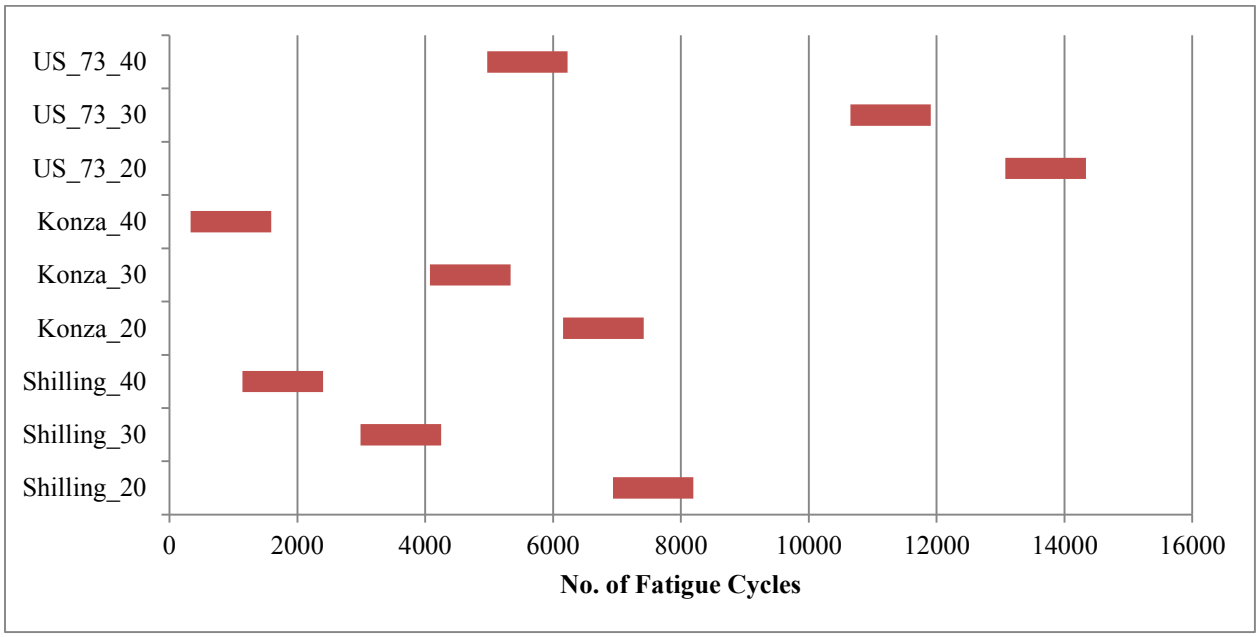


**Figure 4.23 95% confidence interval of VECD test results**

For dynamic modulus test results, the factor, RAP content, and combined effect of factors were not found to be significant; therefore, prediction was based only on RAP source. Confidence intervals are presented in Figure 4.24 for dynamic modulus test results. In general, this figure predicts expected ranges of dynamic modulus values from mixtures containing three RAP sources regardless of content.

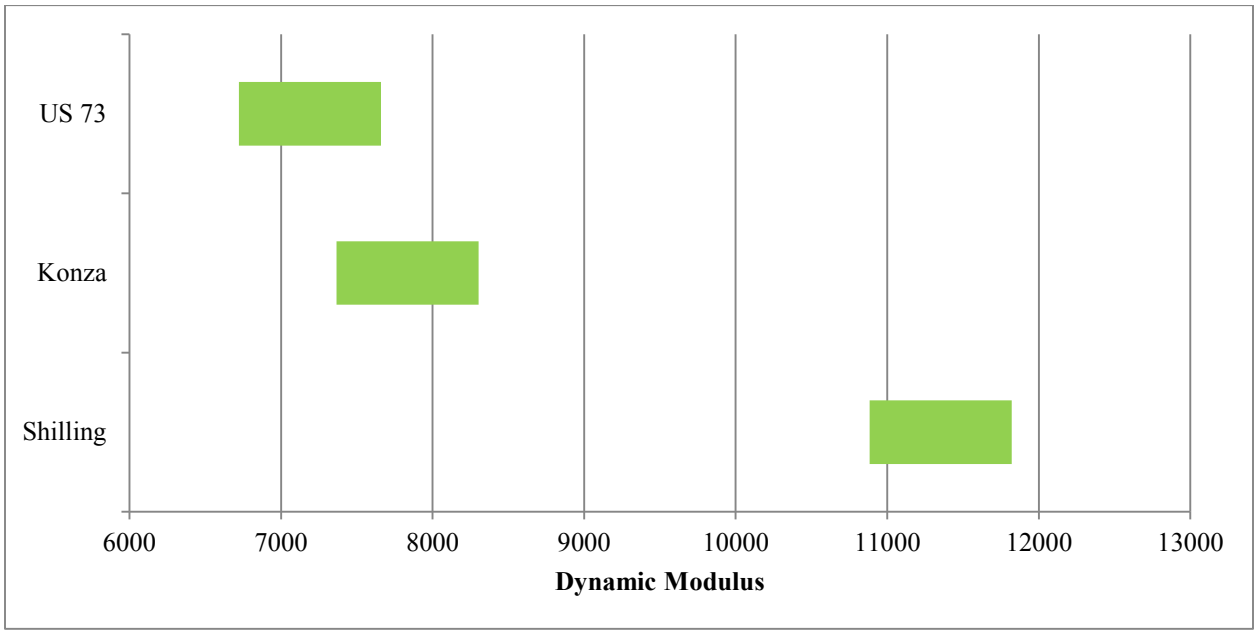


**Figure 4.24 95% confidence interval of dynamic modulus test results**

### 4.6.5 Comparison of Cracking Tests

Mean results obtained from the S-SCB test, the OT test, the dynamic modulus test, and the VECD test were compared using the Tukey's pairwise comparison method in order to find best performing combination of RAP source and RAP content and most promising cracking evaluation test.

Data used in the analysis was first checked for homogeneity of variance, the null hypothesis was checked by the model likelihood ratio test, and the homogenous variance assumption was found to be true for all datasets. In the next step, data was checked for normality. Table 4.10 shows normality test results of the S-SCB test data. The dataset was normally distributed, as justified by the normal probability plot for the dataset illustrated in Figure 4.25.

**Table 4.10 Normality test results of SCB test data**

| Normality Test | p-value |
|---|---|
| Shapiro-Wilk | 0.954 |
| Kolmogorov-Smirnov | 0.097 |
| Anderson-Darling | 0.406 |

Tukey's pairwise comparison method is considered to be the most powerful tool for controlling Type-I error rate (Kuehl 2000). Least squared means for S-SCB test results were grouped using this method. Depending on the grouping, mean results of the tests were compared in order to identify the better performing tests. The basic assumption was that the more capable the test was to capture statistically significant differences between the mixtures, the more the test was suitable for determining cracking potential. In other words, the test was capable of accurately evaluating effects of factors. Pairwise comparison of the means for S-SCB test results are shown in Table 4.11. Normal probability plot for SCB test results are presented in Figure 4.25.

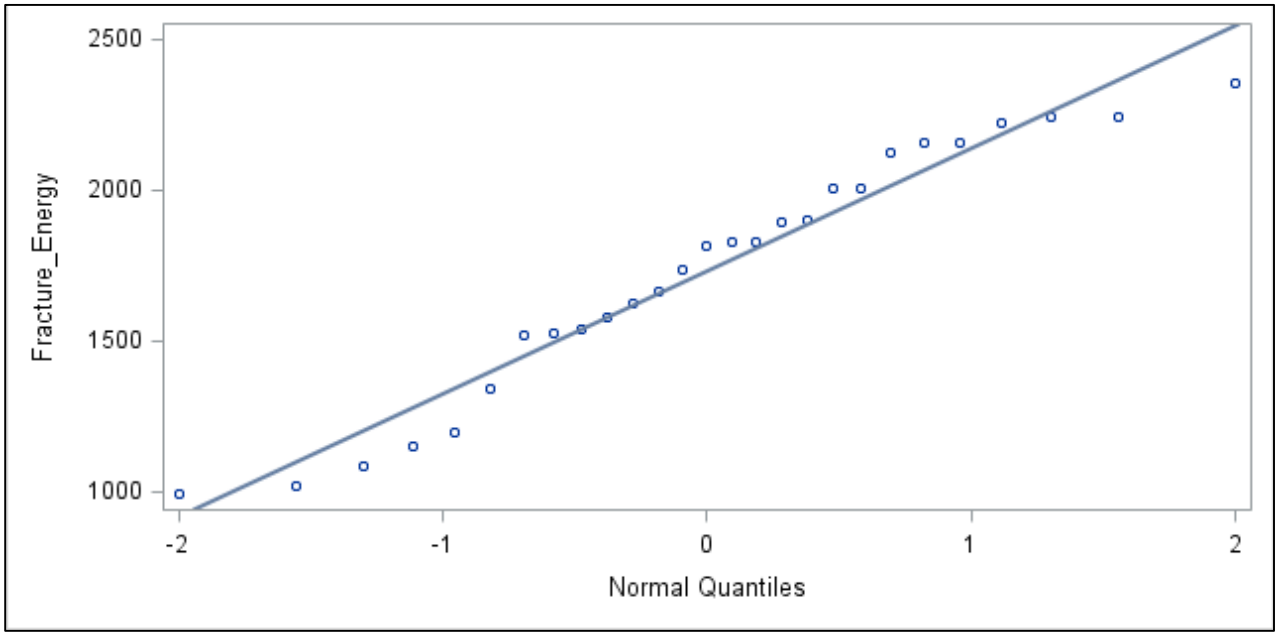


**Figure 4.25 Normal probability plot of FE**

**Table 4.11 Tukey pairwise comparison of SCB test results**

| Asphalt Content (%) | 4.3 | 4.7 | 4.8 | 4.1 | 4.4 | 4.5 | 4.3 | 4.9 | 4.8 |
|---|---|---|---|---|---|---|---|---|---|
| Shilling_40 | A | | | | | | | | |
| Shilling_20 | | A | | | | | | | |
| Shilling_30 | | | AB | | | | | | |
| Konza_40 | | | | AB | | | | | |
| Konza_30 | | | | | ABC | | | | |
| US_73_40 | | | | | | BC | | | |
| Konza_20 | | | | | | | BC | | |
| US_73_20 | | | | | | | | C | |
| US_73_30 | | | | | | | | | C |

Assumptions for this test included independence of observations and homogeneity of variance. Comparison of significance was done based on adjusted p-value of each pair: if the p-value was lower than the level of significance ($\alpha = 0.05$), two compared mixtures had statistically significant differences. In Table 4.11, mixtures identifications are coded by source name and RAP content (%). Asphalt content of the mixture was reported in the corresponding columns. As shown in this table, mixtures bordered with the same colored box demonstrated no significant difference in their mean FE values. For example, the mixtures with 40% Shilling RAP and 20% Shilling RAP are different, but the difference was not statistically significant at 95% confidence level. Several overlapping did not allow formation of a full block. The best performing mixture contained 30% US 73 RAP at a binder content of 4.8%. Overall, the test was able to determine six blocks of similar means those showed significant difference among them.

OT test results were also checked for normality using the same methods previously mentioned. Table 4.12 and Figure 4.26 show p-values and normal probability plot, respectively. The dataset was found to be normally distributed.

**Table 4.12 Normality test results of OT test**

| Normality Test | p-value |
|---|---|
| Shapiro-Wilk | 0.9649 |
| Kolmogorov-Smirnov | 0.0965 |
| Anderson-Darling | 0.3020 |

Tukey pairwise comparison results are shown in Table 4.13 The extent of overlapping was more concentrated according to results of this test. The mixture with 20% Shilling RAP performed the best in this test and 30% Konza RAP mixture performed the worst. The test captured six blocks of similar least squared means.

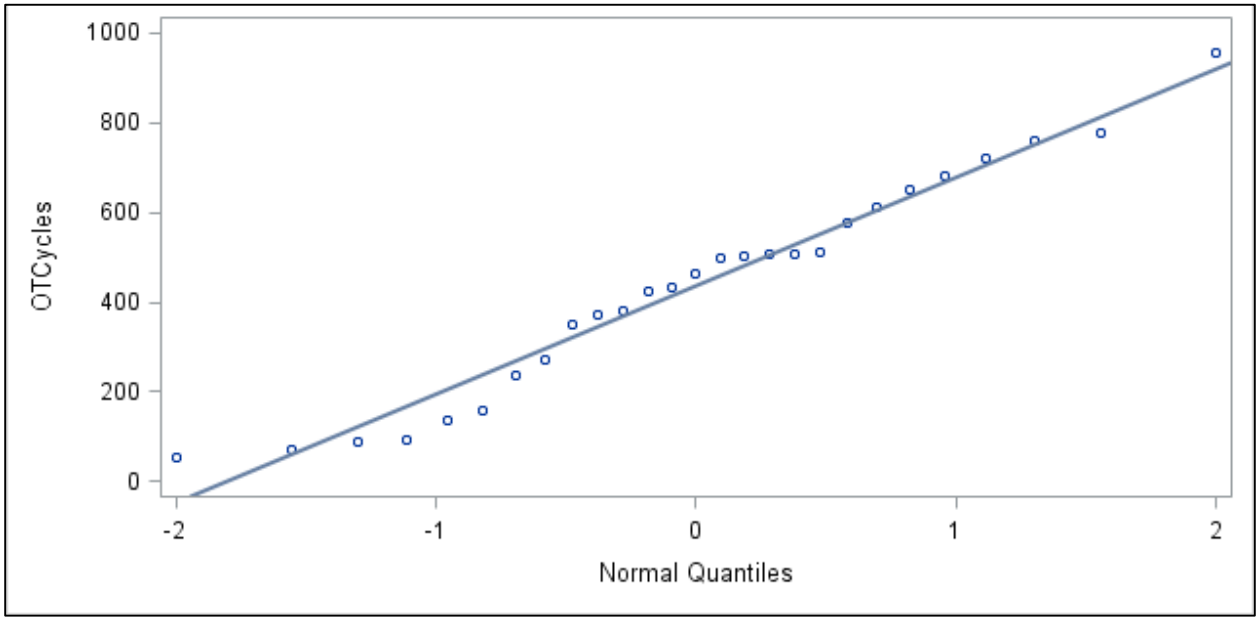


**Figure 4.26 Normal probability plot of OT cycles**

**Table 4.13 Tukey pairwise comparison of OT test results**

| Asphalt Content (%) | 4.7 | 4.9 | 4.8 | 4.5 | 4.8 | 4.1 | 4.3 | 4.3 | 4.4 |
|---|---|---|---|---|---|---|---|---|---|
| Shilling_20 | A | | | | | | | | |
| US_73_20 | | AB | | | | | | | |
| US_73_30 | | | ABC | | | | | | |
| US_73_40 | | | | ABC | | | | | |
| Shilling_30 | | | | | BC | | | | |
| Konza_40 | | | | | | BC | | | |
| Konza_20 | | | | | | | DC | | |
| Shilling_40 | | | | | | | | D | |
| Konza_30 | | | | | | | | | D |

For statistical analysis of dynamic modulus test results, dynamic modulus values of 10 Hz and 21 $^{0}$C were used. As mentioned, the dynamic modulus test was not suitable for evaluation of the effects of RAP source and RAP content on cracking performance. However, results were re-analyzed and compared to other test results. Results from the dynamic modulus and VECD tests were tested for normality. Test outcomes are presented in Tables 4.14 and 4.15 and Figures 4.27 and 4.28. Both datasets were found to be normally distributed.

**Table 4.14 Normality test results of dynamic modulus test**

| Normality Test | p-value |
|---|---|
| Shapiro-Wilk | 0.88 |
| Kolmogorov-Smirnov | 0.18 |
| Anderson-Darling | 0.91 |

**Table 4.15 Normality test results of VECD test**

| Normality Test | p-value |
|---|---|
| Shapiro-Wilk | 0.93 |
| Kolmogorov-Smirnov | 0.12 |
| Anderson-Darling | 0.59 |

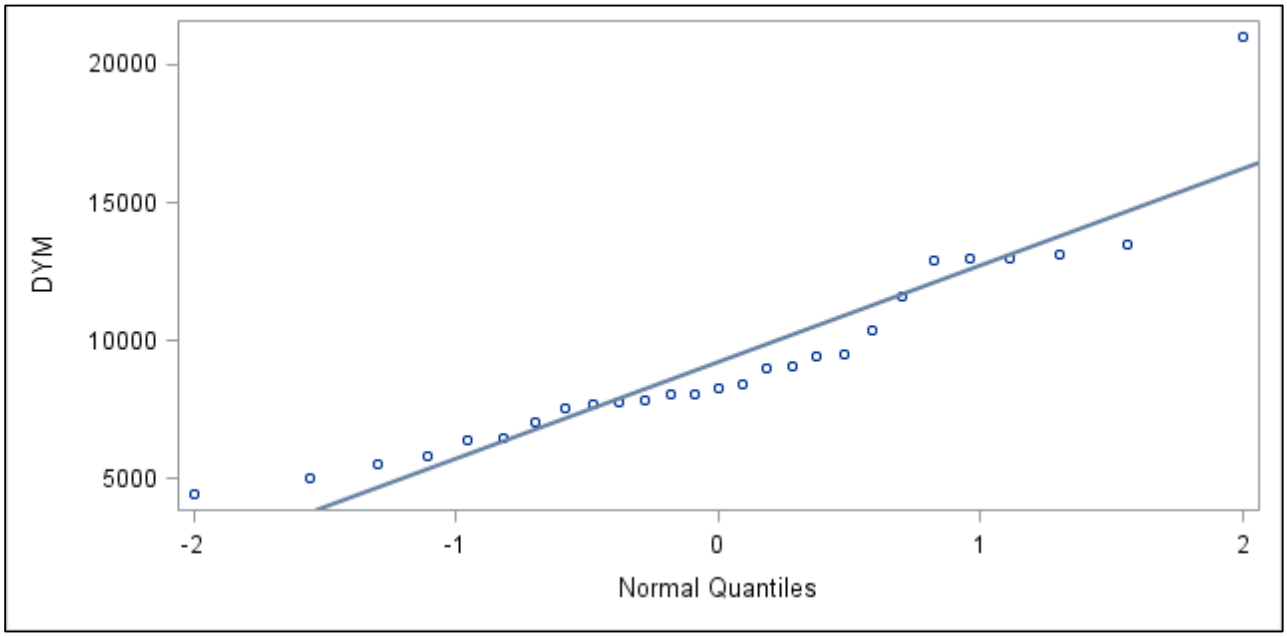


**Figure 4.27 Normal probability plot of dynamic modulus results**

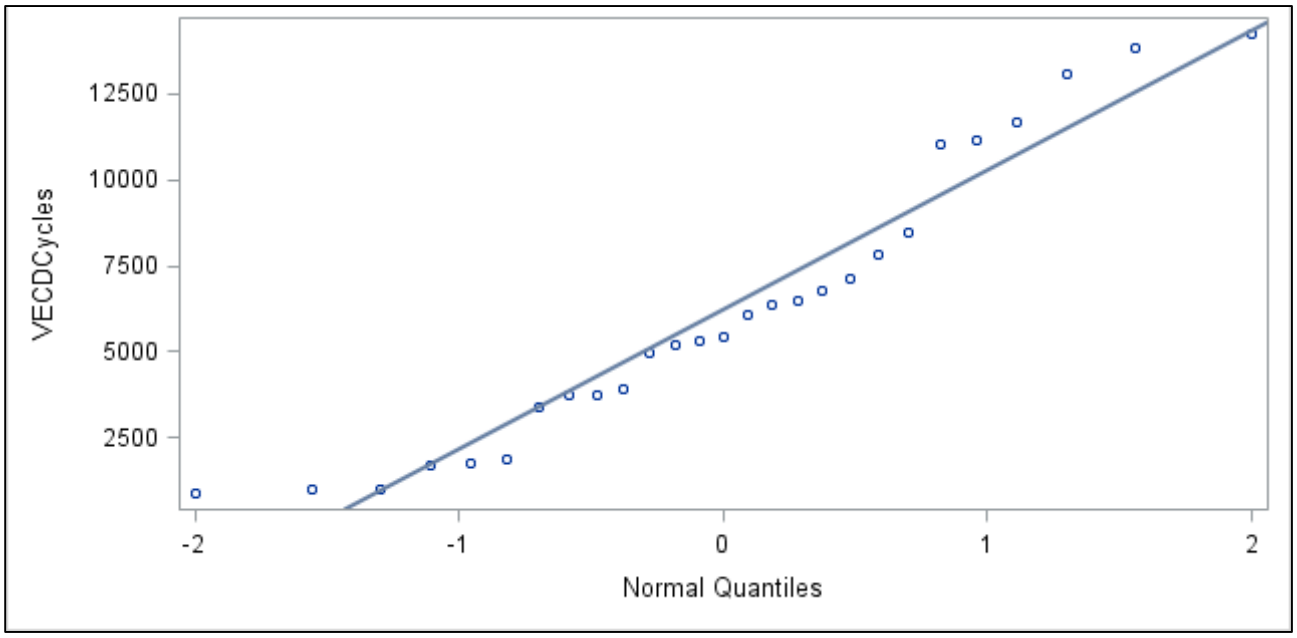


**Figure 4.28 Normal probability plot of fatigue cycles of VECD test**

In Tables 4.16 and 4.17, Tukey pairwise comparison groups are presented for the means of dynamic modulus test results and VECD test results, respectively. Mixtures enclosed in boxes of identical color did not show any significant difference in their means. According to dynamic modulus test results, the test identified only three blocks, and the overlapping zone was much larger than other tests, indicating less identification of differences.

**Table 4.16 Tukey pairwise comparison of dynamic modulus test results**

| Asphalt Content (%) | 4.3 | 4.8 | 4.3 | 4.9 | 4.7 | 4.8 | 4.1 | 4.4 | 4.5 |
|---|---|---|---|---|---|---|---|---|---|
| Shilling_40 | A | | | | | | | | |
| Shilling_30 | | AB | | | | | | | |
| Konza_20 | | | AB | | | | | | |
| US_73_20 | | | | AB | | | | | |
| Shilling_20 | | | | | AB | | | | |
| US_73_30 | | | | | | AB | | | |
| Konza_40 | | | | | | | AB | | |
| Konza_30 | | | | | | | | AB | |
| US_73_40 | | | | | | | | | B |

For VECD test results, three individual blocks were identified. Overlapping blocks were smaller in range, and eight groups overall were formed. According to this test, the mixture containing 20% RAP from US 73 showed optimum fatigue performance.

**Table 4.17 Tukey pairwise comparison of VECD test results**

| Asphalt Content (%) | 4.9 | 4.8 | 4.7 | 4.3 | 4.5 | 4.4 | 4.8 | 4.3 | 4.1 |
|---|---|---|---|---|---|---|---|---|---|
| US_73_20 | A | | | | | | | | |
| US_73_30 | | B | | | | | | | |
| Shilling_20 | | | C | | | | | | |
| Konza_20 | | | | CD | | | | | |
| US_73_40 | | | | | DE | | | | |
| Konza_30 | | | | | | EF | | | |
| Shilling_30 | | | | | | | F | | |
| Shilling_40 | | | | | | | | G | |
| Konza_40 | | | | | | | | | G |

Based on analysis, the test with most potential for assessing cracking potential of a mix with RAP is the VECD test, followed by the OT and S-SCB tests for capturing desired variability in cracking performance. The dynamic modulus test was not significant for evaluating the effect of RAP source and RAP content on cracking performance of HMA mixtures.

# Chapter 5 - Conclusions and Recommendations

## 5.1 Conclusions

The objective of this research was to evaluate cracking resistance of Superpave mixtures with high RAP contents and various RAP sources. A total of nine mixtures were tested in four cracking test setups as well as in the moisture susceptibility test. The following conclusions were drawn based on analysis results:

1) Modified Lottman test results indicated that TSR decreased with increasing RAP content, but the values were greater than 80%, as required by KDOT, for six mixtures with RAP from Shilling and US 73 sources. Three mixtures containing 20, 30, and 40% Konza RAP failed to achieve minimum TSR in this test.
2) The S-SCB test compared mixtures based on FE and stiffness parameters. With increasing RAP content, rate of energy release and stiffness parameters increased. Mixtures with RAP from US 73 performed better than mixtures with two other sources of RAP. Differences in FE values for various RAP content and source were not found to be statistically significant because of dominant interaction effect between the RAP source and the RAP content at the 95% confidence interval. Overall, this test was able to identify differences in performance of various mixtures.
3) The R-SCB test showed anomalous results for the evaluation of fatigue performance. For six mixtures from the first and third sources of RAP, performance decreased with increasing RAP content. For second source of RAP, however, the mixture containing 40% RAP performed the best.

4) The OT test provided straightforward evaluation of mixtures; mixtures passing a minimum of 300 OT cycles were considered to satisfactorily resist reflective cracking, but mixtures with 40% RAP from the first and second RAP sources failed in this category. Statistical analysis results identified that the OT test is capable of cracking performance of HMA mixtures and identifying interaction effect of RAP content and RAP source. Therefore, prediction was made for each individual mixture using 95% confidence interval.
5) Typical trends of decreasing dynamic modulus values with increasing temperature and decreasing dynamic modulus values for low frequencies were observed in the dynamic modulus test results. However, the test results proved that the dynamic Modulus test did not accurately evaluate cracking performance. High variability associated with the test may have contributed to this statistical conclusion.
6) The VECD test compared mixtures according to the number of standard fatigue cycles. Fatigue performance decreased with increasing RAP content. Mixtures with RAP from US 73 performed better than the other two sources. Statistically, dominance of individual RAP content or RAP quality was not found. Damage characteristic curves were produced for all mixtures, and performance was assessed on damage parameter values, the higher the better. Remaining fatigue life of the mixtures was also simulated for corresponding stress and strain levels. The VECD test identified the highest number of significant differences among test results.
7) Mixtures with total binder content of 4.5 to 4.9% performed satisfactorily. Mixtures with 40% RAP were satisfactory for two sources, but the other source

displayed anomalous results. However, for up to 30% RAP content, mixtures performed well.

## 5.2 Recommendations

RAP properties those had been included in this study were binder content and gradation of RAP sources. Study results show that the stiffening effect of RAP affects outputs of various test results; therefore, further study should include these RAP properties. For all tests, RAP source was found to be a significant, sometimes dominant, source of variance. If RAP sources individually perform, one prescription of quantity is not possible to be given at least for higher quantity of RAPs. Characterization of RAP quality is essential for satisfactory performance. As a future research scope, characterization of RAP binder at the elemental level may help characterizing RAPs to provide better guidance to designers.

# References


AASHTO PP 61-13 (2013). "Standard Practice for Developing Dynamic Modulus Master Curves for Hot Mix Asphalt (HMA) Using the Asphalt Mixture Performance Tester (AMPT)" Proposed Protocol, American Association of State Highway and Transportation Officials, Washington, DC.

AASHTO T 283 (2007). "Resistance of Compacted Asphalt Mixtures to Moisture-Induced Damage," Standard Specification, American Association of State Highway and Transportation Officials, Washington, DC.

AASHTO TP 107-14 (2014). "Determining the Damage Characteristics Curve of Asphalt Mixtures from Direct Tension Cyclic Fatigue Test." Test Protocol, American Association of State Highway and Transportation Officials, Washington, DC.

AASHTO TP 62-07 (2013). "Standard Method of Test for Determining Dynamic Modulus of Hot-Mix Asphalt Concrete Mixtures" Test Protocol, American Association of State Highway and Transportation Officials, Washington, DC.

Adamson, J. M., Mathias, C. L., Andrews, R. C. (1996). "Deep Pavement Moisture Barriers Using Pressure Injection of a Lime-flyash Slurry." Second Malaysian Road Conference, Kuala Lumpur, Malaysia.

Al-Qadi, I. L., Abuawad, I. M., Dhasmana, H., Coenen, A. R. (2014). "Effects of Various Asphalt Binder Additives/Modifiers on Moisture-Susceptible Asphaltic Mixtures." Journal of Civil Engineering Studies, Illinois Center for Transportation Series No. 14-004, ISSN: 0197-9191.

Al-Qadi, I. L., Abuwad, I. M. (2014). "Effects of Various Asphalt Binder Additives/Modifiers on Moisture Susceptible Asphalt Mixtures," Civil Engineering Studies, Illinois Center for Transportation Series No. 14-004, ICT-R27*078.

Al-Qadi, I. L., Ozer, H., Lambros, J., Lippert, D. L. (2015). "Testing Protocols to ensure Mix Performance w/High RAP and RAS." Webinar: Illinois Center for Transportation, University of Illinois at Urbana-Champaign, Illinois.

Anderson, T. L. (1995). "Fracture Mechanics, Fundamentals and Applications." First Edition, Taylor and Francis, NY.

Aziz, S. R. (2013). "Evaluation of Cracking Resistance of Superpave Mixtures in Kansas." Master's Thesis, Kansas State University, Manhattan, Kansas.

Aziz, S. R. (2013). “Evaluation of Cracking Resistance of Superpave Mixtures in Kansas.” Master’s Thesis, Kansas State University, Manhattan, Kansas.

Bhasin, A., Button, J. W., Chowdhury, A. (2004). “Evaluation of Simple Performance Tests on Hot-Mix Asphalt Mixtures from South Central United States.” Journal of the Transportation Research Board, Vol. 1891, pp. 147-181.

Bonaquist, R. (2007). “Can I Run More RAP?.” Journal of Hot Mix Asphalt Technology, National Asphalt Pavement Association, Vol. 12, Issue 5.

Bonaquist, R. (2011). “Effect of Recovered Binders from Recycled Shingles and Increase RAP Percentages on Resultant Binder PG.” Report No. WHRP 11-13, Washington Department of transportation, Madison.

Bonaquist, R. (2013). “Impact of Mix Design on Asphalt Pavement Durability.” Transportation Research Circular, Transportation Research Board, Washington D. C.

Brown, E. R., Hainin, M. R, Cooley, A., Hurley, G. (2004). “NCHRP Report 531: Relationship of Air Voids, Lift Thickness, and Permeability in Hot-Mix Asphalt Pavements.” Transportation Research Board of the National Academies, Washington, D.C., 2004.

Brown, E. R., Hainin, M. R., Cooley, A., Hurley, G. (2004). “Relationship of Air Voids, Lift Thickness, and Permeability in Hot-Mix Asphalt Pavements.” NCHRP Report 531: Transportation Research Board of the National Academies, Washington, D.C.

Buss, A. F., Williams, R. C. (2013). “Investigation of Warm-Mix Asphalt for Iowa Roadways, Phase II.” Final Report: Tech Transfer Summaries, paper 53.

Cho, Y. H., Park, D. W., Hwang, S. D. (2010). “A Predictive Equation for Dynamic Modulus of Asphalt Mixtures Used in Korea.” Journal of Construction and Building Materials, Vol. 24, Issue. 4, pp. 513-519.

Chong, K. P., Kuruppu, M. D. (1984). “New Specimen for Fracture Toughness Determination for Rock and Other Materials.” International Journal of Fracture, Vol. 26, Issue 2, pp. 59-62.

Christensen, D. W., Hanz, A., Velasquez, R., Arshadi, A., Bahia, H (2013). “Refinement of Current WisDOT HMA Mixture Application Guidelines Related to NMAS and Aggregate Characteristics.” Final report: Project 0092-12-01, Wisconsin Highway Research Program, Wisconsin Highway Research Program, Madison.

Cooper III, S. (2014). “Semi-Circular Bend: Sample Preparation, Testing, and Analysis.” Louisiana Asphalt Pavement Association Annual Meeting, Point Clear, Alabama.

Cooper, S. III. (2014). "Semi-Circular Bend: Sample Preparation, Testing and Analysis." Louisiana Asphalt Pavement Association Annual Meeting, Louisiana Transportation Research Center.

Copeland, A. (2011). "Reclaimed Asphalt Pavement in Asphalt Mixtures: State of the Practice." Report No. FHWA-HRT-11-021, Federal Highway Administration, McLean, Virginia.

Daniel, J. S., Kim, Y. R. (2002). "Development of a Simplified Fatigue Test and Analysis Procedure Using a Viscoelastic Continuum Damage model." Journal of the Association of Asphalt Paving technologists, Vol. 71, pp. 619-650.

Daniel, J. S., Lachance, A. (2005). "Mechanistic and Volumetric Properties of Asphalt Mixtures with RAP," Journal of Transportation Research Board, Issue. 1929, pp. 28-36.

Devol, J. R. (2008). "Texas Overlay Tester Project." Technotes, Washington State Department of transportation, Washington.

FHWA (2011). "Highway Statistics 2008." Federal Highway Administration, U.S. Department of Transportation. <http://www.fhwa.dot.gov/policyinformation/statistics/2008/ hm12.cfm> (Accessed on May 7, 2015).

Ghauch, Z. G., Abou-Jaude, G. G. (2013). "Strain Response of Hot-mix Asphalt Overlays in jointed Plain Concrete pavement due to Reflective Cracking." Journal of Computer and Structures, Vol. 124, pp. 38-46.

Hossein, A., Sheikhmotevali, M. A. (2013). "Application of Bitumen Rheological Parameters to Predict Thermal Cracking Behavior of Polymer Modified Asphalt Mixture." Journal of Construction and Building Materials, Vol. 66, pp. 259-267.

Hu, S., Zhou, F., and Scullion, T. (2011). "Factors That Affect Cracking Performance in Hot- Mix Asphalt Mix Design." Journal of the Transportation Research Board, Vol. 2210, pp. 37-46.

Huang, B., Shu, X., Zuo, G. (2013). "Using Notched Semi Circular Bending Fatigue Test to Characterize Fracture Resistance of Asphalt Mixtures." Journal of Engineering Fracture Mechanics, Vol. 109, pp. 78-88.

Huang, B., X. Shu, and Y. Tang, (2005). "Comparison of Semicircular Bending and Indirect Tensile Strength Tests for HMA Mixtures." American Society of Civil Engineers Geotechnical Special Publication, Issue 130-142, pp. 177-188.

Huang, L, Keming, C., Zeng, M. (2009) "Evaluation of Semicircular Bending Test for Determining Tensile Strength and Stiffness Modulus of Asphalt Mixtures." Journal of Testing and Evaluation, Vol. 37, pp. 122-128

Huber, G. (2013). "History of Asphalt Mix Design in North America, Part II: Superpave." Asphalt Institute Journal: Asphalt, Vol. 28, pp. 25-29.

Kandahl, P. S., Parker, F. J (1998). "Aggregate Tests Related to Asphalt Concrete Performance in Pavements." NCHRP Report 405: Transportation Research Board of the National Academies, Washington, D. C.

Kandhal, P. S., and Chakraborty, S. (1996). "Effect of Asphalt Film Thickness on Short and Long-Term Aging of Asphalt Paving Mixtures." Journal of the Transportation Research Board Vol. 1535, pp. 83-90.

Kansas Test Method KT-15 (2004). "Bulk Specific Gravity and Unit Weight of Compacted Hot Mix Asphalt." Kansas Department of Transportation, Topeka, Kansas.

Kansas Test Method KT-39 (2014). "Theoretical Maximum Specific Gravity of Asphalt Paving Mixtures, Kansas Department of Transportation." Topeka, Kansas.

Kansas Test Method KT-56 (2014). "Resistance of Compacted Asphalt Mixtures to Moisture Induced Damage." Kansas Department of Transportation, Topeka, Kansas.

Karlsson, R., Isacsson, U. (2006). "Material-Related Aspects of Asphalt Recycling—State-of-the-Art." Journal of Materials in Civil Engineering, Vol. 18, Issue 1, pp. 81-92.

Kevin, P., Nazarian, S. (2014). "Improved Overlay Tester for Fatigue Cracking." Project Report: Texas Department of Transportation, RiP 36805.

Khosravifar, S., Schwartz, C. W., Goulias, D. G. (2015). "Mechanistic Structural Properties of Foamed Asphalt Stabilised Base Materials." International Journal of Pavement Engineering, Vol. 16, Issue. 1, pp. 27-38.

Kim, Y. R., Baek, C., Underwood, B. S., Subramanian, V., Guddati, M. N., & Lee, K. (2008). "Application of Viscoelastic Continuum Damage Model Based Finite Element Analysis to Predict The Fatigue Performance Of Asphalt Pavements," KSCE Journal of Civil Engineering, Vol. 12(2), pp. 109-120.

Kim, Y.R., Guddati, M.N., Underwood, B.S., Yun, T.Y., Subramanian,V., Savadatti., S. (2009). "Development of a Multiaxial Viscoelastoplastic Continuum Damage Model for Asphalt Mixtures," Project Report: Federal Highway Administration, US Department of Transportation, Report No. FHWA-HRT-08-073.

Kuehl, R. O. (2000). "Design of Experiments: Statistical Principles of Research Design and Analysis." 2nd Edition, Duxbury Press, California.

Lee, H. D., Winkle, C. V., Carlson, R., Mokhtari, A., Ahmed, T., Kim, H., Tang, S., Williams, C. (2015). "Development of Quality Standards for Inclusion of High Recycled Asphalt Pavement Content in Asphalt Mixtures – Phase II." Final Report TR-658, Public Policy Center, University of Iowa, Iowa City, Iowa.

Lee, S., Mun, S., Kim, R. (2011). "Fatigue and Rutting Performance of Lime-modified Hot-mix Asphalt Mixtures." Construction and Building Materials, Vol. 25, issue 11, pp. 4202-4209.

Li, X., and Marasteanu, M. (2004). "Evaluation of the Low Temperature Fracture Resistance of Asphalt Mixtures using the Semi Circular Bend Test." Journal of the Association of Asphalt Paving Technologists, Vol. 73, pp. 401-426.

Li, X., M. O., Marasteanu, R. C., Williams, T. R., Clyne (2008). "Effect of Reclaimed Asphalt Pavement (Proportion and Type) and Binder Grade on Asphalt Mixtures." Journal of the Transportation Research Board, No. 2051, pp. 90–97.

Li. J., Oh, J., Naik, B., Simate, G. S., Walubita, L. F. (2014). "Laboratory Characterization of Cracking-resistance Potential of Asphalt Mixes Using Overlay Tester." Journal of Construction and Building Materials, Vol. 70, pp. 130-140.

Martin, A.E., Edith, A., Kutay, M. E., Lawrence, J., Luo, X., Lytton, R. (2013). "Comparison of Fatigue Analysis Approaches for Hot-Mix Asphalt to Ensure a State of Good Repair." Technical Report SWUTC/13/600451-00012-1, Texas A&M Transportation Institute, College Station, Texas.

McDaniel, R. S., H., Soleymani, R. M., Anderson, P., Turner, Peterson, R., (2000). "NCHRP Web Document 30: Recommended Use of Reclaimed Asphalt Pavement in the Superpave Mix Design Method." Transportation Research Board of the National Academies, Washington, D.C., 2000. <http://onlinepubs.trb.org/onlinepubs/nchrp/nchrp_w30-a.pdf.> Accessed May 30, 2015.

Meininger, R.C., Nichols, F.P. (1990). "Highway Materials Engineering. Aggregates and Unbound Bases." Publication No. FHWA-HI-90-007, NHI Course No. 13123, Federal Highway Administration, Washington, D.C.

Monismith, C. L., Secor, K. E., Blackner, E. W. (1961). "Asphalt Mixture Behavior in Repeated Flexure," Journal of Association of Asphalt Paving Technologists," Vol. 30, pp. 188–122.

Monismith, C. L., Secor, K. E., Blackner, E. W. (1961). "Asphalt Mixture Behavior in Repeated Flexure." Journal of Association of Asphalt Paving Technologists, Vol. 30, pp. 188–122.

NAPA (2010). "Asphalt Pavement Recycling Facts." <http://moasphalt.org/facts/environmental/facts.htm> (accessed on May 30, 2013).

NAPA (2013). "Asphalt Pavement Overview." <http://www.asphaltpavement.org/index.php?option=com_content&view=article&id=14&Itemid=34> (accessed on May 5, 2015).

Nicholls, J. C., McHale, M. J., Griffths, R. D. (2008). "Best Practice Guide for Durability of Asphalt Pavements." Road Note, Vol. 42, Transport Research Laboratory, Workingham, Berkshire, United Kingdom.

Ozer, H., Al-Qadi, I. L., Kanaan, A. (2012). "Laboratory Evaluation of High Asphalt Binder Replacement with Recycled Asphalt Shingles (RAS) for a Low N-Design Asphalt Mixture." Civil Engineering Studies, Illinois Center for Transportation Series No. 12-018, ISSN: 0197-9191.

Paris, P., Erdogan, F. (1963). "A Critical Analysis of Crack Propagation Laws," Journal of Basic Engineering, Transactions of the American Society of Mechanical Engineers, pp. 528-534.

Pell, P. S., Cooper, K. E. (1975) "The Effect of Testing and Mix Variables on the Fatigue Performance of Bituminous Materials." Journal of Association of Asphalt Paving Technologists, Vol. 44, pp.1-12.

Podolsky, J., Buss, A., Williams, R. C., Eric C. (2014). "Comparative Performance of Bio-derived/chemical Additives in Warm Mix Asphalt at Low Temperature." Journal of Materials and Structures, International Union of Testing and Research Laboratories, Vol. 26, Issue 2, pp. 304-311.

Ren, R., Geng, L., An, H., Wang, X. (2015). "Experimental Research on Shear Fatigue Characteristics of Asphalt Mixtures Based on Repeated Uniaxial Penetrating Test." Journal of Road materials and Pavement Design, Vol. 16, Issue 2, pp. 459-468.

Roque, R., Zou, J., Kim, Y. R., Baek, C. M., Thirunavukkarasu, S., Underwood, B.S., Guddati, M.N. (2011). "Top-Down Cracking of Hot Mix Asphalt Layers: Models for Initiation and Propagation." Final Report NCHRP 1-42A, Transportation Research Board of the National Academies, Washington, D.C.

Roylance, D. (2001). "Introduction to Fracture Mechanics." Department of Materials Science and Engineering, Massachusetts Institute of Technology, Cambridge, MA.

Saadeh, S., Eljairi, O. (2011). "Development of a Quality Control Test Procedure for Characterizing Fracture Properties of Asphalt Mixtures." Project Report: 10-24, University Transportation Centers Program, USDOT.

Sabahfar, N. (2012). “Use of High-Volume Reclaimed Asphalt Pavement (RAP) for Asphalt Pavement Rehabilitation.” Master’s Thesis, Kansas State University, Manhattan, Kansas.

Sabahfar, N. (2012). “Use of High-Volume Reclaimed Asphalt Pavement (RAP) for Asphalt Pavement Rehabilitation.” Master’s Thesis, Kansas State University, Manhattan, Kansas.

Sakhaeifar, M. S., Kim, Y. R., Kabir, P. (2015). “New Predictive Models for the Dynamic Modulus of Hot Mix Asphalt.” Journal of Construction and Building Materials, Vol. 76, pp. 221-231.

SAS Institute Inc. (2011). SAS User Guide for Windows, Release 9.3. Cary, NC. 2011.

Scullion, T., Walibita, L., F., Faruk, A., Hoeffner, J. (2012). “The Overlay Tester (OT): Sensitivity Evaluation and Comparison to Other Crack Test Methods.” Project Summary Report: Texas Department of Transportation, P0-6607, College Station, Texas.

Shakiba, M., Darabi, M. K., Abu Al-Rub, R. K., Taesun, Y., Little, D. N. (2013). “Continuum Coupled Moisture-Mechanical Damage Model for Asphalt Concrete.” Journal of the Transportation Research Board, Vol. 2372, pp. 72-82.

Shen, J., Amirkhanian, S., Miller, J. A. (2007). “Effects of Rejuvenating Agents on Superpave Mixtures Containing Reclaimed Asphalt Pavement.” Journal of Materials in Civil Engineering, Vol. 19, pp. 376-388.

Shu, X., Huang. B., and Vukosavljevic, D. (2008). “Laboratory Evaluation of Fatigue Characteristics of Recycled Asphalt Mixture.” Journal of Construction and Building Materials, Vol. 22, No. 7, pp. 207-213.

Tan, Y., Shan, L., Kim, Y. R., Underwood, S. (2012). “Healing Characteristics of Asphalt Binder.” Journal of Construction and Building Materials, Vol. 27, Issue. 1, pp. 570-577.

TEX-248-F (2014). “Overlay Test.” Texas Department of Transportation, Texas.

Tong, Y., Lou, R., Lytton, R. L. (2015). “Moisture and Aging Damage Evaluation of Asphalt Mixtures Using The Repeated Direct Tensional Test Method,” Vol. 5, Issue 5, pp. 397-410.

Underwood, B. S., Kim, Y. R. (2012). “Simplified Viscoelastic Continuum Damage Model as Platform for Asphalt Concrete Fatigue Analysis.” Journal of the Transportation Research Board, Vol. 2296, pp. 36–45.

Underwood, B. S., Kim, Y. R. (2014). “A Four Phase Micro-Mechanical Model for Asphalt Mastic Modulus,” Journal of Mechanics of Materials, Vol. 75, pp. 13-33.

Valdes, G., Perex-Jimenez, F., Miro, R., Martinez, A., Botella, R. (2011). "Experimental Study of Recycled Asphalt Mixtures with High Percentages of Reclaimed Asphalt Pavement (RAP)." Journal of Construction and Building Materials, Vol. 25, pp. 1289-1297.

Walubita, L. F., Faruk, A. N., Das, G., Hossain, T. A., Zhang, J., Scullion, T. (2012). "The Overlay Tester: A Sensitivity Study to Improve Repeatability and Minimize Variability in the Test Results." Project Report: FHWA/TX-12/0-6607-1, Federal Highway Administration, Washington D. C.

Walubita, L. F., Hoeffner, J. K., Scullion, T. (2013). "New Generation Mix-Designs: Laboratory-Field Testing and Modifications to Texas HMA Mix-Design Procedures." Technical Research Report: FHWA/TX-12/0-6132-3FHWA, Texas A&M Transportation Institute (TTI), College Station, Texas.

West, R., Willis, R., Brown, R., Blow, M. (2014). "Improved Performance of Reclaimed Asphalt Pavement Mixes." Final Report: Study SD2011-08, Office of Research, South Dakota Department of Transportation, South Dakota.

Xie, Z., Shen, J., Earnest, M., Li, B., Jackson, M. (2014). "Fatigue Performance Evaluation of Porous European Mix (PEM) with Crumb Rubber Modified Binders Using Simplified Viscoelastic Continuum Damage Model." 94$^{Th}$ Annual Meeting: Transportation Research Board, Washington D. C.

Yao, H., You, Z., Li, L., Lee, C. H. (2013). "Rheological Properties and Chemical Bonding of Asphalt Modified with Nanosilica." Journal of Materials in Civil Engineering, Vol. 25, Issue. 11, pp. 1619-1630.

Yu, H., Shen, S. (2012). "Impact of Aggregate Packing on Dynamic Modulus of Hot Mix Asphalt Mixtures Using Three-Dimensional Discrete Element Method." Journal of Construction and Building Materials. Vol. 26, Issue. 1, pp. 302-309.

Zaumanis, M., Mallick, R. B. (2014). "Review Of Very High-Content Reclaimed Asphalt Use in Plant-Produced Pavements: State of The Art." International Journal of Pavement Engineering, Vol. 16:1, pp. 39-55.

Zhou, F., Hu, S., Scullion, T. (2006). "Integrated Asphalt (Overlay) Mix Design with Balancing both Rutting and Cracking Requirements." Technical Report FHWA/TX-05/5123-1, Texas Transportation Institute (TTI).

Zhou, F., Scullion, T. (2004). "User Manual for TxDOT's New Overlay Tester." Project Report: FHWA/TX-05/0-4467-P3, Federal Highway Administration, Washington D. C.

Zhou, F., Scullion, T. (2005). "Developing an Upgraded Overlay Tester System to Characterize the Reflection Cracking Resistance of Asphalt Concrete." Project Summary Report: 0-4467-S, Texas Transportation Institute, the Texas A&M University System, College Station, Texas.

# Appendix A - Cracking Test Results

## 5.1 Semi-Circular Bending Test: Fracture Energy Results

| RAP Source | RAP Content (%) | Area Under (P-u) Curve (J) | Ligament Area ($m^2$) | Fracture Energy ($J/m^2$) | Average Energy ($J/m^2$) | Std. Dev | COV (%) |
|---|---|---|---|---|---|---|---|
| Shilling | 20 | 5.8858 | 0.00725 | 2242.9 | 2098.7 | 180.9 | 8.6 |
| | | 5.6612 | 0.00725 | 2157.4 | | | |
| | | 4.9745 | 0.00725 | 1895.7 | | | |
| | 30 | 5.8892 | 0.00725 | 2244.2 | 2064.9 | 214.4 | 10.4 |
| | | 5.5713 | 0.00725 | 2123.1 | | | |
| | | 4.7956 | 0.00725 | 1827.5 | | | |
| | 40 | 5.2671 | 0.00725 | 2007.2 | 2173.8 | 175.4 | 8.1 |
| | | 5.6613 | 0.00725 | 2157.4 | | | |
| | | 6.1846 | 0.00725 | 2356.8 | | | |
| Konza | 20 | 4.0371 | 0.00725 | 1538.5 | 1632.2 | 98.5 | 6.0 |
| | | 4.5525 | 0.00725 | 1734.9 | | | |
| | | 4.2598 | 0.00725 | 1623.3 | | | |
| | 30 | 4.3656 | 0.00725 | 1663.6 | 1769.4 | 92.1 | 5.2 |
| | | 4.8057 | 0.00725 | 1831.3 | | | |
| | | 4.7584 | 0.00725 | 1813.3 | | | |
| | 40 | 5.8410 | 0.00725 | 2225.9 | 1884.0 | 350.0 | 18.6 |
| | | 4.0054 | 0.00725 | 1526.4 | | | |
| | | 4.9852 | 0.00725 | 1899.8 | | | |
| US 73 | 20 | 2.5993 | 0.00725 | 990.5 | 1161.2 | 176.0 | 15.2 |
| | | 3.5219 | 0.00725 | 1342.1 | | | |
| | | 3.0206 | 0.00725 | 1151.1 | | | |
| | 30 | 2.5412 | 0.00725 | 968.4 | 1187.6 | 337.7 | 28.4 |
| | | 2.6710 | 0.00725 | 1017.9 | | | |
| | | 4.1367 | 0.00725 | 1576.4 | | | |
| | 40 | 5.2653 | 0.00725 | 2006.5 | 1612.2 | 377.1 | 23.4 |
| | | 4.1332 | 0.00725 | 1575.1 | | | |
| | | 3.2935 | 0.00725 | 1255.1 | | | |

## 5.2 Semi-Circular Bending Stiffness Parameters

| RAP Source | RAP Content (%) | Load (KN) | Displacement (mm) | c(L/D) | Sample Thickness, t (mm) | Stiffness Modulus (MPa) | Average Modulus (MPa) | Std Dev. | COV (%) |
|---|---|---|---|---|---|---|---|---|---|
| Shilling. | 20 | 2543.7 | 0.0019 | 0.8 | 50 | 21420.5 | 20491.1 | 1414.1 | 6.9 |
| | | 2516.2 | 0.0019 | 0.8 | 50 | 21189.1 | | | |
| | | 2004.3 | 0.0017 | 0.8 | 50 | 18863.7 | | | |
| | 30 | 3172.0 | 0.0015 | 0.8 | 50 | 33834.8 | 29439.9 | 8056.3 | 27.4 |
| | | 3863.6 | 0.0018 | 0.8 | 50 | 34342.9 | | | |
| | | 2769.5 | 0.0022 | 0.8 | 50 | 20141.9 | | | |
| | 40 | 4608.2 | 0.0012 | 0.8 | 50 | 61442.9 | 58594.2 | 5566.0 | 9.5 |
| | | 3587.4 | 0.0011 | 0.8 | 50 | 52180.4 | | | |
| | | 3885.0 | 0.0010 | 0.8 | 50 | 62159.2 | | | |
| Konza | 20 | 2354.5 | 0.0014 | 0.8 | 50 | 26908.2 | 26804.4 | 439.9 | 1.6 |
| | | 2632.2 | 0.0016 | 0.8 | 50 | 26321.8 | | | |
| | | 2548.4 | 0.0015 | 0.8 | 50 | 27183.0 | | | |
| | 30 | 2467.4 | 0.0015 | 0.8 | 50 | 26318.7 | 27406.9 | 1249.5 | 4.6 |
| | | 2713.1 | 0.0016 | 0.8 | 50 | 27130.5 | | | |
| | | 2517.5 | 0.0014 | 0.8 | 50 | 28771.4 | | | |
| | 40 | 3135.7 | 0.0016 | 0.8 | 50 | 31357.3 | 33843.1 | 2247.0 | 6.6 |
| | | 2456.4 | 0.0011 | 0.8 | 50 | 35730.0 | | | |
| | | 2798.4 | 0.0013 | 0.8 | 50 | 34441.8 | | | |
| US 73 | 20 | 1549.6 | 0.0019 | 0.8 | 50 | 13048.8 | 11124.3 | 2374.4 | 21.3 |
| | | 1482.4 | 0.0028 | 0.8 | 50 | 8470.9 | | | |
| | | 1481.7 | 0.0020 | 0.8 | 50 | 11853.2 | | | |
| | 30 | 1893.6 | 0.0015 | 0.8 | 50 | 20198.8 | 18313.4 | 1639.7 | 9.0 |
| | | 1829.7 | 0.0017 | 0.8 | 50 | 17220.7 | | | |
| | | 2080.6 | 0.0019 | 0.8 | 50 | 17520.6 | | | |

| | | | | | | | | | |
|---|---|---|---|---|---|---|---|---|---|
| | 40 | 2414.7 | 0.0020 | 0.8 | 50 | 19317.9 | 18466.2 | 819.6 | 4.4 |
| | | 2320.9 | 0.0021 | 0.8 | 50 | 17683.0 | | | |
| | | 2414.7 | 0.0021 | 0.8 | 50 | 18397.7 | | | |

## 5.3 Texas Overlay No. of OT Cycles

| RAP Source | RAP Content (%) | Air Void (%) | Initial Peak Load (kN) | No. of OT Cycles | Average Duration (min) | Average No. of OT Cycles | Std. dev | COV (%) |
|---|---|---|---|---|---|---|---|---|
| Shilling | 20 | 7.2 | 2.341 | 956 | 134 | 805 | 140 | 17.4 |
| | | 7.3 | 2.418 | 778 | | | | |
| | | 7.0 | 2.296 | 680 | | | | |
| | 30 | 7.3 | 2.799 | 348 | 80 | 477 | 117 | 24.5 |
| | | 7.4 | 2.987 | 576 | | | | |
| | | 7.2 | 2.903 | 507 | | | | |
| | 40 | 7.3 | 3.432 | 91 | 21 | 128 | 34 | 26.9 |
| | | 7.1 | 3.219 | 134 | | | | |
| | | 7.0 | 3.186 | 159 | | | | |
| Konza | 20 | 7.3 | 2.615 | 236 | 48 | 296 | 75 | 25.2 |
| | | 7.1 | 2.769 | 380 | | | | |
| | | 7.0 | 2.599 | 273 | | | | |
| | 30 | 7.2 | 1.917 | 54 | 12 | 71 | 16 | 22.7 |
| | | 7.4 | 2.069 | 72 | | | | |
| | | 7.3 | 2.318 | 86 | | | | |
| | 40 | 7.2 | 2.989 | 372 | 73 | 435 | 65 | 14.9 |
| | | 7.0 | 3.098 | 432 | | | | |
| | | 7.1 | 3.185 | 502 | | | | |
| US 73 | 20 | 7.8 | 1.152 | 612 | 97.7 | 626 | 126 | 20.1 |
| | | 6.5 | 1.773 | 508 | | | | |
| | | 7.4 | 1.612 | 758 | | | | |
| | 30 | 6.5 | 0.848 | 498 | 93 | 561 | 140 | 24.9 |
| | | 7.0 | 0.581 | 721 | | | | |
| | | 7.2 | 0.713 | 464 | | | | |
| | 40 | 7.1 | 0.581 | 649 | 47.3 | 529 | 112 | 21.3 |
| | | 6.9 | 0.495 | 512 | | | | |
| | | 7.4 | 0.395 | 426 | | | | |

## 5.4 Dynamic Modulus Test Results

| Sample ID | Temperature ('C) | Dynamic Modulus (MPa) at different Loading Frequencies (Hz) | | | | | |
|---|---|---|---|---|---|---|---|
| | | **25** | **10** | **5** | **1** | **0.5** | **0.1** |
| 20_I | 4 | 16190 | 15059 | 14198 | 12413 | 11586 | 9589 |
| 20_II | | 15390 | 13883 | 13120 | 11146 | 10234 | 7581 |
| 20_III | | 14511 | 14822 | 13757 | 11210 | 10074 | 7481 |
| Mean | | 15363.7 | 14588 | 13691.7 | 11589.7 | 10631.3 | 8217 |
| Std. Dev | | 839.8 | 621.9 | 542 | 713.7 | 830.6 | 1189.2 |
| COV (%) | | 5.5 | 4.3 | 4 | 6.2 | 7.8 | 14.5 |
| 20_I | 21 | 11532 | 9502 | 7799 | 6033 | 5880 | 5928 |
| 20_II | | 9192 | 8052 | 7446 | 6224 | 5558 | 5108 |
| 20_III | | 11447 | 10384 | 7739 | 5324 | 5016 | 4997 |
| Mean | | 10723.7 | 9312.7 | 7661.3 | 5860.3 | 5484.7 | 5344.3 |
| Std. Dev | | 1327.1 | 1177.5 | 188.9 | 474.2 | 436.6 | 508.5 |
| COV (%) | | 12.4 | 12.6 | 2.5 | 8.1 | 8 | 9.5 |
| 20_I | 37 | 6749 | 5347 | 4578 | 3942 | 2312 | 1925 |
| 20_II | | 6331 | 5493 | 4992 | 3977 | 2674 | 1944 |
| 20_III | | 7149 | 5399 | 4667 | 3216 | 2746 | 1780 |
| Mean | | 6743 | 5413 | 4745.7 | 3711.7 | 2577.3 | 1883 |
| Std. Dev | | 409 | 74 | 217.9 | 429.6 | 232.6 | 89.7 |
| COV (%) | | 6.1 | 1.4 | 4.6 | 11.6 | 9 | 4.8 |
| 30_I | 4 | 13140 | 11868 | 10802 | 8410 | 7404 | 5238 |
| 30_II | | 12800 | 11478 | 10555 | 8556 | 7765 | 6054 |
| 30_III | | 10564 | 9097 | 8616 | 7307 | 7563 | 5816 |
| Mean | | 12168 | 10814.3 | 9991 | 8091 | 7577.3 | 5702.7 |
| Std. Dev | | 1399.5 | 1500 | 1197.2 | 682.9 | 180.9 | 419.6 |
| COV (%) | | 11.5 | 13.9 | 12 | 8.4 | 2.4 | 7.4 |
| 30_I | 21 | 9221 | 8407 | 7835 | 6744 | 5381 | 4698 |
| 30_II | | 10615 | 9464 | 8551 | 6663 | 5948 | 4476 |
| 30_III | | 8589 | 7840 | 7158 | 5661 | 5091 | 4013 |
| Mean | | 9475 | 8570.3 | 7848 | 6356 | 5473.3 | 4395.7 |
| Std. Dev | | 1036.6 | 824.2 | 696.6 | 603.2 | 435.9 | 349.5 |
| COV (%) | | 10.9 | 9.6 | 8.9 | 9.5 | 8 | 8 |
| 30_I | 37 | 6427 | 5673 | 4148 | 3542 | 2815 | 2172 |
| 30_II | | 6428 | 5126 | 4230 | 4438 | 2731 | 2276 |
| 30_III | | 6322 | 5411 | 4758 | 3373 | 2878 | 2810 |

| | | | | | | | |
|---|---|---|---|---|---|---|---|
| Mean | | 6392.3 | 5403.3 | 4378.7 | 3784.3 | 2808 | 2419.3 |
| Std. Dev | | 60.9 | 273.6 | 331.1 | 572.4 | 73.7 | 342.3 |
| COV (%) | | 1 | 5.1 | 7.6 | 15.1 | 2.6 | 14.1 |
| 40_l | 4 | 9337 | 8286 | 8636 | 7049 | 6323 | 4611 |
| 40_ll | | 8671 | 7889 | 7205 | 5741 | 5135 | 3811 |
| 40_lll | | 10478 | 9557 | 8804 | 6993 | 6128 | 4246 |
| Mean | | 9495.3 | 8577.3 | 8215 | 6594.3 | 5862 | 4222.7 |
| Std. Dev | | 913.8 | 871.3 | 878.7 | 739.5 | 637.1 | 400.5 |
| COV (%) | | 9.6 | 10.2 | 10.7 | 11.2 | 10.9 | 9.5 |
| 40_l | 21 | 8192 | 5032 | 4463 | 3224 | 2558 | 1866 |
| 40_ll | | 5602 | 4442 | 3893 | 2801 | 2424 | 1696 |
| 40_lll | | 6703 | 5815 | 5115 | 3740 | 2273 | 1410 |
| Mean | | 6832.3 | 5096.3 | 4490.3 | 3255 | 2418.3 | 1657.3 |
| Std. Dev | | 1299.8 | 688.8 | 611.5 | 470.3 | 142.6 | 230.4 |
| COV (%) | | 19 | 13.5 | 13.6 | 14.4 | 5.9 | 13.9 |
| 40_l | 37 | 4284 | 3535 | 3024 | 2056 | 1732 | 1074 |
| 40_ll | | 4561 | 3599 | 3093 | 2131 | 1822 | 1193 |
| 40_lll | | 5559 | 4550 | 3880 | 2553 | 2185 | 1394 |
| Mean | | 4801.3 | 3894.7 | 3332.3 | 2246.7 | 1913 | 1220.3 |
| Std. Dev | | 670.6 | 568.4 | 475.5 | 267.9 | 239.8 | 161.7 |
| COV (%) | | 14 | 14.6 | 14.3 | 11.9 | 12.5 | 13.3 |

## 5.5 Phase Angle Values

| Sample ID | Temperature ($^0$C) | Phase Angle ($^0$) at Different Loading Frequency (Hz) | | | | | |
|---|---|---|---|---|---|---|---|
| | | 25 Hz | 10 Hz | 5 Hz | 1 Hz | 0.5 Hz | 0.1 Hz |
| 20_l | 4 | 13.5 | 34.2 | 32.3 | 22.5 | 23.6 | 25.9 |
| 20_ll | | 17.9 | 36.8 | 35.5 | 27.8 | 25.3 | 22.8 |
| 20_lll | | 10.1 | 11.8 | 12.5 | 14.1 | 15.4 | 18.3 |
| Mean | | 13.8 | 27.6 | 26.8 | 21.5 | 21.4 | 22.3 |
| Std. Dev | | 3.9 | 13.8 | 12.5 | 6.9 | 5.3 | 3.8 |
| COV (%) | | 28.2 | 49.9 | 46.6 | 32.1 | 24.7 | 17.0 |
| 20_l | 21 | 21.3 | 39.4 | 38.4 | 29.2 | 30.1 | 31.6 |
| 20_ll | | 25.8 | 29.8 | 35.9 | 32.5 | 33.5 | 28.9 |
| 20_lll | | 17.3 | 18.0 | 19.1 | 21.9 | 22.8 | 25.3 |
| Mean | | 21.5 | 29.1 | 31.1 | 27.8 | 28.8 | 28.6 |
| Std. Dev | | 4.2 | 10.7 | 10.5 | 5.4 | 5.5 | 3.1 |
| COV (%) | | 19.7 | 37.0 | 33.7 | 19.5 | 19.0 | 10.9 |
| 20_l | 37 | 17.8 | 31.5 | 36.5 | 27.6 | 31.5 | 26.5 |
| 20_ll | | 21.1 | 30.0 | 37.5 | 28.3 | 32.4 | 27.4 |
| 20_lll | | 22.2 | 21.2 | 22.2 | 24.8 | 25.5 | 27.7 |
| Mean | | 20.4 | 27.6 | 32.1 | 26.9 | 29.8 | 27.2 |
| Std. Dev | | 2.3 | 5.6 | 8.5 | 1.9 | 3.7 | 0.6 |
| COV (%) | | 11.3 | 20.2 | 26.6 | 6.9 | 12.5 | 2.4 |
| 30_l | 4 | 11.6 | 11.8 | 12.5 | 14.6 | 15.5 | 18.0 |
| 30_ll | | 18.9 | 16.7 | 15.6 | 15.5 | 12.3 | 11.3 |
| 30_lll | | 7.4 | 9.6 | 7.6 | 8.7 | 9.4 | 11.5 |
| Mean | | 12.6 | 12.7 | 11.9 | 12.9 | 12.4 | 13.6 |
| Std. Dev | | 5.8 | 3.6 | 4.0 | 3.7 | 3.0 | 3.8 |
| COV (%) | | 46.1 | 28.7 | 33.8 | 28.6 | 24.5 | 28.0 |
| 30_l | 21 | 14.2 | 15.9 | 14.8 | 17.3 | 18.2 | 20.9 |
| 30_ll | | 13.2 | 14.7 | 17.5 | 16.4 | 19.1 | 17.6 |
| 30_lll | | 9.7 | 13.9 | 11.6 | 13.6 | 14.5 | 16.7 |
| Mean | | 12.3 | 14.8 | 14.6 | 15.8 | 17.3 | 18.4 |
| Std. Dev | | 2.4 | 1.0 | 2.9 | 1.9 | 2.4 | 2.2 |
| COV (%) | | 19.3 | 6.7 | 20.1 | 12.1 | 14.2 | 12.1 |
| 30_l | 37 | 10.6 | 14.9 | 16.7 | 19.3 | 20.2 | 23.1 |
| 30_ll | | 11.3 | 15.8 | 12.6 | 13.7 | 17.2 | 23.8 |
| 30_lll | | 11.4 | 13.5 | 14.5 | 16.6 | 17.5 | 19.9 |
| Mean | | 11.1 | 14.7 | 14.6 | 16.5 | 18.3 | 22.3 |
| Std. Dev | | 0.4 | 1.1 | 2.0 | 2.8 | 1.7 | 2.1 |
| COV (%) | | 3.7 | 7.7 | 14.0 | 16.9 | 9.1 | 9.3 |
| 40_l | 4 | 15.9 | 12.7 | 10.9 | 12.7 | 13.7 | 16.9 |

| | | | | | | | |
|---|---|---|---|---|---|---|---|
| 40_ll | | 18.5 | 17.6 | 11.5 | 13.5 | 11.5 | 17.4 |
| 40_lll | | 9.5 | 29.8 | 31.9 | 22.9 | 18.7 | 21.6 |
| Mean | | 14.6 | 20.0 | 18.1 | 16.4 | 14.6 | 18.7 |
| Std. Dev | | 4.6 | 8.8 | 11.9 | 5.7 | 3.7 | 2.6 |
| COV (%) | | 31.5 | 43.8 | 66.0 | 34.8 | 25.4 | 13.9 |
| 40_l | 21 | 28.2 | 18.4 | 19.7 | 22.8 | 28.3 | 27.3 |
| 40_ll | | 25.9 | 21.4 | 18.4 | 23.6 | 27.5 | 26.8 |
| 40_lll | | 31.5 | 34.8 | 33.5 | 23.9 | 25.0 | 27.1 |
| Mean | | 28.5 | 24.9 | 23.9 | 23.4 | 26.9 | 27.0 |
| Std. Dev | | 2.8 | 8.7 | 8.4 | 0.6 | 1.7 | 0.2 |
| COV (%) | | 9.8 | 35.2 | 35.1 | 2.4 | 6.5 | 0.8 |
| 40_l | 37 | 21.7 | 29.5 | 24.6 | 27.7 | 28.6 | 31.7 |
| 40_ll | | 17.9 | 32.8 | 25.7 | 27.8 | 25.3 | 21.3 |
| 40_lll | | 17.8 | 20.2 | 21.4 | 24.8 | 25.8 | 29.0 |
| Mean | | 19.1 | 27.5 | 23.9 | 26.8 | 26.5 | 27.3 |
| Std. Dev | | 2.2 | 6.6 | 2.2 | 1.7 | 1.8 | 5.4 |
| COV (%) | | 11.6 | 23.9 | 9.4 | 6.5 | 6.6 | 19.8 |

## 5.6 VECD Cycles

| RAP Source | RAP Content | Air Void (%) | No. of fatigue Cycles | Average No. of cycles | Std. Dev | COV (%) |
|---|---|---|---|---|---|---|
| Shilling | 20 | 7.1 | 6391 | 7567 | 1071 | 14.2 |
| | | 7.0 | 8486 | | | |
| | | 7.0 | 7824 | | | |
| | 30 | 6.8 | 3396 | 3619 | 193 | 5.3 |
| | | 6.5 | 3730 | | | |
| | | 6.8 | 3731 | | | |
| | 40 | 7.0 | 1700 | 1771 | 92 | 5.2 |
| | | 7.0 | 1875 | | | |
| | | 7.0 | 1739 | | | |
| Konza | 20 | 7.1 | 7109 | 6788 | 309 | 4.6 |
| | | 7.2 | 6765 | | | |
| | | 7.1 | 6491 | | | |
| | 30 | 7.3 | 4986 | 4705 | 697 | 14.8 |
| | | 7.3 | 3911 | | | |
| | | 7.4 | 5218 | | | |
| | 40 | 7.2 | 1009 | 960 | 76 | 7.9 |
| | | 7.5 | 873 | | | |
| | | 7.5 | 1000 | | | |
| US 73 | 20 | 7.1 | 14238 | 13705 | 598 | 4.4 |
| | | 7.1 | 13820 | | | |
| | | 7.1 | 13059 | | | |
| | 30 | 6.5 | 11665 | 11281 | 336 | 3.0 |
| | | 6.5 | 11134 | | | |
| | | 6.8 | 11044 | | | |
| | 40 | 6.8 | 5310 | 5598 | 414 | 7.4 |
| | | 7.1 | 5413 | | | |
| | | 7.0 | 6073 | | | |

## 5.7 Fatigue Life Prediction Parameters

| RAP Source | RAP Content | Dynamic Modulus (MPa) | K1 | K2 | K3 | Strain Levels (με) | | |
|---|---|---|---|---|---|---|---|---|
| | | | | | | 300 | 500 | 700 |
| Shilling | 20 | 12999 | 2.8E-129 | 3.29 | 34.45 | 106905.8 | 19912.18 | 6581.994 |
| | 30 | 12726 | 2.3E-129 | 3.42 | 34.45 | 24514.01 | 4272.594 | 1351.866 |
| | 40 | 12180 | 1.8E-129 | 3.24 | 34.45 | 9389.652 | 1794.153 | 603.1213 |
| Konza | 20 | 8317 | 1.7E-127 | 3.11 | 35.64 | 174506.8 | 35633.84 | 12514.24 |
| | 30 | 6673 | 2.2E-126 | 3.17 | 35.64 | 603.6487 | 119.5429 | 41.14318 |
| | 40 | 8358 | 1.6E-128 | 3.35 | 35.64 | 4800.338 | 867.1186 | 280.8986 |
| US 73 | 20 | 9313 | 2.9E-127 | 5.65 | 36.9 | 837652.2 | 46732.42 | 6982.242 |
| | 30 | 8570 | 1.8E-129 | 5.89 | 37.95 | 821015.3 | 40519.32 | 5584.291 |
| | 40 | 5096 | 2.4E-127 | 6.12 | 39.8 | 576316.2 | 25289.86 | 3225.84 |